EVALUATION AND STRENGTHENING OF ELEVATED SLAB ON GRADE WITH FIBER-REINFORCED POLYMER (FRP) LAMINATES

by

NATAWUT CHAIWINO

Presented to the Faculty of the Graduate School of

The University of Texas at Arlington in Partial Fulfillment

of the Requirements

for the Degree of

DOCTOR OF PHILOSOPHY

THE UNIVERSITY OF TEXAS AT ARLINGTON

August 2018

Acknowledgements

First and foremost, I would like to express my utmost gratitude to my advisor Dr. Nur Yazdani for his valuable guidance, consistent support, and encouragement through the entirety of this research. I am grateful to Dr. Laureano Hoyos, Dr. Suyun Ham and Dr. Ratan Kumar for readily accepting to serve on my dissertation committee as well as for their advice. My appreciate also goes to the former members of my advisory committee, Dr. Mohammad Razavi, Dr. Yeonho Park, and Dr. Wen Chan for their helpful suggestions at the beginning of my research. I will be always grateful to the Department of Civil Engineering at UT Arlington for providing me with supports and facilities to perform my research work.

I am thankful to my friends, Dr. Eyosias Beneberu, Yazan Almomani, Santosh Timilsina, Mina Riad, Tariq Al Jaafreh, Towfiqul Alquadir, Zaid Momani, and Ankita Lad for all the helpful, amusing, and amazing moments.

I am deeply grateful to my parents and lovely sister who stood by my side from the beginning until the completion of my PhD study.

July 1, 2018

Abstract

EVALUATION AND STRENGTHENING OF ELEVATED SLAB ON GRADE WITH FIBER-REINFORCED POLYMER (FRP) LAMINATES

Natawut Chaiwino, PhD

The University of Texas at Arlington, 2018

Supervising Professor: Nur Yazdani

Elevating a residential house appears to be one of the most effective techniques to eliminate or alleviate flood losses. In general, the elevation procedures involve raising a house as well as its typical slab-on-grade (SOG) foundation and supporting it with an additional support system. The unconcerned effects of the drastic changes in support condition could lead to severe structural damages and failure of houses. After elevated, thus, such slabs must be properly supported and retrofitted, for which the available methodology and know-how is almost nonexistent. The fiber reinforced polymer (FRP) application, considered as a promising technique in the rehabilitation of concrete structures, are utilized in this study to improve the structural performance of an elevated SOG.

The main objectives of the research is to investigate and evaluate the flexural behavior of a full-scale elevated SOG with low reinforcement ratio and the effect of using externally bonded carbon FRP (CFRP) and glass FRP (GFRP) laminates to retrofit such slabs. The current study includes three distinct phases: experimental investigation of two full-scale slabs subjected to static load, finite

element analyses of test slabs to verify with the experimental results, and parametric study to expand the results using validated numerical models. The results show a delay of the crack initiation and propagation, as well as an increase in the ultimate load capacity of 30% over the control with the use of a single layer of CFRP laminates. The experimental and theoretical were found to correlate well in terms of the load-deflection responses, crack development, and modes of failure.

Table of Contents

List of Figures

List of Tables

Chapter 1
Introduction

1.1 Background

Severe flooding has caused substantial economic losses in coastal communities and flood-prone areas throughout the state of Texas and other states, as evidenced from flooding history. In 2015, extensive flash flooding washed away hundreds of homes and caused additional damage on more than 1,000 homes in Wimberley, San Marcos, and Hays County in Texas (Janner, 2015). In 2016, flooding destroyed 1,000 homes in Houston and caused more than 5 billion dollars in damage (Yan and Lavandera, 2016). Hurricane Harvey produced one of the worst catastrophic disasters in US history in 2017 (Figure 1-1). According to the report from the Federal Emergency Management Agency (FEMA) on September 22, 2017, nearly 80,000 homes in Texas had at least 18 inches of floodwater and 23,000 of those had experience of more than 5 feet. More than 1.5 billion dollars in federal funds were provided to people impacted by the disaster (FEMA, 2017).

Elevating a residential house above the Base Flood Elevation (BFE) has widely been used as a mitigation method to eliminate or minimize flood damages (FEMA P-312, 2014). In the elevation procedures, after a residential house is elevated, additional foundation members, such as piers and steel beams, are necessarily provided to support a slab Figure 1-2 (a). Open foundations, as shown in Figure 1-2 (a), are required for elevated homes in areas with high-velocity water flow to reduce the hydrodynamic and breaking wave loads, according to the

Figure 1-1 Texas homes affected by Hurricane Harvey (Phillip, 2017)

National Flood Insurance Program (NFIP) criteria, the community's floodplain management regulations, and building codes (FEMA, 2013). In areas subjected to low-velocity wave action, closed foundations are permitted (Figure 1-2 (b)). However, the most common foundation type for residential houses in Texas is slab-on-grade (SOG) foundation. Since the slab forms the floor of the house, and occasionally the foundation as well, elevating the house and slab together is convenient and economical. Slab-on-ground or slab-on-grade is defined as a slab that directly rests on the soil or selected fill and bears on the soil underneath (ACI 360R, 2010). The drastic change in support condition after elevation causes unanticipated bending moments and shear forces in a slab. Such slabs, therefore, must be properly supported and retrofitted.

The use of fiber reinforced polymer (FRP) laminates is a promising technique in the rehabilitation of concrete structures, in terms of life-span cost benefit, high strength-to-weight ratio, high stiffness-to-weight ratio, excellent

(a) Open foundation (b) Closed foundation

Figure 1-2 Types of elevated homes (Arkdevinc, 2018)

durability, and low environmental impact (Hollaway, 2010). FRP system consists of the fibers and resins combined to form the composite laminate, and applicable bonding agent utilized to bond the laminate to the substrate (ACI 440.2R, 2017). Previous research indicated that FRP strengthening results in an increase in flexural strength of concrete structural members ranging from 10% up to 500% (Ritchie et al., 1991; Sharif et al., 1994; Mosallam and Mosalam, 2003).

1.2 Problem Statement

Since SOG foundations are generally found in warmer environments where ground freezing and thawing is rarely concerned, they are prevalent in the southern portion of the United States, such as in Texas, Louisiana, Mississippi, Alabama and Florida. The total number of NFIP policies in force in Texas is 675,813 (FEMA, 2018). Approximately 70% of the total NFIP policies in force are for single-family residential homes, as presented in Figure 1-3. It is assumed that approximately 25% of homes in the Special Flood Hazard Area (SFHA) do not have an NFIP policy. Based on published data, it is also assumed that at least 60% of single-

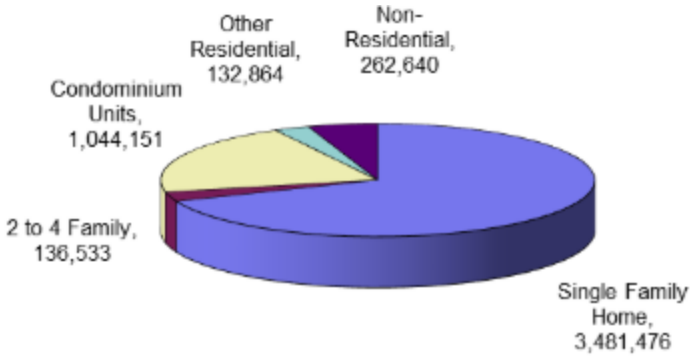

Figure 1-3 Total NFIP policies in force by occupancy type (FEMA, 2018)

family homes in the South have SOG foundations (Census Bureau, 2008). From the assumptions above, an estimated 2,100,000 single-family homes with SOG foundations are in the SFHA in the southern part of United States. Thus, a very large number of SOG homes with significant potential for damage in flood prone areas have been recommended to retrofit to prevent future flood damage. Although many of these homes have been constructed based on earlier codes or with no building code, it is necessary to consider the requirements of the current building codes and standards. The International Residential Code (IRC) requires that concrete SOG floors be designed and constructed in accordance with the IRC or the American Concrete Institute (ACI) 332 Code provisions (IRC 2015; ACI 332, 2014). These guidelines do not require that SOGs be reinforced, and they do not contain design provisions for elevated slabs. Elevated slabs must be designed in accordance with ACI 318 Code Provisions. ACI 318 allows a plain concrete slab to be used only when a slab is continuously supported. It also considers plain concrete to be unreinforced concrete, and concrete that contains less reinforcement than its minimum requirement (ACI 318, 2014). SOGs typically

reinforced with a single layer of welded wire fabric (WWF) will be classified into the latter category. Therefore, elevating SOG homes with slabs that are either unreinforced or contain typical reinforcement would violate the code.

In addition, the slab reinforcement should be placed in the upper one-third of the slab to provide crack control (ACI 360R, 2010). However, the reinforcement often rests at or near the bottom of the slab, as shown in Figure 1-4 (a), due to common construction practices for placing the WWF. As a result, the reinforcement has insufficient concrete covering as shown in Figure 1-4 (b), and can be subjected to corrosion over time. Both of these effects can cause a substantial reduction in any structural capacity of slabs, adding to the possibility of structural cracking and inadequate safety. An understanding of the elevation procedures and elevated SOG behaviors, including placement of elevation support beams and piers (number, position, cross-sectional area), load carrying capacity, mode of failure, and any needed strengthening of the elevated slabs to ensure the safety of the home occupants has not been determined in depth to date. In previous research,

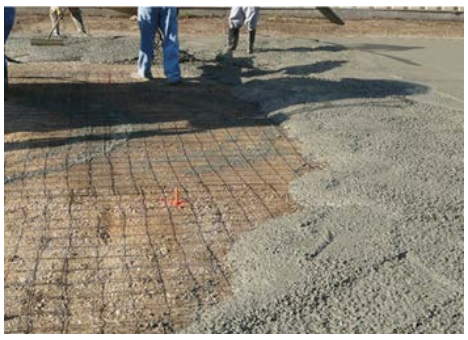

(a) Improper WWF placement

(b) Exposed WWF

Figure 1-4 WWF reinforcement issues

the study focuses on experimental and theoretical investigations that were done on reduced scale slab or full-scale slab with simplified rigid support systems. Both cases are not sufficient to capture the flexural failures in positive and negative moment regions, in particular for unique support systems of elevated SOG.

1.3 Objectives

The research experimentally investigates the structural behaviors of both non-retrofitted and CFRP-retrofitted elevated SOG with low WWF reinforcement ratio on the pile and beam foundation system. In addition, theoretically study on the effect of a wide range of varied parameters related to such slabs, which include slab thickness, concrete strength, support beam span, support beam spacing, and types of FRP, is performed. The main objectives of the research are as follows:

- Perform a numerical model to simulate the failure scenarios of a typical elevated SOG, before and after retrofit, subjected to the minimum live load for residential houses.
- Conduct experimental tests on full-scale slabs with the pile and beam foundation system to investigate the overall response of the slabs.
- Evaluate the performance of CFRP strengthened slabs reinforced by WWF on the pile and beam foundation system.
- Validate the 3D finite element models based on the test results.
- Develop numerical models to investigate and compare the response of SOG before and after elevation.

- Perform nonlinear analyses of elevated SOG with a wide range of parameters through the validated models.
- Evaluate the effect of variables in the parametric study to identify the level of each variable influencing the failure of elevated SOG.
- Develop a series of design charts that will provide the safe load capacity for non-retrofitted and CFRP-retrofitted elevated SOG.

1.4 Organization of the Dissertation

The remainder of the dissertation is organized and described as follows:

Chapter 2- Literature Review

A background literature review is performed in this chapter to review previous theoretical and experimental studies on typical SOG, foundation support for elevated SOG, house elevation procedures, unreinforced concrete slab, carbon FRP and glass FRP retrofitted slab.

Chapter 3- Test Specimen Design and Numerical Modeling

This chapter represents the description, preliminary analysis and design of the test slabs and their support system conducted on simulation modeling according to various codes. The numerical results utilized to determine the experimental program is also presented.

Chapter 4- Experimental program

The construction of full-scale test slabs, instrumental setup, and static load tests are described in this chapter. The results of observations from experimental tests are then presented.

Chapter 5- Result Validation and Discussion

The approaches for model validation is introduced. Nonlinear finite element models are then calibrated with test results to validate the models. The discussion of experimental and numerical results are described.

Chapter 6- Parametric Study

This chapter presents the results and discussions of each parameter variation that influence the response of elevated SOG.

Chapter 7- Conclusions and Recommendations

The summary of findings and conclusions from the theoretical and experimental study are presented. Recommendations for further research are finally discussed.

Chapter 2

Literature Review

2.1 Introduction of Elevated SOG

2.1.1 Slab on Grade

SOG for a residence typically consists of concrete slab with the minimum thickness of 4 inches (WRI TF-700, 2007), and welded wire reinforcement (WWR) required for temperature and shrinkage crack control (WRI TF-205, 2003). Slab thickness depends on their application and may increase to 5 or 6 inches for those subjected to heavy loads, such as garages. However, SOG should be considered the localized occurrences of reduction in thickness up to 0.75 inches (ACI 117, 2010). The causes of unequal thickness involve uneven subgrade, inadequate compaction of concrete, and concrete deterioration. This type of slabs can be supported by thickened edge or foundation wall along the perimeter. In some cases with long slab dimensions, additional footings or a thickened slab are necessary at the center of the slab. Since reinforced by minimal WWF reinforcement, SOGs can be considered as plain concrete slabs (Mosallam and Mosalam, 2003). The minimum 28-day compressive strength of concrete used for residential SOG construction is 2500 psi (WRI TF-700, 2007). For construction which will be exposed to adverse soil conditions that can be detrimental to the concrete, a higher compressive strength may be required. Joints are placed in concrete slabs to control the location and limit the width of random cracks. Subgrade drag equation can be used to determine the amount of reinforcement

based on joint spacing, allowable stress of reinforcement, and the dead weight of the slab (WRI TF-705, 2003).

2.1.2 Elevation Procedure

Elevation procedure is one of the most critical issues that can cause massive distress in concrete slabs of elevated homes, leading to the reduction in structural capacity of the slabs. The main steps of the typical elevation process are described herein and shown in Figure 2-1 (FEMA P-312, 2014). Steel beams are firstly inserted underneath the slab through the excavated tunnels in both directions (Figure 2-1(a)). The lifting jacks are then placed below the support beams. The house and SOG are lifted gradually to ensure that the house is level (Figure 2-1(b)). Wooden cribbing is used as temporary supports for steel beams. When the house is lifted up to the desired height, new footing and foundations are constructed (Figure 2-1(c)). If the slab was originally supported by foundation walls and footings, the footings might be left in place and the existing walls are extended upward to support. If the slab was originally supported by its own thickened edge or grade beam, an entirely new foundation must be constructed. Permanent openings on the foundation walls (if provided) for flood waters are created. Once the new foundation is completed, the house is lowered onto it (Figure 2-1(d)). Open foundations with piers may be used in lieu of continuous walls if the area below the house will be used for parking or it is required for Coastal High Hazard Areas and floodplains with high flow velocities (Figure 2-1(f)). The lifting process for open foundations is similar as above. Once the house is lifted up to the desired height,

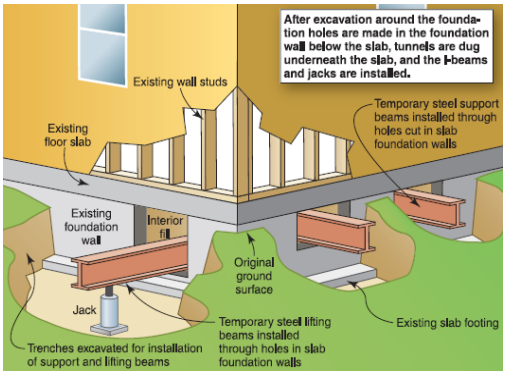

(a) Beam and lifting jack installation

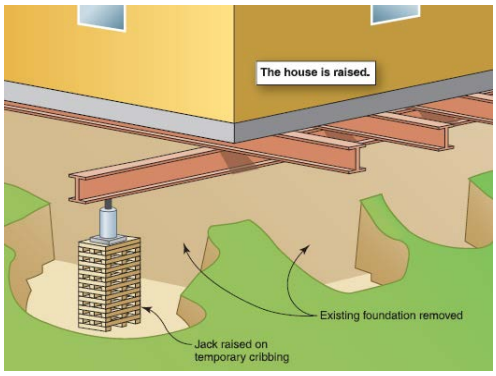

(b) Increment elevating

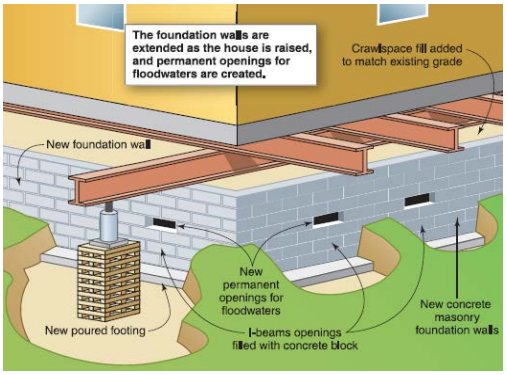

(c) Foundation wall with openings

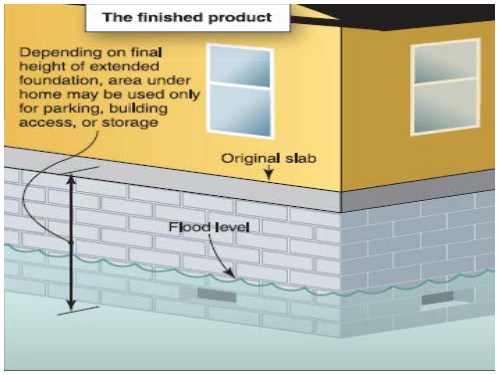

(d) Elevated SOG on closed foundation

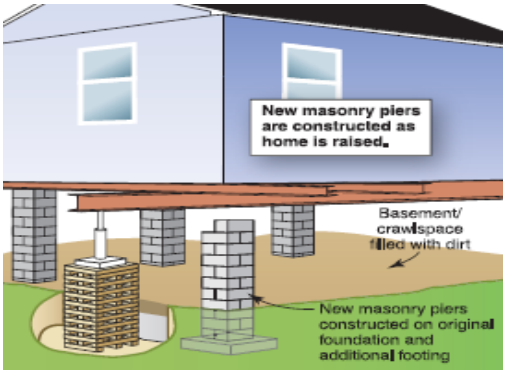

(e) Support columns

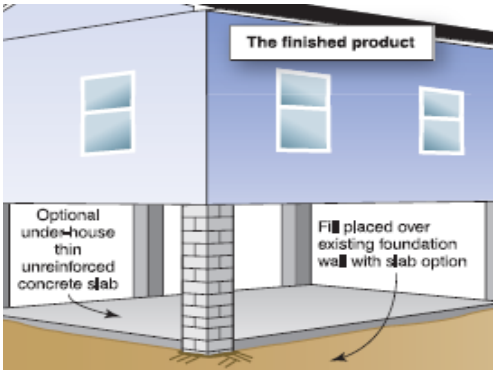

(f) Elevated SOG on open foundation

Figure 2-1 SOG elevation procedure (FEMA P-312, 2014)

new piers or columns are constructed below it instead of foundation walls (Figure 2-1(e)).

2.2 Strengthening of Concrete Structures

Concrete structures may require repair or strengthening during their service life due to structural deficiencies. Causes of them are as a result of construction defects, design errors, an increase in design loads, functional changes, and damages caused by accidents (Carolin, 2003). Compared to a complete replacement or reconstruction of such deteriorated structures, strengthening or repair is often more economical and expedited solution which has been received significant attention all over the world (Bisby and Williams, 2004). Therefore, numerous strengthening methods have been developed and become successful applications for prolonging the service life of deficient concrete structures. The well-known methods that have been used since the last decade for strengthening and repairing concrete structures include cement grout, shot concrete, section enlargement, injection techniques, external plate bonding, and external post-tensioning (Klaiber et al., 1987; Banu and Taranu, 2010). Some techniques, such as epoxy injection generally used to fill fine internal cracks or patching mortar usually required for area cracks, are merely for restoring the damaged concrete to the same previous conditions, but not for enhancing the strength of concrete structures (Seniwongse, 2008). Among these traditional strengthening and repair techniques, external post-tensioning and external plate bonding are considered as the most remarkable methods, in particular when increasing strength is required.

2.2.1 External Post-Tensioning

The application of external post-tensioning involves placing prestressing tendons outside the concrete members to transfer prestressing force to concrete by means of end anchorages and deviator, which must be strong enough to resist the additional prestressing forces (Saibabu et al., 2009). Figure 2-2 depicts a bridge strengthened with the external post-tensioning system whose external prestressing tendons are placed through the hollow section of the box girder (Suntharavadivel and Aravinthan, 2014). This technique is primarily employed in bridge engineering, and practical for both single span and continuous span bridges (Lorenc and Kubica, 2006). The benefits of this strengthening method include maintaining an elastic behavior under higher loads, enhancing ultimate resistance, decreasing overall deflection due to the service loads, and improving fracture and fatigue response (Chen and Gu, 2005). However, several drawbacks of this technique collected from the sites are reported by Daly and Witarnawan (1997).

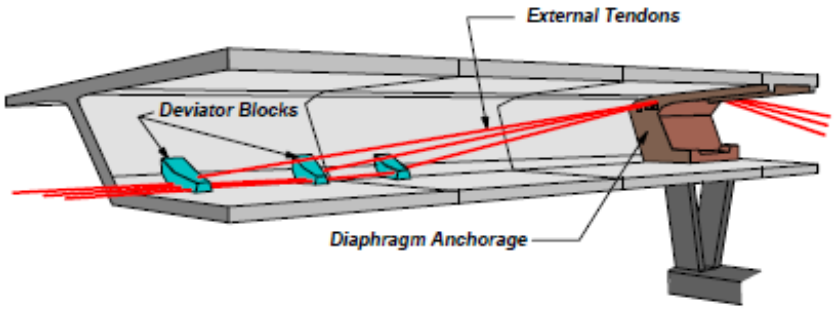

Figure 2-2 Layout of the external post-tensioning method on a bridge (Suntharavadivel and Aravinthan, 2014)

Installation of deviators, anchorages, and tendons can be difficult due to the limited space and access. In the installation process, drilling and welding existing concrete structures should be carefully conducted in less critical areas to avoid more damages and reduction in structural performance of under-strength structures. The details of deviator and anchorage are also required to handle stress concentrations taken placed in the existing concrete members. The tendons, being external, are vulnerable to corrosion, exposed to contamination by birds and susceptible to accidental damages such as fire. Since additional stress is applied to a deficient structure, a precise analysis is required to formulate the tendon configuration. A profound understanding of the stress distribution in the deck and, if necessary, additional investigations must be performed to determine the existing stress in a prestressed member for the safety of the bridge.

2.2.2 External Plate Bonding

The technique increases strength and stiffness of existing concrete members using steel plates or FRP plates which are glued by epoxy resin and anchored to the concrete substrate. The use of steel plate bonding to strengthen building members, such as reinforced concrete (RC) beams and slabs (Figure 2-3 (a)), as well as concrete bridges (Figure 2-3 (b)) have been worldwide since the past. Various studies of this repair and strengthening methods were executed on small-scale specimens in laboratories (Van Gemert, 1980; Zhang et al., 2001; Ebead and Marzouk 2002) to full-scale application for a set of concrete bridges at a motorway interchange (Raithby, 1980). The results from the previous research

stated above indicated that bonding of steel plates to concrete elements could impressively increase the cracking load and the load carrying capacity. Moreover, the investigations exhibited an increase in stiffness of the specimens strengthened by steel plate bonding. This method, therefore, has been recognized to be an effective solution to improve structural performance.

(a) Strengthened RC beam (b) Strengthened bridge girder

Figure 2-3 External steel plate bonding (Horse, 2018)

Although it has been known as a successful strengthening technique, the external steel plate bonding has many disadvantages (Hollaway and Leeming, 1999). A few significant drawbacks are summarized herein. Since a steel plate is externally attached to a structural member and is exposed to the natural environments, unlike an internal reinforcement, it can be easily subjected to the corrosion which could decrease the bond strength. It was demonstrated that a substantial amount of corrosion mostly occurred at the steel/epoxy interface and can lead to a reduction in strength of concrete members (Macdonald and Calder, 1982). Steel plates are inflexible causing the difficulty in applying to complex shapes such as curved surfaces. The self-weight of the plates are also problematic

to handle on site, and the installation process then requires an external pressure to hold the plate during cure of an epoxy resin. Due to the weaknesses of steel plates in the external plate bonding method, advanced composite materials such as FRP sheet were successfully developed as a replacement of steel plates.

2.3 FRP Strengthening

2.3.1 FRP Characteristics

In the 1980's, FRP plates were introduced and demonstrated to be more beneficial than traditional steel plates in strengthening and repairing applications (Kaiser, 1989). Compared with conventional strengthening methods such as external steel plates bonding, the fibers and epoxy resins are relatively expensive than steel, but the installation cost of FRP systems are mostly more economical (Nanni, 1999). The previous study proposed by Meier (1992) also indicated that although the price per unit volume of FRP composites is 4 to 20 times higher than that of steel, the savings in the installation procedure can compensate the costly materials in a strengthening project. However, FRP dramatically exceeds steel when the strength-to-weight ratio is considered. The investigation on bridge rehabilitation revealed that a 2-kg FRP provides same strength as does 47-kg steel (Peshkam and Leeming, 1994). In addition, FRP is a lightweight and noncorrosive material, and is available in various forms ranging from factory-made laminates to dry fiber sheets (ACI 440.2R, 2017). Consequently, it is easy to carry and handle, and does not significantly increase an additional load caused by self-weight on an existing structure. It does not need corrosion-resistant applications which are

necessary for steel plate bonding system. Due to its flexibility, before it is cured, FRP sheet can overcome the disadvantage of steel plate with regard to the limitation of working space and access, as well as the application on the curved surfaces. However, deficiency of FRP laminates subjected to fire hazard was stated. The investigations on the performance of CFRP-strengthened beams and bridge girders under extreme temperature exposure were carried out by Deuring (1994) and Beneberu (2016), respectively. Both studies exhibited that the CFRP laminates progressively lost their bond and detached from the concrete surface. The use of fire insulation, however, could protect the FRP system, concrete, prestressing strand, mild reinforcement, and alleviate structural damages from fire hazard Beneberu (2016).

Commercially available FRP materials can be categorized based on high strength fibers used to fabricate them into three types: aramid, carbon, and glass FRP. The main characteristics of FRP materials created from three different fiber types are compared and shown in Table 2-1. These FRPs generally have fiber volume ratio of approximately 65 percent and all fibers run in a single direction. In general practices, glass fiber reinforced polymer (GFRP) is the most popular reinforcing composite material since it is inexpensive and widely available. However, the durability of GFRP sheet should be concerned particularly for structural application involving concrete (Hollaway and Leeming, 1999).

Table 2-1 Comparison of characteristics of different FRP types (Meier, 1995)

Characteristics	Carbon	E-glass	Aramid
Tensile strength	Very good	Very good	Very good
Compressive strength	Very good	Good	Inadequate
Stiffness	Very good	Adequate	Good
Long term behavior	Very good	Adequate	Good
Fatigue behavior	Excellent	Adequate	Good
Bulk density	Good	Adequate	Excellent
Alkaline resistance	Very good	Inadequate	Good
Cost	Adequate	Very good	Adequate

Santoh et al. (1983) presented that CFRP sheets have higher performance against moisture, solvents, light acids, and possess better durability. In general, CFRP materials exhibit higher tensile strengths compared to steel, and greater stiffness than either GFRP or aramid fiber reinforced polymer (AFRP). As a result, GFRP laminates would need to be three times thicker than CFRP laminates in order to obtain the same tensile stiffness (Hollaway and Leeming, 1999). In addition to increasing the stiffness and strength of reinforced concrete members, the application of CFRP laminates is significantly improve their fatigue behavior (Inoue et al., 1995; Shahawy and Beitelman, 1999). From the foregoing reasons and the information in Table 2-1, the benefits of using CFRP laminates over GFRP and AFRP laminates for structural strengthening and rehabilitation are clear in terms of strength, stiffness, durability and fatigue.

2.3.2 Shear Strengthening

FRP systems used for shear strengthening applications generally are the externally bonded FRP systems (Belarbi and Acun, 2013). Numerous studies demonstrate that the shear capacity of concrete beams can be enhanced by the use of FRP U-shape wrapping (Uwrap), in which fibers are in the transverse direction to the beam (Chajes et al., 1995; Taerwe et al., 1997). Khalifa et al. (2000) experimentally studied the response of continuous RC beams strengthened with externally bonded CFRP wraps. A total of 27 full-scale beams was tested to investigate the effects of six variables, which include steel stirrups, the shear span-to-depth ratio (a/d), CFRP amount and distribution, bonded surface, fiber orientation, and end anchor. The results indicated that externally bonded CFRP laminates could increase the shear capacity ranging from 22% to 145%. The CFRP application showed its effectiveness in enhancing the shear capacity of RC beams in positive and negative moment regions and in both rectangular and T beams. The anchor can apparently improve the shear capacity of the beam. The CFRP had more beneficial effects on the shear strength of beams without shear reinforcement than that of beams with sufficient shear reinforcement. For the beam failed by debonding failure, the shear strength may not increase with increasing amount of CFRP because it significantly depends on the CFRP-to-concrete interfacial bond. The contribution of CFRP systems to shear capacity of beams appeared to increase with an increased a/d ratio. A U-wrap technique was more effective than applying CFRP only to the beam sides.

Bukhari et al. (2010) conducted the experimental work to evaluate the contribution of CFRP sheets to the shear capacity of continuous RC beams strengthened with the various configurations of CFRP sheets. The experimental program consisted of one control beam and six CFRP-strengthened beams. Out of six strengthened beams, four beams were attached with CFRP sheets, in which the main fibers were oriented perpendicular to the longitudinal axis of the beam. The other two strengthened beams with the different compressive strengths of 44 MPa and 60 MPa were bonded with CFRP sheets, in which the main fibers were oriented at 45 degrees to the longitudinal axis of the beam. It was found that shear strength of the beams was improved with the CFRP strengthening. In addition, the shear strength of the beam was considerably enhanced when orienting the CFRP sheets at 45 degrees so that the fibers were perpendicular to the shear cracks.

The magnitude of the increase in strength and stiffness of concrete beams and the modes of failure are related to the orientation of the FRP sheets. Although placing the CFRP sheets perpendicular to the cracks results in a substantial increase in strength and stiffness, the failure mode is more brittle in comparison with placing the CFRP sheets obliquely to the cracks (Norris et al., 1997).

The use of externally bonded FRP systems also showed the effectiveness in enhancing shear strength of the slab (Erki and Heffernan, 1995; Chen and Li, 2000; Wang, 2002). The experimental investigation of the punching shear behavior of interior RC slab-column connections externally strengthened with CFRP strips was carried out by Sharaf et al. (2006). Six full-scale, 2000-mm-square x 150-mm-thick (approximately 80-in-square x 6-in-thick) slab specimens were constructed

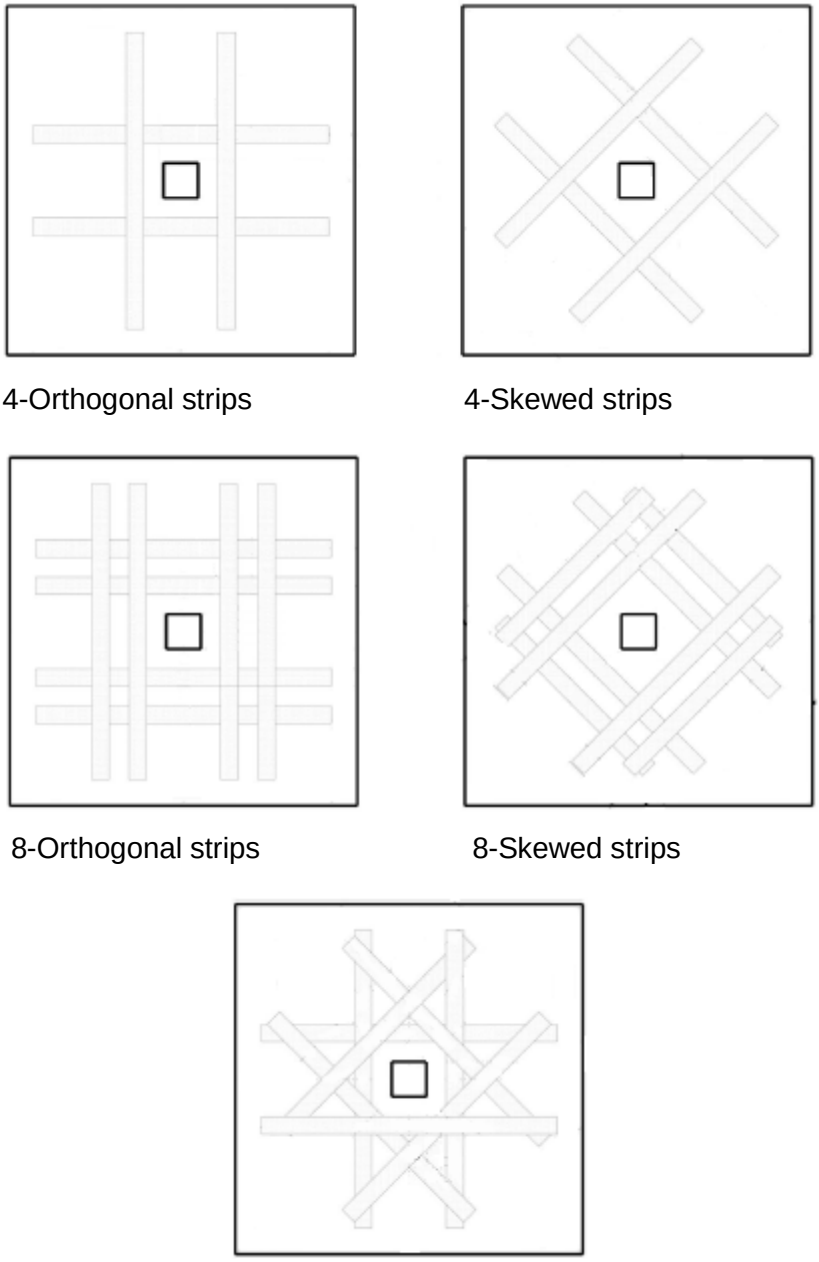

Figure 2-4 CFRP strengthened specimens (Sharaf et al., 2006)

with the column stubs at the middle of the slab. Five of them were strengthened using a different number of CFRP strips and various CFRP arrangement as presented in Figure 2-4. The slabs were simply supported along their edges, and loads were applied on the stubs until failure of the slabs. It was concluded that the punching capacity of specimens strengthened with four and eight CFRP strips enhanced up to 7% and 16%, respectively, compared to the un-strengthened specimen. This implies that the increase in punching shear capacity was nearly proportional to the increase in the area of CFRP laminates. The strengthened specimens exhibited a stiffer behavior than the control. In addition, the skewed strip orientation allowed the specimens to fail with greater deflection compared to the orthogonal strip orientation.

Abdulrahman et al. (2017) experimentally and numerically investigated the effectiveness of CFRP strengthening on flat slab to column corner connections. The experimental work involved testing four large-scale specimens, of which two slabs were constructed with the openings adjacent to the columns. Each 2000-mm-square x 80-mm-thick (approximately 80-in-square x 3-in-thick) slab was supported by four 160-mm-square x 720-mm-high (approximately 6-in-square x 30-in-high) columns cast monolithically with the slab. One specimen without the opening was kept un-strengthened to serve as the control. CFRP sheets of a width of 50 mm (2 in) were bonded to the top surface of all the remaining slabs around four columns in an orthogonal configuration. A steel frame was used to transmit the applied concentrated load from a hydraulic jack and distribute to the slabs to simulate a uniformly distributed load. The nonlinear finite element

models were created to gain further insight into the punching shear behaviors of the slabs. Moreover, alternative CFRP configurations for shear strengthening were examined numerically through the validated model. It was found that using the CFRP sheets resulted in an increase in the punching shear capacity by 11% for the slab without the opening and by up to 23% for the slab with openings. A single diagonal CFRP strip of the slab corner appeared to be the most efficient configuration to upgrade the ultimate load of the slab. At the ultimate load, however, the load enhancements of all strengthened slabs were comparatively small, and the stresses in the CFRP laminates were relatively low. Thus, applying an increased amount of CFRP sheets might not result in substantial load enhancements or be economic.

2.3.3 Flexural Strengthening

Extensive research has been accomplished to evaluate the flexural performance of structural members, such as beams and slabs, strengthened with various types of FRP. The experimental study on improvements in flexural strength of 24 RC beams strengthened with carbon fabric was implemented by GangaRao and Vijay (1998). The concrete beams had the identical dimensions of 150 mm x 300 mm (approximately 6 in x 12 in) but were reinforced with the different amount of internal reinforcement bars. Out of 24 specimens, 16 test beams were wrapped with four different strengthening schemes varying in longitudinal or transverse ply configurations of carbon fabric or in depths of wrapping. The beams were tested through the four-point bending test. It was observed that the average ultimate

strengths were increased by 57% and 100% for two sets of beams. The conclusions could be drawn based on the difference in the ultimate strength enhancement between two sets of beams. The ultimate capacity of strengthened beams had higher percentage increase when the more number of longitudinal layers of carbon fabric was applied. The ultimate strength of wrapped beams with a lower amount of internal reinforcement also had greater percentage increase than that of strengthened beams with a higher amount of internal reinforcement. Moreover, the results indicated that ultimate strength and stiffness performance of damaged beams repaired with carbon fiber and undamaged strengthened beams were similar. The beam-bending theory could predict ultimate load capacities of wrapped beams.

Although GFRP has a lower tensile strength and modulus of elasticity than CFRP, it is considered as an alternative solution to strengthen and rehabilitate concrete members due to its high ductility and relatively low price. The study was conducted by Attari et al. (2012) to investigate the effectiveness of strengthening systems for RC beams using CFRP, GFRP, and hybrid FRP sheets. Six RC beams were externally strengthened with different FRP types and configurations, and a control beam was un-strengthened. The beam specimens had dimensions of 100 mm x 160 mm (approximately 4 in x 6 in) with a length of 1500 mm (60 in). All the specimens had the identical geometry with the same steel reinforcements and were tested to failure using the four-point bending device. The author concluded that the beams wrapped with a twin-layer of glass- and carbon-fiber composite achieved a strength capacity enhancement of 114% in comparison with the control.

The U-wrap configuration yielded the best results regarding flexural strength improvement and the internal force redistribution. The interesting findings showed that strengthening concrete beams using CFRP and GFRP materials having an equivalent ultimate load per unit length provided similar results. The use of a GFRP material or a single layer of hybrid composite for flexural strengthening exhibited a comparatively high elongation at rupture and improved the ductility.

Bonding FRP composites can enhance the flexural capacity of concrete beams and slabs; however, there are the chances of premature failures due to delamination (Balendran et al., 2001). A number of studies have demonstrated that the mode of failure can become more brittle after strengthening an under-reinforced concrete beam with FRP laminates (Thomsen et al., 2004)

Besides, Thomsen et al. (2004) presented the findings of the experimental study on RC beams focusing on the failure modes due to the loss of composite action between concrete substrates and FRP plates. The effects on the failure mechanisms of RC beams caused by four parameters including length, width, and stiffness of FRP plates, and types of loading were examined. It was observed that, for beam subjected to point loads, there is a certain FRP length that changed the failure modes from debonding to plate end peeling (also referred to as concrete cover delamination). The peak bond stress in long FRP sheets took place under the point loads, while it occurred at the end of shorter FRP plates. Wider FRP laminates of equal cross section tend to decrease the bond stress at the FRP-concrete interface, and very large plates could change the mode of failure from debonding to FRP rupture. The stiffness of FRP sheets considerably influenced

the structural response and failure mode of the strengthened beams. For an equal reinforcing index, the interface shear stresses at the end of GFRP plate, of which the axial stiffness was relatively less, were lower than those at CFRP plate end. When sufficient anchorage length was provided to prevent plate end delamination, CFRP-strengthened beams exhibited greater ultimate loads in comparison with GFRP-strengthened beams. Unlike the applied point loads in the four-point bending test, the distributed load did not create a discontinuity in the FRP force, resulting in a lower chance of mid-span debonding.

The successful applications of FRP composites in enhancing flexural capacity of both one-way and two-way concrete slabs were also continuously reported (Arockiasamy et al., 1996; Lam and Teng, 2001; Seim et al., 2001; Mosallam and Mosalam, 2003; Teng et al., 2003; Arduini et al., 2004; Al-Rousan et al., 2012). Selected studies were summarized herein.

Seim et al. (2001) investigated the effect of FRP fabric and strips on one-way RC slabs. Thirteen scaled slabs 2290 mm long x 480 mm wide x 102 mm thick (approximately 90 in long x 19 in wide x 4 in thick) were tested in flexure. Three slabs were strengthened with CFRP fabric and seven were reinforced with CFRP strips. A glass fiber chopped layer was applied on a single slab and the other two were used as control specimens. Depending on the material types and configuration of FRP, the load capacity of the strengthened slabs can be increased up to 370%. However, the application of CFRP strengthening system changed the failure modes of the slabs from the ductile failure associated with the yielding of steel reinforcement to FRP-concrete delamination, or FRP rupture, or crack growth

through the outer layer of the FRP strips. The results also indicated that the use of FRP fabric which completely covered the surface of the slab significantly enhanced load carrying capacity, although the number of fibers applied was considerably greater than that in the FRP strips. Furthermore, the use of FRP fabric resulted in 50 to 70% higher levels of deformation at ultimate loads in comparison with the FRP strips.

Mosallam and Mosalam (2003) studied the effectiveness of using FRP to retrofit and repair unreinforced and reinforced concrete slabs. Twelve simply supported two-way slabs with dimensions of 2670 mm x 2670 mm x 76 mm (approximately 105 in x 105 in x 3 in) were tested under uniformly distributed load. Nine unreinforced slabs were fabricated with 6 x 6- W1.4 x W1.4 WWF at 32 mm (1.25 in) from the tension surface of the slab specimens. The light WWF was considered as non-structural reinforcement, and it was expected not to contribute extensively to ultimate limit states of the slab. Three reinforced slabs were fabricated with #3 rebar. A total of eight unreinforced and reinforced slabs were strengthened externally with 2 layers of CFRP or 3 layers of GFRP over 50% of slab areas. The FRP configuration is depicted in Figure 2-5. The specimens were classified into retrofitted and repaired specimens. To demonstrate the repair applications, slabs were partially damaged with the pressure of approximately 85% of the ultimate load. After that, the pre-cracked slabs were repaired using epoxy and carbon/epoxy laminates. The retrofitted and repaired specimens were tested to failure. A pressure was applied using a high-pressure water bag at the loading rate of 3.45 kPa/min (72 psf/min).

Figure 2-5 FRP strengthened specimen (Mosallam and Mosalam, 2003)

It was found that the structural capacity of both unreinforced and reinforced slabs could be upgraded using the FRP strengthening system. For the retrofitted specimens, the use of FRP composites resulted in a significant increase of the structural capacity up to 500% and 200% for unreinforced slabs and reinforced slabs, respectively. For the repaired specimens, the FRP system restored not only the original capacity of the pre-cracked slabs but also enhanced the strength of the repaired slabs more than 540% on average. The test results also indicated that the specimens in all cases experienced the relatively large deformations, which was 1/45 of the clear span length, before failure. Furthermore, the common failure mode was a localized compression failure of the concrete with partial debonding near the ultimate load.

Arduini et al. (2004) tested 26 specimens including one-way RC slabs with no overhang (5000 mm x 1500 mm x 240 mm or approximately 197 in x 59 in x 9.5 in) and a cantilevered overhang (6500 mm x 1500 mm x 240 mm or approximately 256 in x 59 in x 9.5 in). The study focused on the positive moment region for slabs

with no overhang and the negative moment region for slabs with a cantilevered overhang. Specimens in each type were different with regard to amounts of internal steel reinforcement and levels of CFRP strengthening. The authors reported that the use of externally bonded CFRP systems increased load-carrying capacity up to 122% compared to the control. Moreover, the increase in load-carrying capacity was more evident for specimens with low steel reinforcement ratios. The conclusions have a good correlation with the tested results from Mosallam and Mosalam (2003).

Chapter 3
Test Specimen Design and Numerical Modeling

This chapter describes various design considerations and approaches for different components of the test specimens including IRC Code, ACI 318 Code, AISC 325 Code, and 3D nonlinear finite element analysis. The experimental specimens are decided based on the literature reviews in the previous chapter. The methodology used to determine the test program are also discussed.

3.1 Methodology

In structural testing, it often is difficult to construct and test on a full-scale version of the actual structural system due to many reasons such as limitations on time frame, budget, research instrumentation and facilities. Determining the suitably scaled samples that still accurately represent the structural behaviors of a full-scale version is very significant and challenging for researchers. In the previous studies described in the literature reviews, experimental tests were mostly done on the reduced scale slabs or the full-scale slabs with simplified rigid support systems. A reduced scale slab can affect the behavior of reinforced concrete's composite. The size of aggregates in concrete cannot always be appropriately scaled. The bond behaviors between a reduced-scale reinforcement bar and concrete may not replicate the full-scale condition. Moreover, reduced scale slabs with a single span are not sufficient to capture the moment redistribution between the center support moment and the mid-span moment of adjacent spans, as well as the flexural failures in positive and negative moment regions. The most

significant issue of a single-span slab is the boundary condition. An actual multi-span elevated SOG is a continuous slab whose boundary conditions are vertical, horizontal and rotational restraint at the end of each span. The restraint of a continuous slab in reality cannot be considered to be perfectly pinned or fixed, but it depends on the type of slab-beam-column connections and the relative stiffness among slab, support beam, and column. Therefore, it is difficult to accurately replicate the boundary condition of an actual continuous slab for a single-span slab. Although a full-scale slab with simplified rigid support systems can overcome the issues experienced in a reduced scale slab, its rigid support may not be allowed to adequately consider the effect of the relatively high deflection of the steel beam used in the unique support systems of elevated SOG.

3.2 Description of Test Specimen

As described in the previous chapter, there generally are two types of support systems for an elevated house; namely, a closed foundation and an open foundation. Since an open foundation must be used for an elevated house in the areas with high-velocity water flow or high BFE, a home in those areas is required to rise to a relatively high elevation above the ground. Also, homeowners trend to increase column spacing for better flow of flood waters and optimum use of the space below their homes. Thus, a support system with beams and piers are widely used in the areas with high-velocity water flow because the beam supports can provide greater column spacing. In a pile and beam support system, an elevated SOG is supported by steel wide-flange beams which are placed on concrete

masonry unit (CMU) columns in only one direction providing greater column spacing along that direction and creating more usable space, e.g., parking garage. In case of severely deteriorated edge beam, as presented in Figure 3-1, additional steel beams are also required along slab parameter. Based on supported beam configuration, an elevated SOG is considered as a one-way slab regardless of plan aspect ratio of the slab.

Figure 3-1 Additional beam supports for deteriorated edge beams

An elevated house in the areas with low-velocity water flow and low BFE is typically raised to a relatively low elevation above the ground and allowed to be supported by a closed foundation. This type of foundation commonly consists of only support piers with the less spacing between each other compared to those in an open foundation. As a result, the additional limited space below a house after elevation can rarely be used or merely used as storage. From the previous reasons, a pile and beam support system appears to be a more functional and

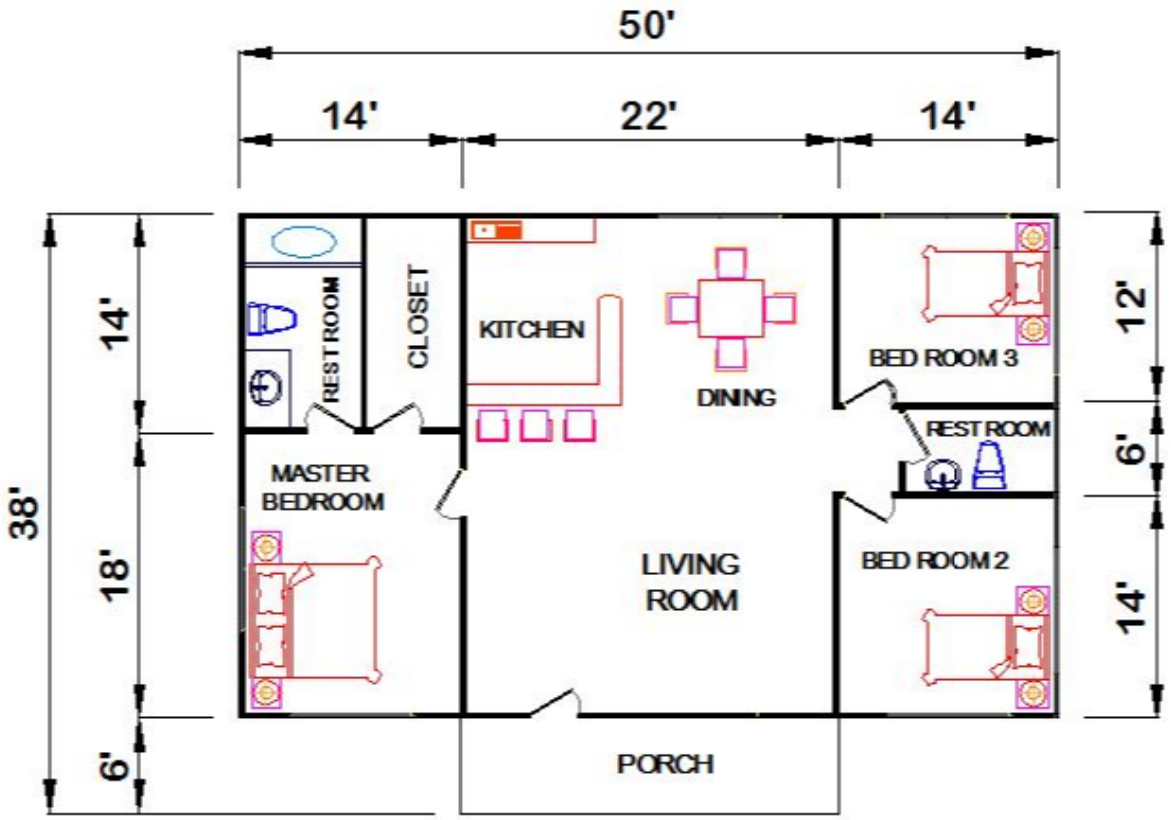

Figure 3-2 Floor plan of a single-family residential home

common option. It is also more hazardous and can cause more severe damages when a slab collapses. Therefore, a pile and beam system was selected as the support of an elevated SOG house in this study.

A house with 1600 square feet of living space was chosen as a typical single-family residential home for this research. The floor plan and dimensions of the selected home are illustrated in Figure 3-2. The layout of support beams and columns for the sample home is shown in Figure 3-3. There were the existing edge beams along the slab parameter. The additional steel beams were placed at equal spacing on the columns in the direction of slab width. Although the edge beams

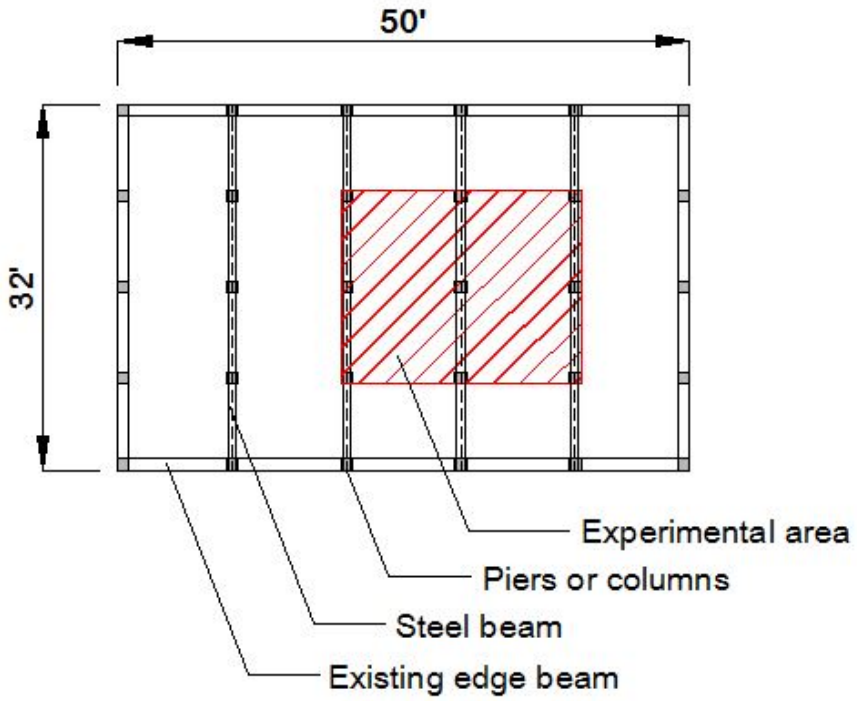

Figure 3-3 Floor plan of a single-family residential home

have significantly higher stiffness than SOGs do, most of them experience severe deterioration. Since there is no specific design criteria or regulation for edge beams of SOG houses, a variety of them with different shapes, dimensions, and internal reinforcement are available on site. Moreover, the deterioration levels of edge beams are diverse in different cases. In order to avoid these uncertainties and produce a conservative scenario, the test slabs were not considered the existence of edge beams. It would require a significant amount of time and resources to construct and test the whole slab of the sample home. Therefore, the section of the slab in the hatched area, as demonstrated in Figure 3-3, was utilized in the experimental program. The test slabs were determined to span two bays in each direction to simulate both positive and negative moment regions. Thus, the moment redistribution and flexural failures in positive and negative moment regions can be investigated, representing more accurately the structural behaviors of a whole elevated SOG home. It should be noted that the results of the test slabs in the experimental program can apply not only to the sample home but also to others with various shapes and sizes supported by beams and piers at the same spacing as test slabs were.

3.3 Design of Test Specimen

The test specimens comprised of five main components; slab, steel beam, CMU column, RC column base, and FRP laminates. The preliminary designs of the test specimens were carried out using two approaches; the hand calculation design and the FEA method.

3.3.1 Slab

ACI 318 (2014) requires plain concrete members under flexure, tension, or shear be supported by continuous vertical structural members. Also, no design code provides the design equations or criteria to determine the ultimate flexural capacity of plain concrete. Since the test slabs behave as one-way slabs due to the support beam configuration, and the basic analysis for continuous beams is the same for one-way slabs (ACI 318, 2014), the maximum stresses at the top and bottom fiber of slab section were calculated using the flexure formula (Gere and Timoshenko, 1997) expressed in Equation 3-1.

$$\sigma_x = \frac{Mc}{I} \qquad 3\text{-}1$$

where

σ_x = the bending stress or the flexural stress

M = the bending moment

c = the distance from neutral axis to the extreme elements

I = the moment of inertia of the cross section

The 1-ft strip of the slab perpendicular to beam direction was used in the hand calculation design. The moment coefficients for equal-span continuous beams from Table 3-22c in AISC 325 (2011) were utilized to calculate the negative and positive moments at the support and mid-span of the slab, respectively. The thickness of the specimens was determined to be four inches according to the typical thickness of the undamaged slab on site. Based on the minimum requirement of concrete compressive strength for a residential SOG home, the compressive strength of 2500 psi was used in the preliminary analysis and design. The tensile strength of concrete in flexure is approximately 10 to 15 percent of the compressive strength (ACI 318, 2014). The lower bound was used, and the tensile strength of the concrete slab was then assumed to be 250 psi. The concrete density was assumed to be 150 lb/ft^3. The minimum uniformly distributed live load of 40 psf required for residential homes was adopted in the analysis (ASCE 7-10, 2010). The factored loads were computed and applied on the slab. Out of the seven basic load combinations in ASCE 7-10 (2010), only the combinations of dead and live load were considered to produce the maximum vertical load. The test slabs were reinforced with 6 x 6- W1.4 x W1.4 WWF, placed near the bottom of the slabs to create the improper placement scenario in construction practices. The existence of WWF was not considered in the hand calculation design but was taken into account in the FEA method. Flexure failure of the slab was determined when the maximum tensile bending stresses induced by the bending moments became greater than the tensile strength of concrete. The details of hand calculations are shown in the Appendix A. After iterative design of a 1-ft slab with

varying support spacing, the failure took place when the column spacing was greater than 7.15 feet. However, this calculation was not considered the effects of internal WWF reinforcement, deflection of steel beam, moment redistribution after crack initiation, crack propagation, and ultimate load of the slab. Thus, FEA models were simulated to investigate those effects in the preliminary design.

3.3.2 Beam

Instead of RC beams which require more construction work, steel beams are selected to be the support in the pile and beam foundation taking into consideration the unsafe working conditions under the elevated house, limited space and time constraints. The typical steel beam for the elevated house is generally over-designed for flexural capacity because it is often controlled by deflection at service load levels. Since a SOG has no internal reinforcement, a small deflection of supports can cause severe damages to the slab. However, a plain concrete slab or a concrete slab with light reinforcement under flexure is not permitted leading to no available design criteria for the allowable deflection of such slabs. As a result, the size of support beams that has a significant influence on the deflection of the slab cannot appropriately be determined. Although a wide range of different beam sizes are used on site due to no guideline and design criteria available, a wide flange beam clearly appears to be the most common type of support beam. In the current research, a W10x33 beam was deployed for the experimental program. The selection of the beam was based on strength, stiffness, and the convenience in construction practices. The steel properties provided by

the supplier are given in Appendix B, and they satisfy tensile requirements in ASTM A992/A992M (2006) as shown in Table 3-1.

Table 3-1 Tensile requirements (ASTM A992/A992M, 2006)

Properties	Requirement
Tensile strength, min ksi	65
Yield point, ksi	50 to 65
Yield to tensile, max	0.85
Elongation in 8 in., min, %	18
Elongation in 2 in., min %	21

3.3.3 Column and Column Base

Similar to support beams, the primary concerns of constructing support columns for an elevated home are matters of safety and convenience in the construction practices. The CMU blocks have been then widely used for this purpose. Besides being dependent on load carrying capacity, the dimensions of columns are controlled by the width of support beams and the available sizes of the products. Figure 3-4 shows three different types of CMU blocks typically used to form the support piers: a hollow concrete block of size (8x8x16) inch, (12x8x12) inch, and (8x8x8) inch. The support piers are generally assembled from CMU, mortar, grout, reinforcing steel, and joint reinforcement.

Since a W-10x33 beam was chosen to be the support beam in the experimental program, of which the flange width is approximately eight inches, in order to provide the sufficient column width for placing the beam, a hollow concrete block of size (12x8x12) inch was employed to construct the support column. The

joint reinforcement installed in each mortar bed between CMU blocks to distribute local temperature and shrinkage stresses were the ladder type. The columns were reinforced by #4 rebar and were designed to satisfy the minimum requirement in ACI 530/530.1 (2013).

(a) 8”x8”x16” (b) 12”x8”x12” (c) 8”x8”x8”

Figure 3-4 Typical CMU block for a pile and beam support system

3.3.4 Column Base

Due to the large size of the experimental specimens, the test was conducted on the concrete pavement outside the laboratory. It would not be convenient to construct the footing foundation beneath the surface of the ground. Therefore, the column base sits on the concrete pavement was chosen to serve as a support for the test specimens instead of RC shallow foundation. 3-ft-square column bases with the thickness of 8 in were constructed and reinforced by #4 rebar. As the column-to-foundation connection was considered to be the critical point in the support system, the vertical reinforcing steel bars in the column were hooked into the column base to provide development length for effective force transfer between the CMU columns and RC foundations.

3.3.5 FRP Laminate

The design concepts and guidelines of the FRP system in ACI 440.2R (2017) were adopted in the preliminary analysis of FRP-strengthened slabs. However, the analysis did not strictly follow certain design limitations related to the ACI 318-14 strength and serviceability requirements for the sake of the research aims. For instance, the ACI 440.2R-17 Code requires the existing strength of the structure still be sufficient to withstand a level of load described by the Eq. (9-1) in the code when the FRP system is damaged. In such a case, the strengthened test slab with damaged FRP system must follow ACI 318-14 Code and would not satisfy the code, in which use of a plain concrete slab under flexure is not permitted.

The FRP sheets were applied to the negative moment area where cracks were expected to occur. The appropriate length of CFRP is required to inhibit debonding, which have been reported as one of the most common failure modes in flexure members. Thus, single-ply CFRP laminates were terminated 4 in. beyond the inflection point, taking into account the issue of FRP end peeling and the minimum requirement of development length in ACI 440.2R-17 code. Moreover, from the recommendation on strengthening limits in the code, additional analysis on the slab strengthened by the FRP laminates was performed to ensure that the failure of the strengthened slabs will be in a flexural mode rather than in a shear mode.

After conducting the initial design, the detailed nonlinear analysis was also performed, and the FRP scheme of the strengthened slab was adjusted taking into

consideration the numerical results. The analysis aims to investigate the overall structural behaviors of the strengthened slab, and then effectively design the test specimens in the experimental program as well.

SikaWrap Hex 117C, a unidirectional carbon fiber fabric, was utilized in the experimental program due to its higher tensile strength and stiffness compared to GFRP and AFRP sheets. Based on the product data sheet from the manufacturer, SikaWrap Hex 117C is recommended using with Sikadur 300 and Sikadur 330 epoxy to form a cured laminate, whose properties and design values are shown in Table 3-2. The properties of adhesive paste necessary for defining the interaction between concrete and CFRP are also shown in Table 3-3.

Table 3-2 Properties and design values of SikaWrap Hex 117C cured laminates

Properties	Design values
Longitudinal tensile strength, psi	1.05×10^5
Longitudinal modulus of elasticity, psi	8.2×10^6
Elongation at break, %	1.0
Thickness, in	0.02

Table 3-3 Properties and design values of Sikadur 330 epoxy

Properties	Design values
Tensile strength (at 7 days), psi	4900
Flexural strength (at 7 days), psi	8800
Flexural modulus (at 7 days), psi	5.06×10^5
Elongation at break (at 7 days), %	1.2

3.4 Numerical Modeling

3.4.1 Finite Element Analysis

An analytical solution to engineering problems can be achieved through the differential equations and basic physical principles such as conservation of energy, equilibrium, and Newton's laws. However, it is often impossible to solve the structures with irregular geometry and complex boundary condition. Analysis of such structures generally is carried out based on simplifying assumptions, yielding the approximated results. FEA is the numerical method that employs the discretization technique to subdivide the mathematical model into small components with simple geometry known as elements or finite elements. The response of each element is indicated by a finite or limited number of degrees of freedom. The behavior of the model is considered from the response of the discrete model achieved by assembling all elements. Thus, FEA has high potential to provide more accurate results, especially in the analysis of complex structures. In this study, FEA was performed using the FEM package ABAQUS (2014). The theories and methodologies applied to develop the 3D nonlinear finite element models are summarized below.

3.4.2 Concrete Damage Model

The failure analysis of concrete structures is associated with nonlinear behavior, attributed to the combination of damage mechanism and plasticity. ABAQUS software offers three crack models for simulating the concrete damage; namely, brittle crack concrete model, smeared crack concrete model, and concrete

damaged plasticity model. The concrete behavior in the present study was characterized by concrete damaged plasticity (CDP) model because it has a capability to represent a complete inelastic response of concrete in compression and tension (Wahalathantri et al., 2011). The assumption of the CDP model is that concrete has two main failure mechanisms; the compressive crushing and the tensile cracking. The stress-strain behaviors of concrete under compression and tension are depicted in Figure 3-5. In order to accurately simulate the compressive and tensile behavior of RC concrete in the CDP model, the inelastic strain $\varepsilon_c^{\sim in}$, the cracking strain $\varepsilon_t^{\sim ck}$, the damage parameter in compression d_c and the damage parameter in tension d_t should be entirely defined according to the following equations.

$$\varepsilon_c^{\sim in} = \varepsilon_c - \varepsilon_{oc}^{el} \quad 3\text{-}2$$

$$\varepsilon_t^{\sim ck} = \varepsilon_t - \varepsilon_{ot}^{el} \quad 3\text{-}3$$

where

ε_{oc}^{el} = the compressive elastic strain corresponding to the undamaged material

ε_{ot}^{el} = the tensile elastic strain corresponding to the undamaged material

ε_c = the compressive strain

ε_t = the tensile strain

The compressive and tensile elastic strain can be determined from the ascending linear portion of the stress-strain curves under compression and tension, respectively. The equations are expressed as:

$$\varepsilon_{oc}^{el} = \sigma_c / E_0 \qquad 3\text{-}4$$

$$\varepsilon_{ot}^{el} = \sigma_t / E_0 \qquad 3\text{-}5$$

where

σ_c = the compressive stress

σ_t = the tensile stress

The initial (undamaged) elastic modulus of concrete E_0 was calculated from $E_0 = 57000\sqrt{f_c'}$ (psi) for the initial analysis. As previously discussed, the concrete compressive strength f_c' and the concrete tensile strength f_t were assumed to be 2500 psi and 250 psi, respectively.

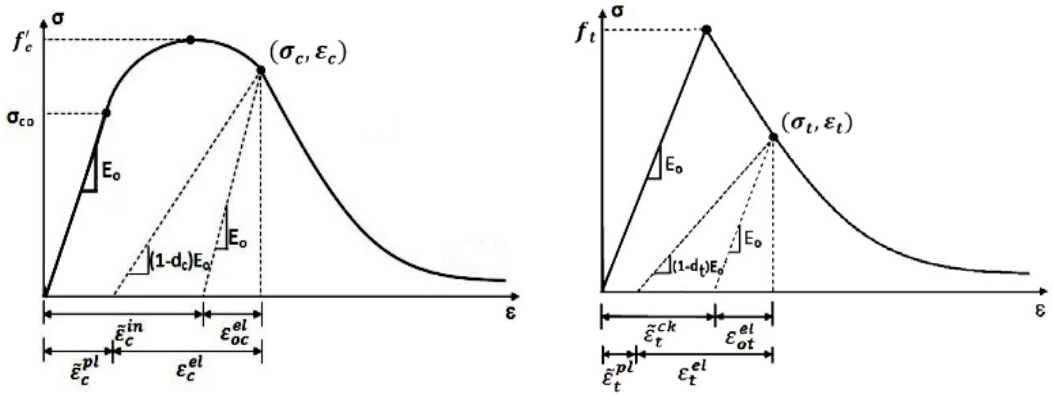

(a) Compression (b) Tension

Figure 3-5 Stress-strain behavior of concrete in the CDP model (ABAQUS, 2014)

Damage parameter is a scalar variable in the range between 0 and 1, representing an undamaged and a fully damaged condition, respectively. It is used to characterize the degradation of the elastic stiffness on the strain softening range of the stress-strain curve (Tao and Chen, 2014). According to a simple model of

plastic degradation appropriate for concrete proposed by Lubliner et al. (1989), the damage parameters of concrete under uniaxial compression and tension are given as:

$$d_c = 1 - \frac{\sigma_c}{f_c'} \quad \text{3-6}$$

$$d_t = 1 - \frac{\sigma_t}{f_t} \quad \text{3-7}$$

Based on geometric relationships in Figure 3-6, the compressive plastic strain $\tilde{\varepsilon}_c^{pl}$ and the tensile plastic strain $\tilde{\varepsilon}_t^{pl}$ are related to the damage parameters as:

$$\tilde{\varepsilon}_c^{pl} = \tilde{\varepsilon}_c^{in} - \frac{d_c}{(1-d_c)}\frac{\sigma_c}{E_0} \quad \text{3-8}$$

$$\tilde{\varepsilon}_t^{pl} = \tilde{\varepsilon}_t^{ck} - \frac{d_t}{(1-d_t)}\frac{\sigma_t}{E_0} \quad \text{3-9}$$

3.4.3 Material Constitutive Behaviors

Numerous models were proposed to develop the stress-strain relationship of concrete under compression (Saenz 1964; Carreira and Chu, 1985; Hsu and Hsu 1994) and tension (Carreira and Chu, 1986; Nayal and Rasheed 2006; Wahalathantri et al. 2011). Since test slabs with minimal structural reinforcement were simply considered as a plain concrete slab, the stress-strain response under uniaxial compression was then computed using the following equation presented by Carreira and Chu (1985):

$$\frac{f_c}{f_c'} = \frac{\beta(\varepsilon/\varepsilon_c')}{\beta - 1 + (\varepsilon/\varepsilon_c')^{\beta}} \quad \text{3-10}$$

where the maximum compressive stress f_c' was taken to be 2500 psi. The compressive strain corresponding to the maximum compressive stress ε_c' = 0.002 was assumed. β is a material parameter that depends on the shape of the stress-strain diagram and is given as:

$$\beta = \frac{1}{1 - \frac{f_c'}{\varepsilon_c' E_0}} \quad for\ \beta \geq 1.0\ and\ \varepsilon \leq \varepsilon_u \qquad 3\text{-}11$$

where the ultimate strain ε_u specified to limit the allowable degree of failure in concrete was assumed to be 0.0035.

Nayal and Rasheed (2006) developed the model based on tension stiffening model presented by Gilbert and Warner (1978) to capture the stress-strain behavior of concrete under uniaxial tension. The primary and secondary cracking stages were represented by two descending parts after the sudden drop at the tensile strain corresponding to the maximum tensile stress ε_{cr}, as shown in Figure 3-6(a). To avoid the run-time error in ABAQUS analysis, the modification of the previous tension stiffening model was done by Wahalathantri et al. (2011) in the sudden drop portion and secondary cracking stage portion, as illustrated in Figure 3-6(b).

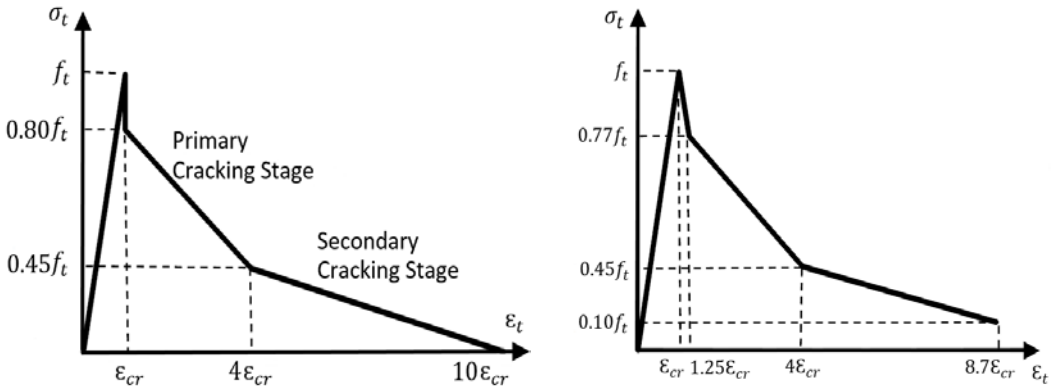

(a) Nayal and Rasheed (2006) (b) Wahalathantri (2011)

Figure 3-6 Tension stiffening model

A bilinear elastic-plastic model was used to describe the stress-strain behavior of the steel and WWF reinforcement. The tangent modulus of the strain-hardening branch was estimated to be one-hundredth of the elastic modulus. Perfect bond was assigned to the interface between the concrete and internal reinforcement. The FRP laminate was modeled as a linear elastic orthotropic material, and its stress-strain response was considered as a linear elastic relationship. The elastic modulus of FRP composites in the direction perpendicular to the fibers E_{12} was assumed to be one-twentieth of that in main direction E_{11}, and Poisson's ratio ν_{12} was assumed to be 0.3 for the analysis.

3.4.4 CFRP-Concrete Interface Model

A bilinear bond-slip model proposed by Lu et al. (2005) was utilized to represent the behavior of the FRP-concrete interface in terms of the local shear stress τ and effective displacement/slip S between the FRP and the concrete as shown in Figure 3-7.

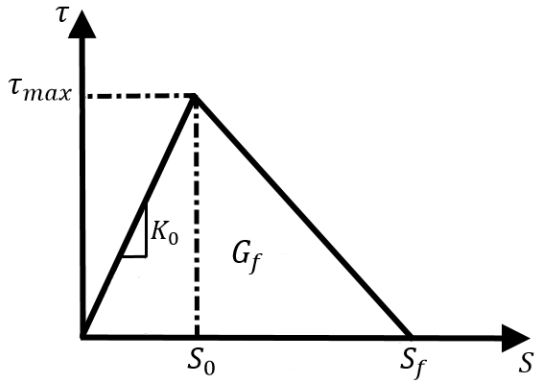

Figure 3-7 Bilinear bond-slip model

The bilinear bond-slip model is defined as follows:

$$\tau = \tau_{max}\frac{S}{S_0} \quad \text{for the ascending part} \tag{3-12}$$

$$\tau = \tau_{max}\frac{S_f - S}{S_f - S_0} \quad \text{for the descending part} \tag{3-13}$$

The maximum bond stress τ_{max} is related to the FRP-to-concrete width ratio β_w and the tensile strength of concrete f_t as:

$$\tau_{max} = 1.5\beta_w f_t \tag{3-14}$$

$$\beta_w = \sqrt{\frac{2.25 - b_f/b_c}{1.25 + b_f/b_c}} \tag{3-15}$$

where b_f and b_c are the width of the FRP laminates and concrete slab, respectively. The slip S_0 corresponding to τ_{max} and the initial stiffness K_0 are described by the linear relationship as:

$$S_0 = \tau_{max}/K_0 \tag{3-16}$$

$$K_0 = K_a K_c/(K_a + K_c) \quad \text{3-17}$$

where $K_a = G_a/t_a$ and $K_c = G_c/t_c$. G_a and G_c are the shear modulus of the adhesive and concrete, respectively. The thickness of adhesive t_a was assumed to be 1 mm. The thickness of concrete t_c was taken to be 5 mm according to the thickness of the concrete layer that debonding was formed within in pull tests carried out by Lu et al. (2005). The interfacial fracture energy G_f is represented by the area under the τ- S curve and is given as:

$$G_f = 0.308\beta_w^2\sqrt{f_t} \quad \text{3-18}$$

Thus, final slip S_f in equation 3-12 can be calculated as:

$$S_f = 2G_f/\tau_{max} \quad \text{3-19}$$

3.4.5 Modeling Methodology

Since geometries, material properties, load patterns and boundary conditions of the test slabs and their supports were symmetric, only half of the specimens were modeled with proper boundary conditions to reduce a computational process and running time. Eight-node linear brick elements with reduced integration (C3D8R) were used for concrete and steel beams. The W00WF was modeled using two-node linear beam elements (B31). Four-node doubly curved thin shell elements with reduced integration (S4R) were used to represent FRP laminates. The FRP-to-concrete interface was defined as surface-

based cohesive behavior which neglects the small interface thicknesses using the above bond-slip constitutive model.

3.4.6 ABAQUS Model

The input data of the ABAQUS models for defining material properties and behaviors of concrete, steel, WWF reinforcement, FRP laminates, and FRP-concrete interface according to the minimum requirement of design codes, theories, methodologies, and assumption mentioned above are summarized in Appendix C.

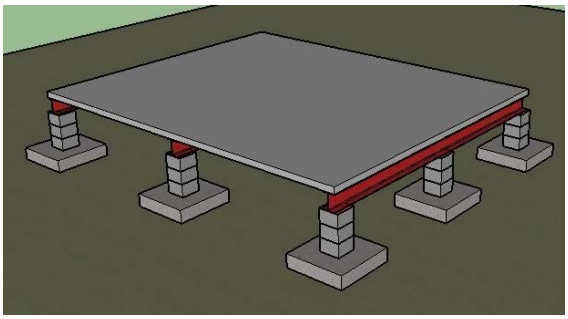

Figure 3-8 The proposed test specimen

The numerical model was created based on the proposed test specimen setup for non-strengthened SOG, referred to as *the control* (Figure 3-8). Half of the specimen with WWF reinforcement was modeled to take advantage of symmetry about the X-Z plane, and the boundary condition of the column was defined to be fixed at the bottom end to represent the translational and rotational restraint due to the column base, as illustrated in Figure 3-9. Numerous models of the control with various slab dimensions, beam span, and beam spacing were repeatedly

analyzed to determine the appropriate dimensions of the test specimen that caused failure of the test slab under the uniformly distributed load. It showed that there was a difference between the results achieved from two approaches; hand calculation and nonlinear FEA. The former method yielded beam spacing of more than 7 ft, while the other provided beam spacing of more than 9 ft. Nevertheless, the results from both approaches were reasonable. The flexure formula was used to compute only the cracking moment M_{cr}, the minimum moment that instigates crack on the slab surface, whereas the nonlinear FEA also considered crack propagation, moment redistribution, and beam deflection. Therefore, the spacing of the support beam for test slabs was taken to be 10 ft.

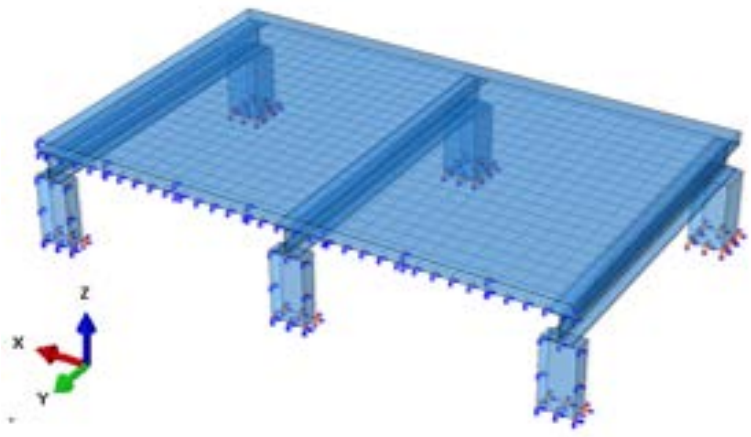

Figure 3-9 ABAQUS model of the control

One of the most useful outputs that can be drawn from the ABAQUS software is the tension damage parameter d_t, which specifies the stiffness degradation of materials. This parameter was then used to explain the crack development and failure behavior of the slab in the preliminary analysis. It indicated

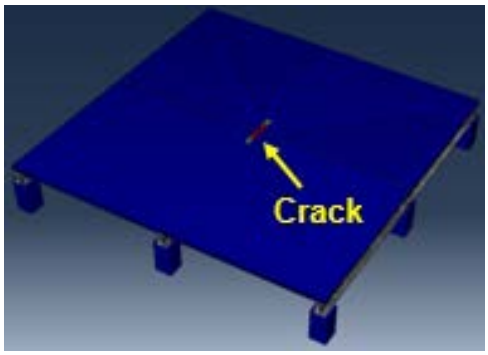

(a) Crack initiation

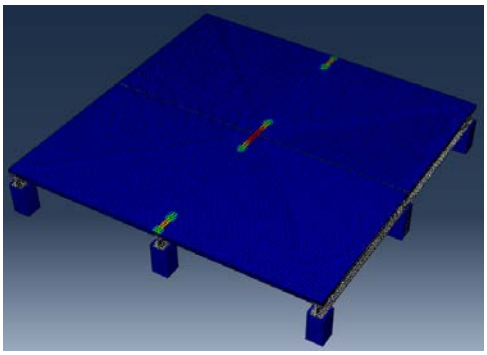

(b) Multiple surface cracks

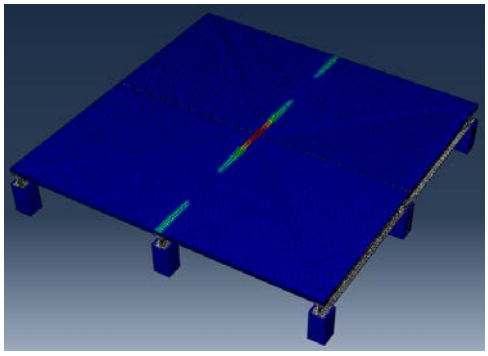

(c) Crack propagation

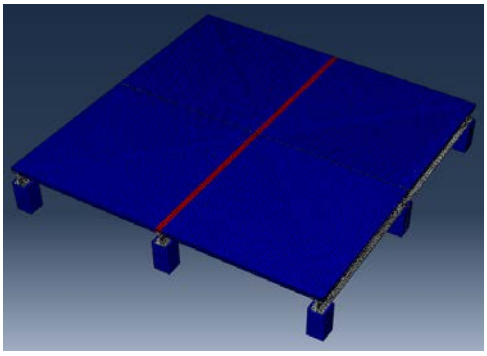

(d) Continuous crack through the slab

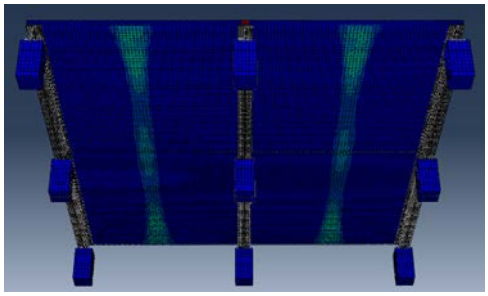

(e) Microcrack

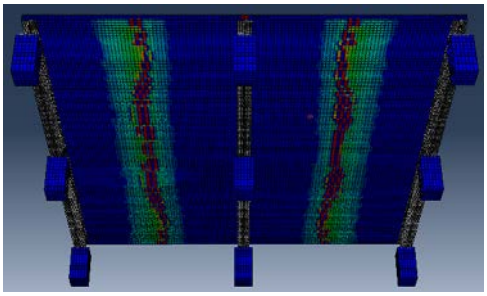

(f) Fully cracked slab

Figure 3-10 Crack patterns of the control

that the first crack took placed on the top surface of the slab at the location of the internal column (Figure 3-10 (a)). With an increased load, the first crack started propagating, while two more cracks occurred at the location of the edge columns along the middle support beam (Figure 3-10 (b)). Visible cracks kept extending toward each other along the beam direction as a higher load was applied (Figure 3-10 (c)), and they eventually connected with each other and form a single continuous crack throughout the top surface of the slab (Figure 3-10 (d)). At this point, the negative moments mostly redistributed to the positive moment region leading to the initiation of the microcracks at the bottom surface of the slab (Figure 3-10 (e)). The propagation of these microcracks rapidly developed with gradually increasing applied load until the failure of the slab at an approximate total load of 98 psf (Figure 3-10 (f)).

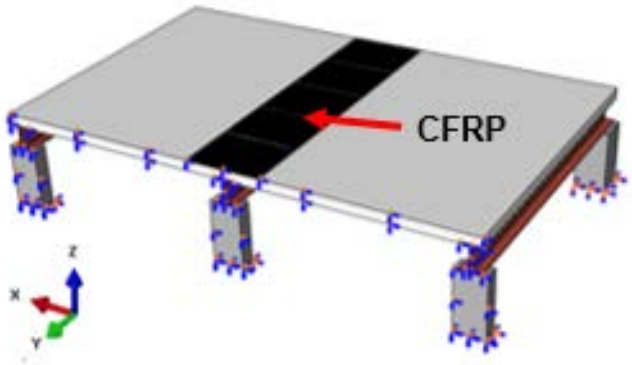

Figure 3-11 ABAQUS model of the FRP-strengthened test specimen

To strengthen the slab for safety, a single-ply unidirectional CFRP laminate was applied on the top of the slab surface along the middle support beam, where the initial cracks occurred, and the fiber direction was oriented perpendicular to the cracks (Figure 3-11). The length of CFRP sheet initially was 8 ft, measured along the fiber direction. After analysis, the slab failed in flexure before CFRP debonding, implying the sufficient development length. The models of strengthened specimens with decreased sizes of the laminates were reanalyzed to provide the optimum use of the material. It finally appeared that CFRP sheets could be reduced from 8 ft to 2.5 ft in length, while the slab was still subjected to the flexural failure mode. The CFRP laminates were employed in the experimental program with the aim of enhancing the flexural capacity of the control by at least 20%. The FEA results exhibited relatively less cracks and slower rate of crack propagation, as compared to the slab without CFRP strengthening. It also showed that the strengthened slab collapsed at an approximate total load of 125 psf, resulting in a 27.5% increase in flexural capacity.

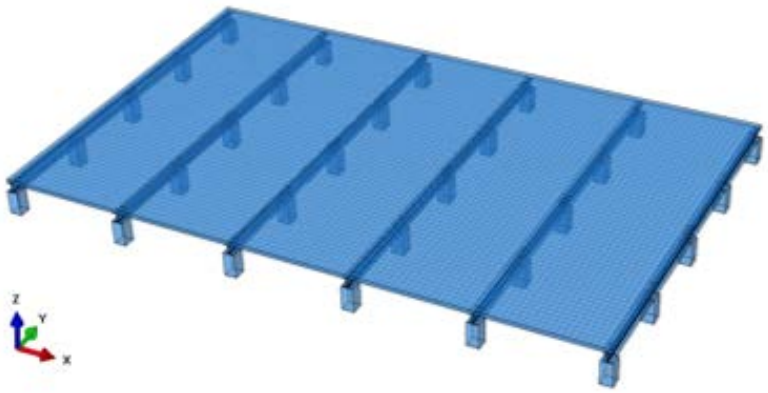

Figure 3-12 ABAQUS model of a typical elevated SOG

Since only the part of a typical elevated SOG was determined to use in the experimental program, it is necessary to certify that the structural behaviors of the selected portion can properly represent those of the whole slab. For this purpose, ABAQUS model in Figure 3-12 was simulated based on a typical floor plan of a single-family residential home in Figure 3-2. Beam spacing and beam span were 10 ft and 8 ft, respectively, which were the same as those in the models of test specimens.

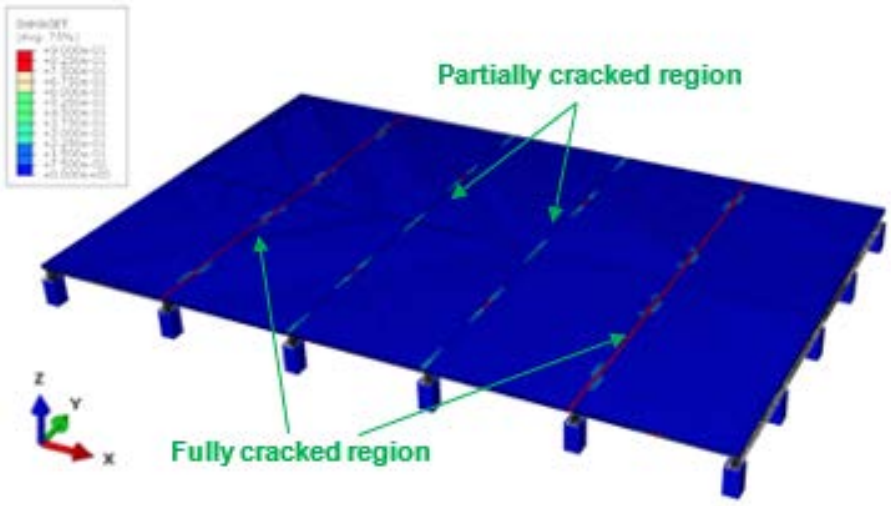

(a) On the top surface of the slab

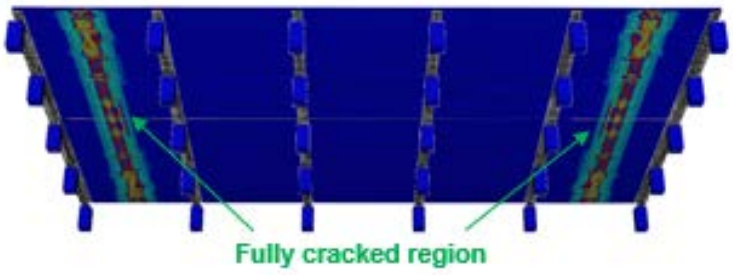

(b) At the bottom surface of the slab

Figure 3-13 Crack patterns of a typical elevated SOG

The FEA results showed remarkable similarities between the test specimen and the typical SOG in terms of crack development and mode of failure. The initial cracks appeared on the top surface of the typical SOG and then propagated throughout the slab along the support beams, and the cracks finally took place at the bottom surface in the positive moment region due to redistribution of the moments, leading to the flexural failure of the slab. It should be noted that continuous slabs always experience more severe cracks in the negative moment regions next to the outer bays than the inner bays. This is because those critical areas are subjected to higher moments according to the moment distribution method. Thus, the typical elevated SOG which was fully cracked at outer bays and partially cracked at the inner bays as depicted in Figure 3-13 (a) behaved in complying with the theory. Figure 3-13 (b) illustrates that the cracks at bottom surface occurred merely in the outer bays and thus caused only those bays to collapse. The ultimate load associated with the collapse of the outer bays was 95 psf, which was slightly less than that of the specimen. Therefore, the proposed specimen can efficiently represent the typical elevated SOG.

Chapter 4
Experimental Program

4.1 Introduction

The experimental work of the current research was conducted at University of Texas at Arlington Research Institute (UTARI). The experimental program comprised constructions of two large-scaled specimens and examinations of the specimens subjected to the uniformly distributed load. Both specimens had the identical geometrical configuration, internal reinforcement details, and support conditions. The results of the analyses and designs discussed in the previous chapter were used to determine the specimens in the experimental program. The layout, cross section, and details of the typical test specimen are presented in Figure 4-1. One specimen was kept un-strengthened as the control, while the other was strengthened externally with a unidirectional CFRP on the top surface of the slab along the middle support beam as depicted in Figure 4-2. The experimental work was done in the open space outside the laboratory because of the large size of the specimens. Water was employed in the load tests to simulate the distributed floor live load required in the design code. The crack development, crack patterns, and failure modes of both test slabs were visually observed during the load test and presented in the final subsection of this chapter. The data collected from the instrumentation during the test, such as strain and deflection, were analyzed in details and discussed in the next chapter.

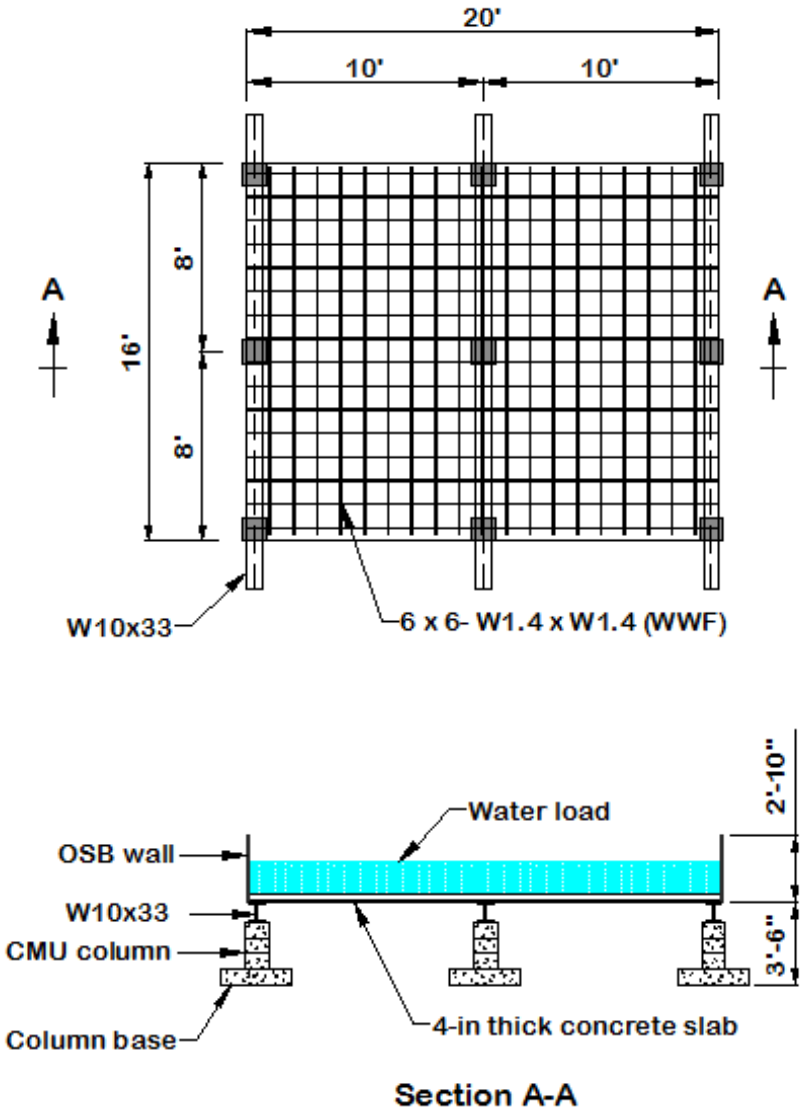

Figure 4-1 Typical test specimen layout and details

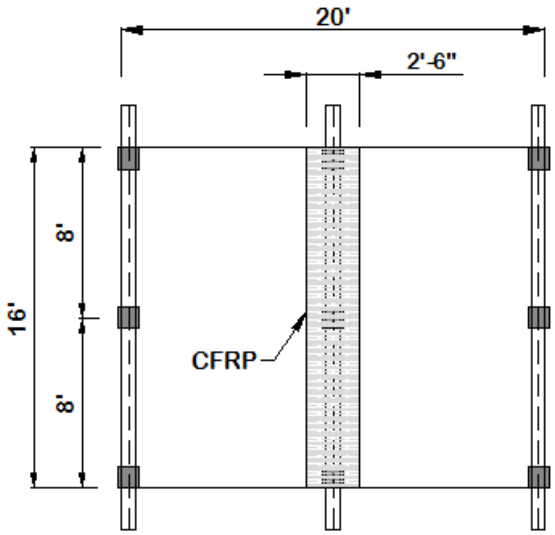

Figure 4-2 Layout of test specimen with CFRP strengthening

4.2 Test Specimen Construction

4.2.1 Test Slab Support

In general, a pile and beam support system is comprised of foundations, columns, and support beams. In the experimental program, however, column bases supported and transferred applied loads from the slabs to the ground instead of foundations. The column base formwork and CMU blocks with open corner were prepared at the UTA CELAB (Figure 4-3). The 2 in x 8 in lumbers were cut and nailed to form the 3-ft-square molds for the column bases. The 8 in x 8 in x 8 in CMU blocks were saw cut at the corner to allow the longitudinal reinforcing bars of the column to extend into the column base. At the site, the layout survey was performed to locate the exact position of the column base. The molds were then placed at the marked locations. The columns were built using a type N mortar

Figure 4-3 Column base formwork (left) and CMU with open corner (right)

to bind CMUs together (Figure 4-4 (a)). The masonry reinforcement ladders, cut to fit the size of concrete blocks as shown in Figure 4-4 (b), were suitably installed in each mortar bed as illustrated in Figure 4-4 (a). The columns were longitudinally reinforced by four #4 rebars which extended through the opening of the blocks into the column base to provide anchorage length (Figure 4-4 (c)). Reinforcement cage of column bases made from four #4 rebars was tied to the extended column rebars and supported by rebar chairs to produce concrete covering. Figure 4-4 (d) shows the arrangement of support columns and bases. The normal strength concrete was then poured, and concrete finishing was done (Figure 4-4 (e) and (f)). After allowing concrete to cure for three days, the 8-in-square columns were enlarged to the 12-in-square columns by covering them with hollow blocks of size (12x8x12) to create more cross-sectional areas for placing steel beam. The elevations of the top surface of the enlarged columns were then adjusted to be equal by topping with high strength mortar, and the top surfaces were leveled simultaneously (Figure 4-5).

(a) CMU assembly with joist reinforcement

(b) Ladder type

(c) Reinforcement cage

(d) Column and base arrangement

(e) Concrete pouring

(f) Concrete finishing

Figure 4-4 Column and column base construction

Figure 4-5 Column enlargement (left) and column elevation adjustment (right)

Finally, twelve W10x33 beams with a length of 10 ft were transported to the site. For each specimen, six of them were placed on the columns by the forklift as shown in Figure 4-6. Since the beam simply sits on the column without welding or bolting, the beam-to-column connection was a friction connection.

Figure 4-6 Steel beam placement

4.2.2 Test Slab

For a temporary slab formwork support, the 4 in x 4 in lumbers cut to the proper length were vertically positioned at the middle between support beams at a spacing of 5 ft. The 4 in x 4 in lumbers also used for horizontal members were screwed to the top of the vertical members (Figure 4-7 (a)). The elevation of slab formwork support was verified using straight 1 in x 2 in lumbers and adjusted with wooden wedges. To avoid large sagging of the test slabs, the 1-1/8 in thick oriented strand board (OSB) was selected to serve as the bottom part of the form. The OSB panels were nailed to the top of the lumber supports, and the sides of the formwork were made by the 2 in x 4 in lumbers screwed along the parameter of the form (Figure 4-7 (b)). A single layer of 6 x 6- W1.4 x W1.4 WWF was laid on the form and scarcely nailed to the OSB panels to hold it in place (Figure 4-7 (c)).

The ready-mix concrete with an anticipated compressive strength of 2500 psi was delivered to the site by two concrete mixer trucks. The slabs were cast from a different mixer truck. The procedures began with performing slump test to determine consistency and workability of fresh concrete and then casting a set of fifteen cylindrical concrete specimens of size 4 x 8-in. for each slab (Figure 4-8 (a)). Concrete was poured into a form, spread by shovels and concrete placers, and thoroughly consolidated by operating a concrete vibrator (Figure 4-8 (b)). A lumber straightedge, known as a screed, was used to strike off and level concrete by drawing it with a slight sawing motion across concrete (Figure 4-8 (c)). A small amount of concrete was kept in front of the screed to fill in certain low spots. A

trowel was utilized to smooth the concrete surface at the edges and corners of the form.

(a) Slab formwork support

(b) Slab formwork

(c) Reinforcement placement

Figure 4-7 Test slab forming


(a) Concrete slump test (left) and concrete test cylinder (right)


(b) Concrete pouring (left) and concrete vibration (right)


(c) Concrete finishing

Figure 4-8 Test slab casting procedure

Concrete curing was immediately accomplished after slab casting to maintain moisture content and temperature in early-age concrete. A water-based concrete curing compound was applied on the entire concrete surfaces, and the slabs were covered by 6-mil-thick plastic sheets as shown in Figure 4-9. After it is cured for seven days when concrete was supposed to gain 65% strength, the formwork was removed. Figure 4-10 illustrates two experimental specimens before the formwork removal.

Figure 4-9 Curing concrete slabs

Figure 4-10 Test specimens

4.2.3 Water Trough

The OSB panels with thickness of 1-1/8 in were fastened to the sides of the slab along the parameter using concrete anchors to form a water trough as illustrated in Figure 4-11. Joists between the panels, in particular at the corners of the slab, were reinforced with tie plates. The trough was 30 in high, and thus uniformly distributed load can be produced up to 156 psf on the specimens when it is full of water (specific weight of water γ_w = 62.4 lbf/ft^3).

Figure 4-11 Attaching OSB sheathing

4.3 CFRP Installation

Since the performance of the CFRP system would be dramatically affected by a slight deviation from the prescribed installation procedures, the CFRP laminates were carefully applied adopting the recommendations from both ACI 440.2R-17 code and the manufacturer documents. The substrate surfaces are required to be a minimum concrete surface profile 3 (CSP 3) for the bond-critical applications, which requires an adhesive bond between FRP and substrates. Figure 4-12 presents the nine different surface profiles ranging based on the level

of roughness from CSP 1 to CSP 9 classified by the International Concrete Repair Institute (ICRI). Both grinding and sandblasting are used to achieve the desired surface profile in the FRP industry.

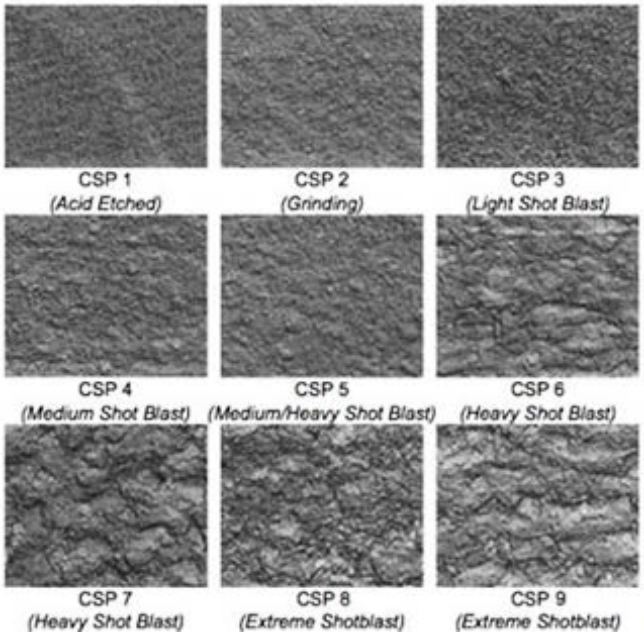

Figure 4-12 ICRI concrete surface profile (CSP)

After removing dirts and existing coatings such as curing compound, sandblasting operation was performed on the top surface of the slab to produce a CSP 4 (Figure 4-13 (a)). The process of applying CFRP started when the substrate and ambient temperature was less than 95 ºF. Sikadur 330 epoxy was mixed (Figure 4-13 (b)) and applied on the slab surface in the negative moment regions where cracks were expected to occur. A set of eight 2 x 2.5-ft CFRP sheets was saturated with Sikadur 300 epoxy (Figure 4-13 (c)) and continuously placed on the slab in which the fibers were perpendicular to the beam direction (Figure 4-13 (d)).

(a) Sandblasting operation

(b) Mixing of Sikadur 330

(c) Saturating CFRP with Sikadur 300

(d) Applying saturated CFRP

(e) Experimental specimen with CFRP laminates

Figure 4-13 CFRP installation

The top surface of the slab was painted in white to improve the efficiency of visual crack observation. The test specimen strengthening with CFRP laminates is shown in Figure 4-13 (e).

4.4 Load Test

4.4.1 Test Setup

The strains and deflections of the specimens corresponding to the applied load were measured by strain gauges and linear variable differential transformers (LVDT's). For the control, five LVDT's were mounted on the floor at different locations as depicted in Figure 4-14 to monitor the vertical deflections of the slab and the steel beam. A total of 11 strain gauges were bonded to the concrete surfaces in both positive and negative moment regions (Figure 4-14). Out of seven strain gauges on the top surface, five of them were located on the beam centerline, and the other two were attached at one ft away from the beam centerline on each side. Four strain gauges on the bottom surface were located at the mid-spans of the slab. For the strengthened specimen, both LVDT's and strain gauges were positioned at the same locations as those of the control as shown in Figure 4-15. However, a different type of strain gauges recommended for FRP applications was installed on the top surface of the slab. After appropriately installed, all strain gauges on the top surfaces of both slabs were coated with EPOWELD epoxy to prevent moisture from water load testing. Figure 4-16 illustrates two types of strain gauges used for concrete and FRP laminates in the experimental program.

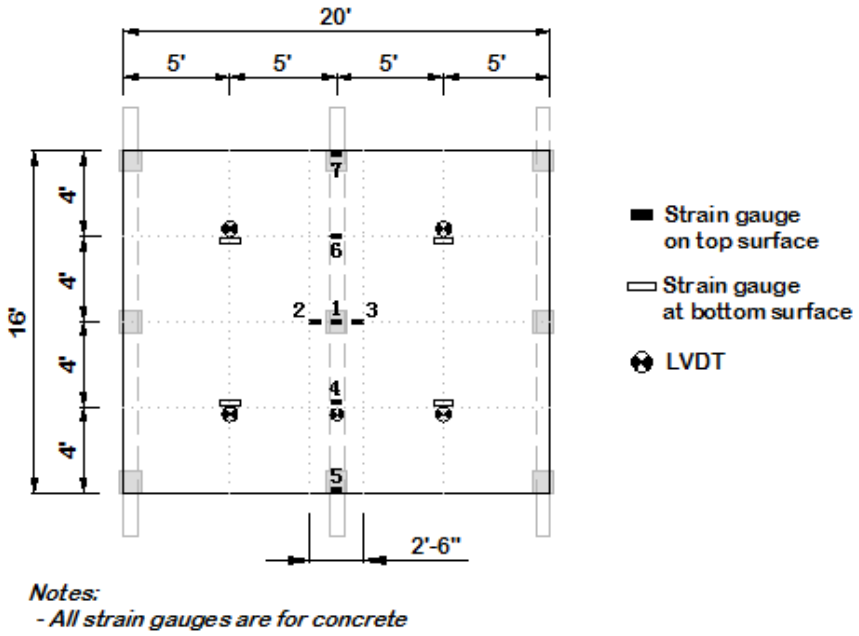

Figure 4-14 Instrumentation of the control

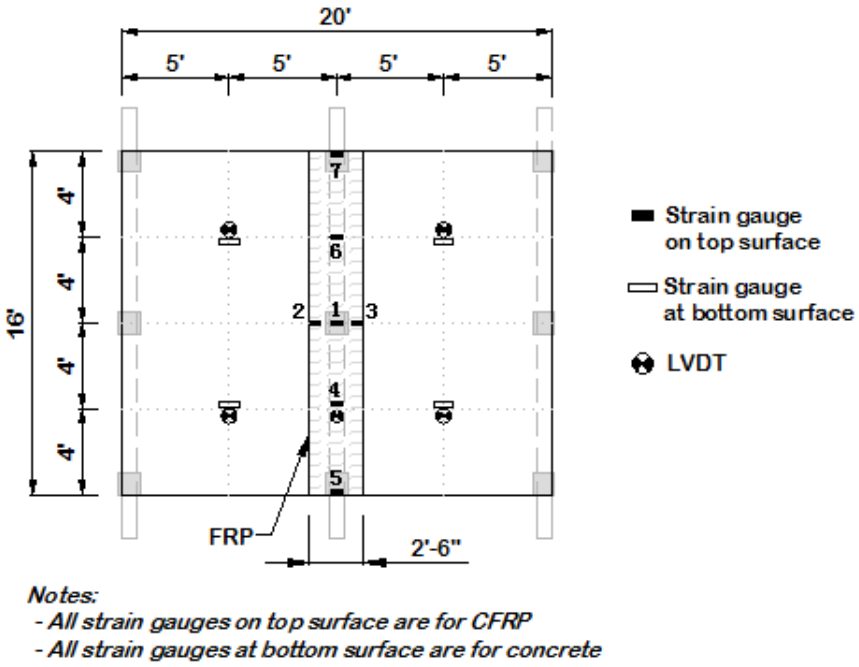

Figure 4-15 Instrumentation of the CFRP-strengthened slab

Figure 4-16 Installation of strain gage for concrete (left) and FRP (right)

The deflection and strain data were collected automatically through a data acquisition system. Figure 4-17 shows the test setup for both specimens. Crack initiation, crack propagation, and FRP delamination was continuously detected during load testing.

Figure 4-17 Experimental setup

4.4.2 Water Load

Both specimens were tested under the uniformly distributed load to replicate the actual SOG subjected to the floor live load specified by ASCE 7-10 code. Prior to starting the load tests, the top surfaces of both slabs were covered by clear 6-mil-thick plastic sheets to avoid water leakage. Loading was applied using water to gradually fill up the trough with constant flow rate at 56 liters/min as shown in Figure 4-18. Based on the slab surface area and the flow rate, filling water created the applied load with the rate of 0.385 psf/min or 23.1 psf/hr. Thus, the applied load could be calculated from the loading time. The height of water was also measured during load testing and computed to verify the applied load. Pressure load could be increased up to 156 psf, which nearly four times greater than minimum load requirement for a residential house. The load was applied to one slab at a time. Load testing was terminated when the specimen failed or the trough was full of water.

Figure 4-18 Load test on the control (left) and the strengthened specimen (right)

4.4.3 Experimental Observation

While loading the control using water, the difference of the water levels between two opposite edges of the slab in the longitudinal direction was observed to be approximately 2 in. However, there was no apparent difference in the water levels along the transverse direction. As the height of water column was increased up to 16 in, a single crack visually detected on the top surface of the slab near the centerline of the middle support beam (Figure 4-19 (a)). The crack on top surface

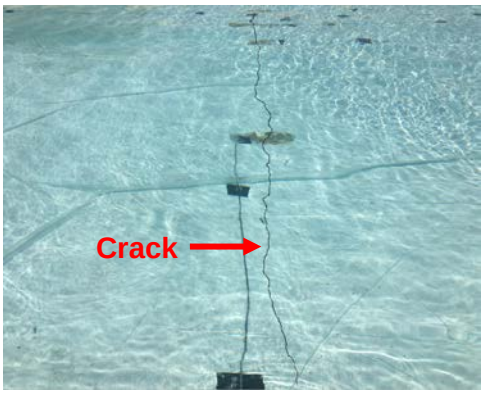

(a) Top surface

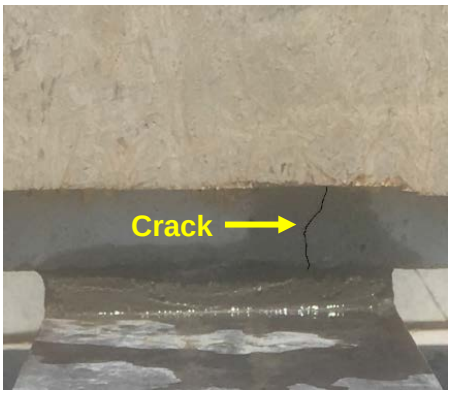

(b) Side surface

(c) Bottom surface

Figure 4-19 Crack development of the control

Figure 4-20 Collapse of the control specimen

also propagated throughout the depth of the slab (Figure 4-19 (b)). Finally, the cracks took place on the bottom surface at the mid-span of both bays immediately before the slab collapsed (Figure 4-19 (c)). The control slab sudden failed with a water column height of 18 in (Figure 4-20). Both spans of the slab did not collapse simultaneously due to the effect of imperfection in the construction process. Nevertheless, the crack at the left mid-span of the slab nearly developed throughout the slab thickness.

The load test for the strengthened specimen was conducted in the same manner. The water column heights measured at several locations were slightly different implying that the slab was accurately leveled. Water load was kept being

applied on the slab until the water level reached the top of the trough, and the load test was then terminated. Figure 4-21 (a) shows the strengthened specimen after load testing with a water column height of 29 in. The slab was still in good condition. Cracks in negative moment region on the top surface of the slab could not be monitored because most parts of the area were covered by CFRP laminates. Based on visual observation, no crack was found on the bottom and side surfaces of the slab (Figure 4-21 (b) and (c)).

(a) CFRP-strengthened slab after load test

(b) Bottom surface of the slab

(c) Side surface at the middle support beam

Figure 4-21 Crack observation on the CFRP-strengthened slab

Chapter 5
Result Validation and Discussion

5.1 Model Validation

A detailed description of the results from the experimental program is presented separately for each specimen. Although both specimens in the experimental program had the identical geometry and support condition, they were cast from two separate concrete batches, and thus their mechanical properties of concrete might be different. In order to compare the experimental results of such specimens with the different concrete properties, the experimental results from each specimen were first utilized to validate finite element models. The validated models of both specimens were then reanalyzed with the same material properties. The numerical results of the specimens were compared and discussed in this chapter.

For each test slab, two sets of five cylindrical concrete specimens collected during slab casting were tested to determine the average compressive strength f_c' and splitting tensile strength f_t in accordance with ASTM C39/39M (2017) and ASTM C496/C496M (2017), respectively. Five CFRP coupon tests were also conducted complying with ASTM D7565/7565M (2010) to estimate the average tensile strength and modulus of elasticity of CFRP laminates. Figure 5-1 shows the cylindrical specimen and coupon tests carried out at the UTA laboratory. The mechanical properties of concrete and CFRP laminates used for model validation were summarized in Table 5-1 and 5-2, respectively.

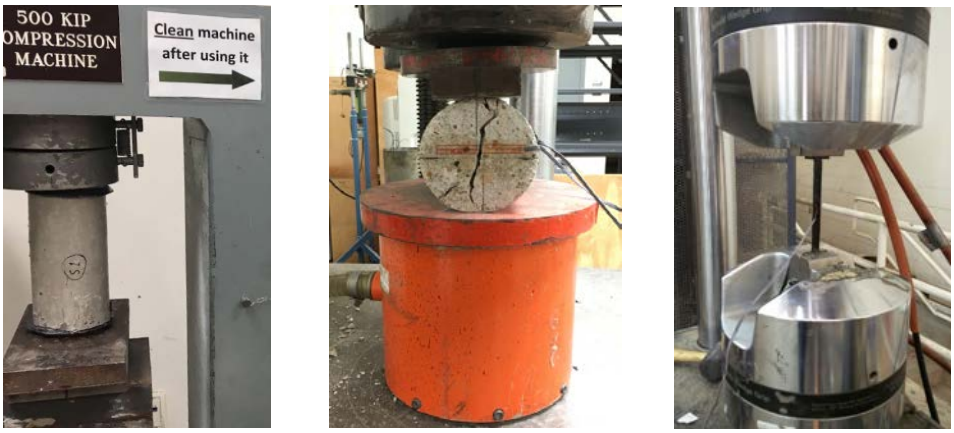

(a) (b)…… ……(c)…..

Figure 5-1 Cylindrical specimen and coupon tests: (a) concrete compressive strength; (b) concrete tensile strength; (c) CFRP tensile strength

The load-deflection responses of the slab and beam from the finite element models were compared to those from the experimental program to calibrate the models. The mid-span deflections of the slabs experimentally measured by two LVDT's per each span were averaged and plotted versus the applied pressure load. The mesh sizes of the finite element models were varied to adjust the results,

Table 5-1 Mechanical properties of test slabs at different ages

Properties	Non-strengthened slab	Strengthened slab
Density, pcf	142	146
Compressive strength, psi	3215	3520
Tensile strength, psi	419	431
Modulus of elasticity, psi	2.52×10^6	2.66×10^6
Age of concrete, day	46	53

Table 5-2 Mechanical properties of cured CFRP laminates

Properties	Cured CFRP laminates
Tensile strength, psi	1.05×10^5
Modulus of elasticity, psi	8.2×10^6
Thickness, in	0.024

particularly in the discrete areas such as contact regions between concrete and CFRP laminates. The load-deflection curves of the slab and beam support for the control show a good agreement between experimental and numerical results indicating that the constitutive models used in the FEM analysis can precisely capture the fracture behavior of the concrete (Figure 5-2). It is noted that the slight difference of the test results between the left and right span of the slab are associated with the effect of imperfection in the construction process. The ultimate

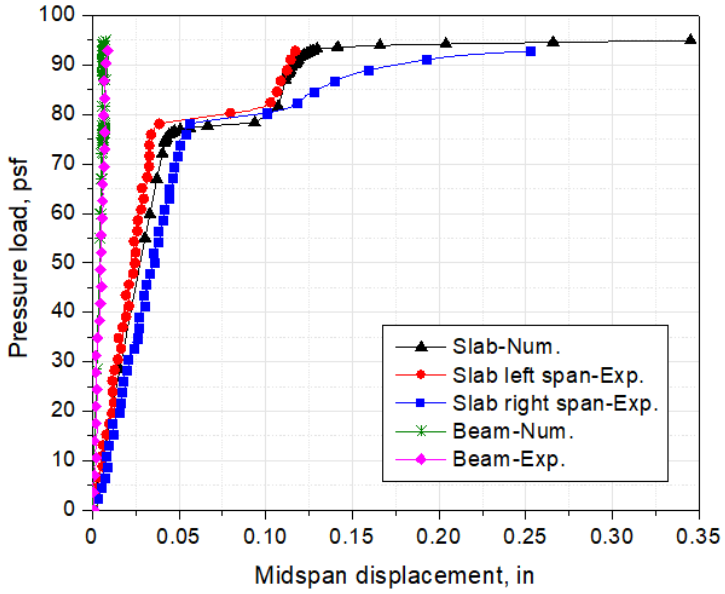

Figure 5-2 Comparisons between experimental and numerical results of the control

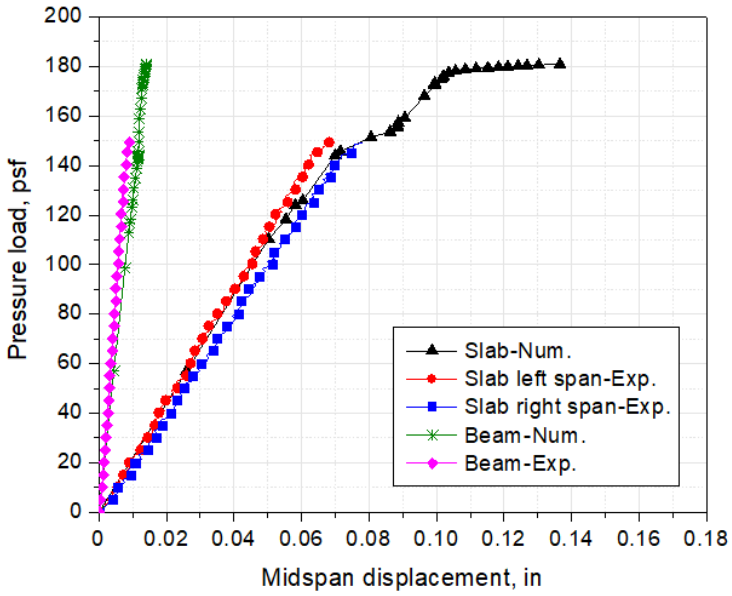

Figure 5-3 Comparisons between experimental and numerical results of the CFRP strengthened specimen

load experimentally measured for the control was 92 psf which caused the failure of the right span of the slab. The deflections corresponding to the ultimate load at the left and right span of the slab were 0.12 and 0.25 in, respectively

Similarly, the load versus deflection of the CFRP strengthened specimen were plotted in Figure 5-3. It was noticed that the experimental results behaved linearly and had a strong correlation with numerical results. Due to the limitation of load capacity in the test, the strengthened slab did not fail with the maximum pressure load of 150 psf, which exceeds three times the minimum live load requirement for a residence (IBC 2012). The deflections corresponding to the maximum applied load at the left and right span of the slab were 0.068 and 0.075 in, respectively. The ultimate load capacity of the strengthened slab, however,

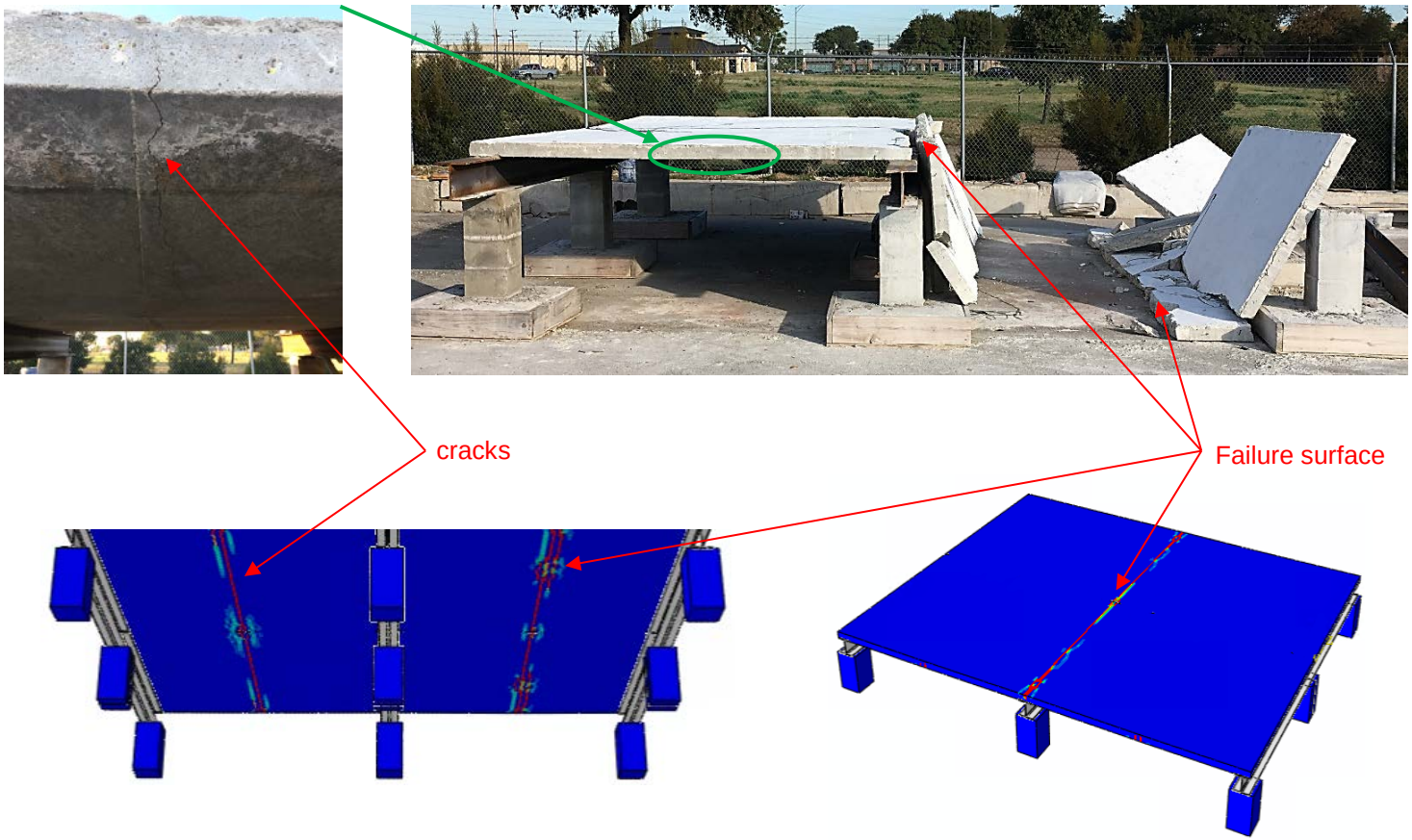

Figure 5-4 Failure surface comparison between experimental and numerical results of the control

was achieved by FEA approach. The pressure load in the FEA model was increased until the slab collapsed. The numerical results exhibited the nonlinear load-deflection behavior with a slightly higher load than the load level in the experimental program. The predicted ultimate load of the strengthened specimen was 180 psf.

The load-deflection response at midspan of the support beam for both specimens increased linearly throughout the tests, and deflection decreased after releasing test loads. This implies that the elastic limit of the steel beams was not reached as expected.

In addition to load-deflection behaviors of the slabs, the crack patterns from experimental and numerical results were also compared to provide accurate validation of the FEA models. It was apparent that all the crack patterns and failure surfaces for the control achieved from the test and the FEA models took place at the same locations as illustrated in Figure 5-4. Besides, the development of cracks also was in an excellent agreement, and its details were discussed in the next section of this chapter. Unlike the control, the strengthened slab did not fail and no crack occurred during the load test. The CFRP sheets were peeled off after the test to investigate the crack underneath. It was found that there was no crack in the negative moment region. Since a visible crack could not be observed, it is conservative to assume the presence of microcracks. At the load of 150 psf, the validated model exhibited the microcracks in the negative moment area near the column locations (Figure 5-5 (a)).There was no crack on top and side surface of the slab in both FEA model and experiment (Figure 5-5 (b) and (c))..

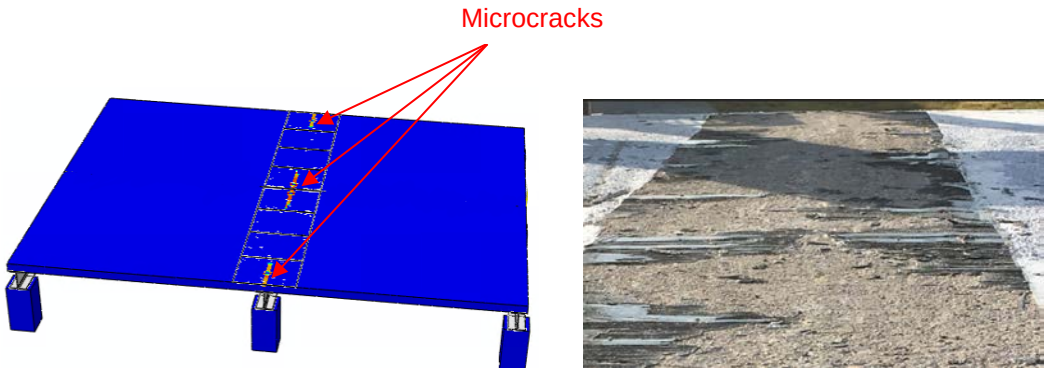

(a)

(b)

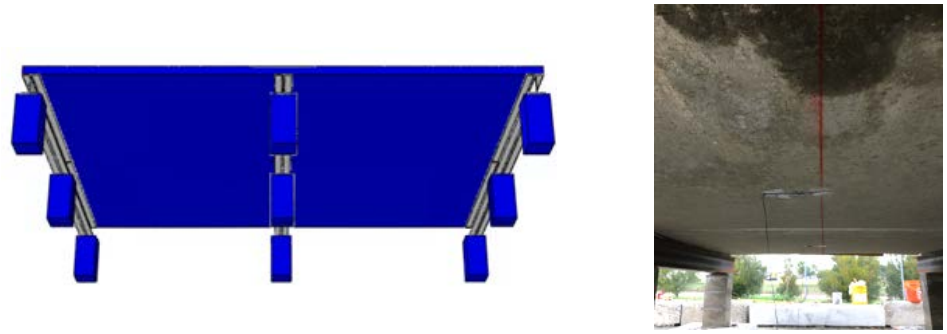

(c)

Figure 5-5 Crack pattern comparison between experimental and numerical results of the strengthened slab: (a) top surface; (b) side surface; (c) bottom surface

5.2 Discussion of Results

After properly validated, FEA model of the strengthened specimen was reanalyzed using the concrete properties of the control. The numerical results of both specimens were discussed in terms of load-deflection response, mode of failure, crack development, and strain distribution.

5.2.1 Load-Deflection Response

The comparison between the load-deflection responses of the un-strengthened and strengthened slabs was shown in Figure 5-6. It should be noted that the self-weight of the slab specimens was not taken into account in the load-deflection curves achieved from the experimental program as presented in Figure 5-2 and 5-3. However, it cannot be neglected in this case because the self-weight of the slab is relatively high compared to the minimum required live load for residential homes. Therefore, the self-weight of concrete and steel was considered in the current comparison. The ultimate load of the un-strengthened and CFRP strengthened slab were 142 psf and 185 psf, respectively, representing the increase in the flexural load capacity of 30.3% over the control slab. The deflection of the strengthened slab was less than that of the control at any load level because the CFRP strengthening system contributed to the overall stiffness of the specimen. Nevertheless, since the deflection corresponding to the ultimate load of the strengthened slab was less, the application of CFRP resulted in a decrease of overall ductility of the structure.

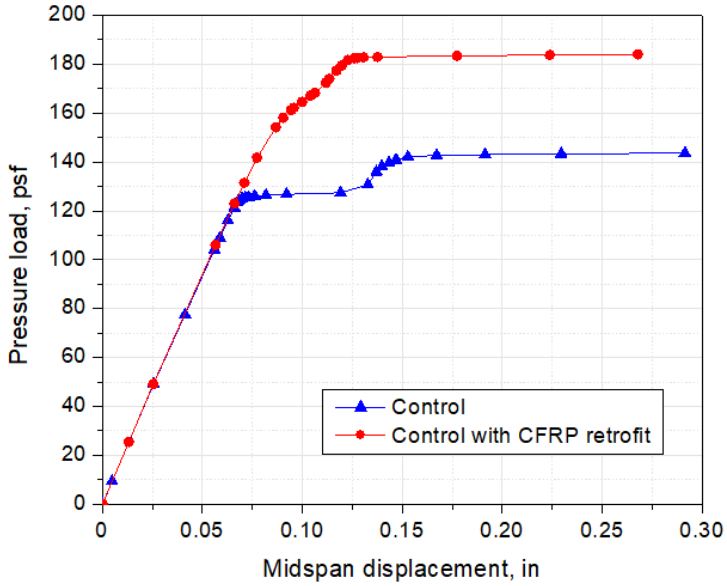

Figure 5-6 Numerical load-displacement relationships

The load-deflection curve of the control consists of four main portions. The initial part is linear until the initiation of the first crack in the negative moment region causing a nonlinear relationship in the load-deflection curves before a sudden increase in the deflection. This significant increase in the deflection with a slight load increment in the second portion indicates that the crack propagated throughout the top surface of the slab. Due to a stiffness reduction at the crack section, the moment in the negative moment region was distributed to the positive moment regions at both mid-spans of the slab. Consequently, the slab could bear more load. As load was continuously increased, the crack in the negative moment region developed along the depth of the slab causing more stiffness reduction at the crack section and more moment distribution to the positive moment region until the failure at the mid-span of the slab. From the foregoing reasons, in the third

portion of the curves the load and deflection increases in a nonlinear relationship with the less slope in comparison with the first portion. The collapse of the slab caused by the flexure failure in the positive moment regions was indicated by the horizontal line in the last portion of the load-deflection behaviors.

The load-deflection curve of the strengthened slab behaves similarly to that of the control and is divided into four distinct portions. However, the curve exhibited the less change in slope after the crack propagated through the slab surface in the negative moment region. This indicates that when the crack occurred in the negative moment region, the tensile stress at the top fiber of the concrete slab was transmitted to the CFRP laminates resulting in the decrease of the crack width and crack tip opening rate.

5.2.2 Failure Mode

Both control and strengthened specimens showed brittle failure modes. However, modes of failure changed from brittle flexure failure for the control slab due to the deficiency of welded wire reinforcement in tension zones to intermediate flexural crack-induced debonding for the strengthened slab. The failure modes were characterized by crack patterns and strain compatibility between the CFRP and the concrete slab as discussed below.

5.2.3 Crack Development

Tension damage parameter, available in the concrete damage plasticity model, was used to capture the evolution of crack in term of the degradation of concrete stiffness. For the control, initiation of cracks on top fiber face started in

the negative moment region at the column locations as previously mentioned due to the deflection of the beam supports. Each initial crack first propagated toward the mid-span of the beams to form throughout the slab along the middle beam line. At this load level, the readings from LVDT's did not show a significant change until the crack developed through the depth of the slab. As the applied load increases, the crack gradually occurred on the bottom face near the mid-span of the slab. Finally, the WWF reinforcement yielded and the crack propagated from the bottom to the top face leading to the sudden failure of the slab in the positive moment region.

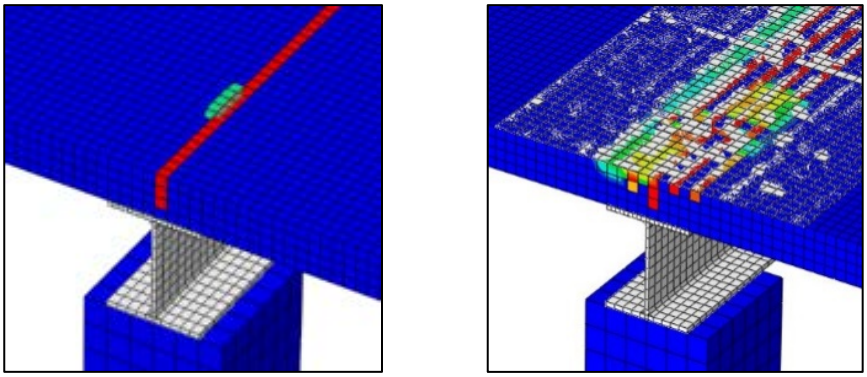

(a) Control specimen (b) Strengthened specimen

Figure 5-7 Crack pattern on the top surface of the slab

The specimen strengthened with the CFRP system experienced similar crack development. However, instead of a single line of crack which occurred on the top surface of the control slab (Figure 5-7(a)), multiple small cracks took place along the middle beam support in the negative moment region (Figure 5-7(b)). After the flexural cracks started on the top face, the CFRP partially debonded at

the locations of cracks. Similar to the control, as the applied load increases, the internal WWF was yielded and followed by flexure failures in the positive moment regions at the mid-spans of the slab as shown in Figure 5-8.

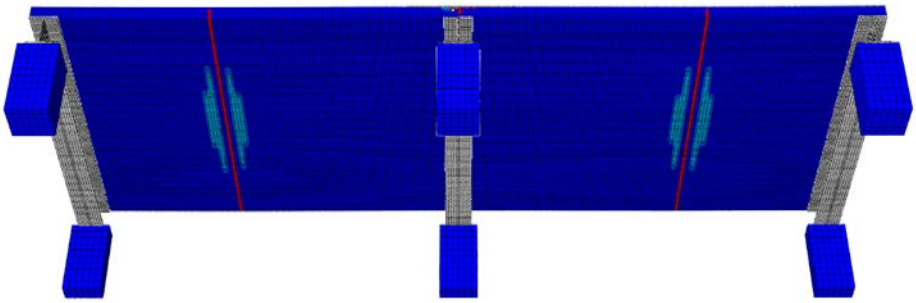

Figure 5-8 Crack pattern at the bottom surface of the strengthened slab

5.2.4 Load-Strain Response

Since the specimens were symmetric in both directions, only a quarter of the slabs was considered. The total load-strain relationships of the concrete elements of the control at five different locations are shown in Figure 5-9. Four locations point “1” to point “4” were on the top surface of the slab in the negative moment region, while the other point “5” was at the mid-span bottom surface in the positive moment region. The strain at point “1” reached the tensile strength of the control which was 0.0166% (166 με) leading to the crack initiation on the top surface of the slab at the interior column location. After that, the strain at point “2” and “3” reached the concrete tensile strength, respectively, causing the failure in the negative moment region at the load level of 128 psf. It is noted that at this load level strain at point “4” significantly decreased and became negative because the crack separated the continuous slab apart, and they behaved as two simple slabs.

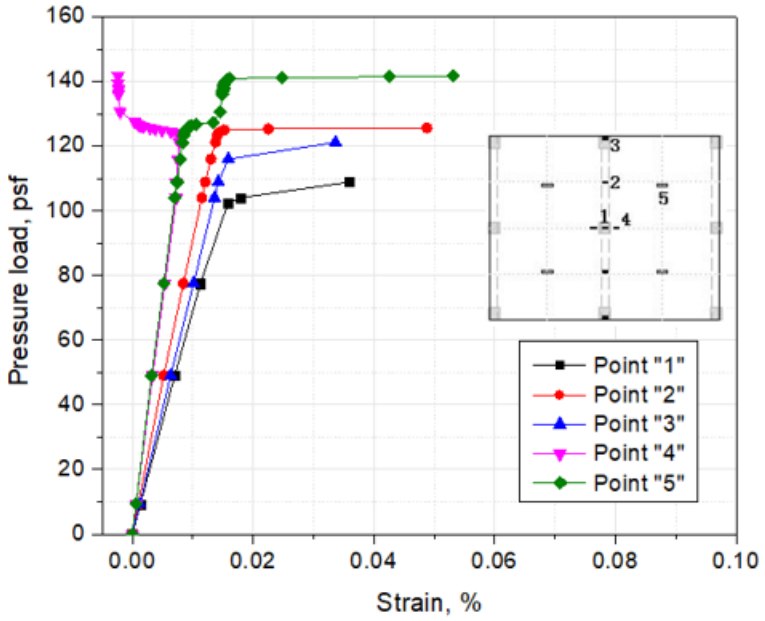

Figure 5-9 Numerical load-strain relationship of the control

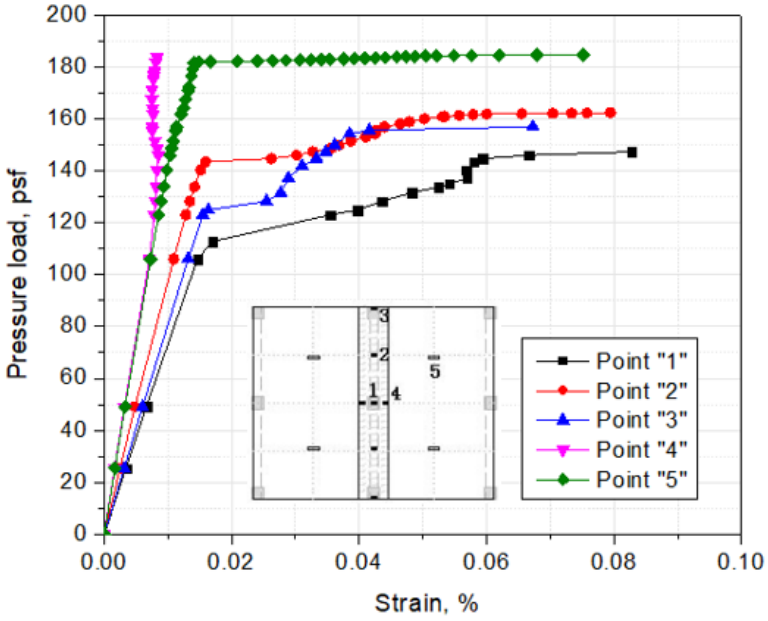

Figure 5-10 Numerical load-strain relationship of the strengthened slab

As a result, the slabs curled upward due to the applied load, and the top surface of the slab was under compression. At the ultimate load of 142 psf, strain at point "5" exceeded the tensile strength as expected.

The total load versus strains of the strengthened slab were also plotted at the same five locations as the control as illustrated in Figure 5-10. The load-strain curves behave similarly to those of the control where strain at point "1", reached the tensile strength first followed by strains at point "2", point "3" and point "5", respectively. However, when the slab failed in the negative moment region, described by the loss of strain compatibility as discussed in the following subsection, strain at point "4" slightly decreased and still was positive value. This

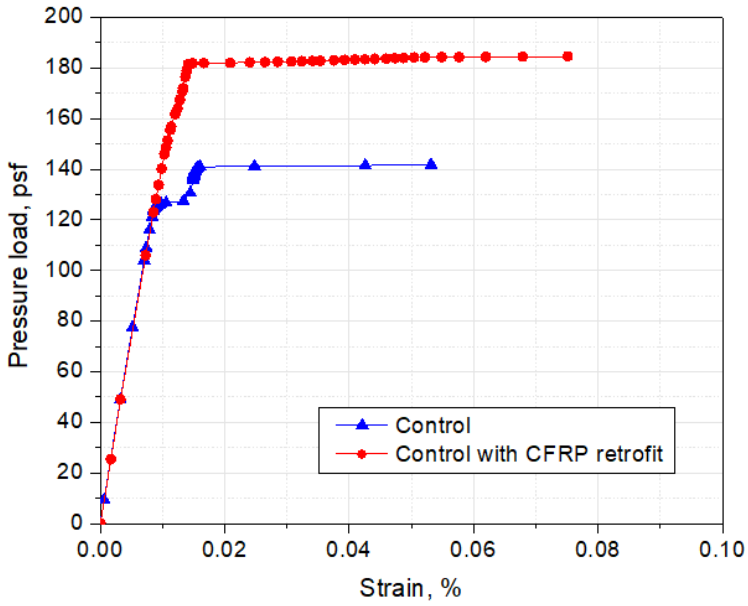

Figure 5-11 Comparison of load-strain relationship of the control and strengthened slab

is because the CFRP laminates debonded partially and were able to transfer stresses across the cracks on the top surface of the slab. Therefore, the slab still was continuous.

Figured 5-11 shows the comparison between load-strain relationship at point “5” of the control and strengthened slab. The ultimate load of the control and strengthened slab are 142 psf and 185 psf, respectively. By using the CFRP strengthening method, the increase of ultimate load is 30.3% which is the same number indicated by load-deflection response.

5.2.5 Strain Compatibility

The total load versus strain of the CFRP and concrete elements in the vicinity of the interface at two selected locations point “1” and “2” were plotted in Figure 5-12 to provide a better understanding of the debonding behavior. At point “1” which locates at the middle of the CFRP sheet where several cracks existed, the initial strain in the CFRP sheet is slightly higher than that in the concrete element adjacent to the interface. These strains are compatible at any load level up to 130 psf which the first microcrack arises. With increased load, the strain in CFRP sheet is not proportional to but still higher than that in the concrete. The intersection of the load-strain curves of CFRP and concrete slab at the total load of 164 psf shows a complete lack of strain compatibility. The corresponding strain of 0.082% which is significantly less than the ultimate strain of CFRP laminates ($\varepsilon_{cfrp,ult}$ = 1%) indicating that the debonding of the CFRP sheets occurred at point “1” before the rupture of the CFRP laminates. As a result, at load level beyond the

intersection point, the strain in the concrete element becomes greater than that in the CFRP laminates.

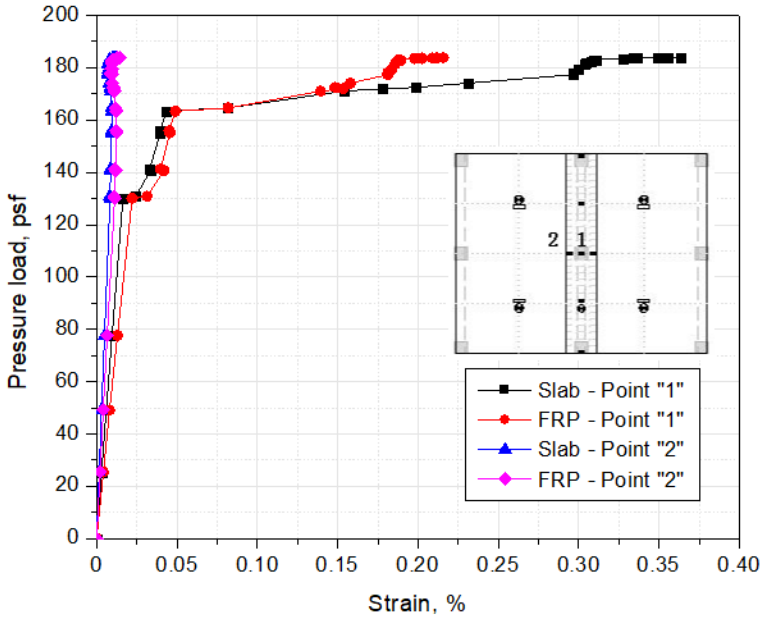

Figure 5-12 Load-strain relationship of CFRP laminate and concrete slab

In contrast, at point “2” near the edge of the CFRP sheet where no crack appeared the load-strain curves of CFRP and concrete does not show an intersection point, and still maintains the compatibility at the ultimate load of the strengthened slab. Therefore, the debonding of CFRP laminates took place only in the cracking areas and the development length of CFRP sheets used in this study was sufficient. This failure pattern of the strengthened slab is identified as intermediate flexural crack-induced debonding.

Chapter 6
Parametric Study

6.1 Introduction

The numerical analyses were extended with variations of the associated parameters. The goal is to gain a better understanding of how each component contributes to the whole system of an elevated SOG in term of load carrying capacity. It also aimed in developing the guideline charts for alternative design parameters and geometries of an existing SOG to provide the optimum use of the additional foundation support system and the optional FRP strengthening method with safety. Furthermore, in the last section of this chapter, the numerical analyses of a typical SOG on the selected types of soils in Texas were implemented to investigate the structural responses of a slab affected by the responses of soils underneath. The validated FEA models from the previous chapter were utilized for these purposes. The simulation modeling was conducted following the criteria in section 3.4 of chapter3.

6.2 Variables and results of Elevated SOG

The parameters and the range of variation in this parametric study were decided based on a common variety of non-elevated and elevated SOG houses. The effects of six parameters on the load carrying capacity of an elevated SOG were examined. Out of six parameters, three of them, the concrete compressive strength, slab thickness, and location of WWF reinforcement are related to an existing SOG itself which cannot be changed in a construction process of elevating

Table 6-1 Parameters and range of variation in parametric study

No.	Parameters (Variables)	Range of Variation	Unit
1	Concrete compressive strength	2500, 3000	psi
2	Beam spacing	5, 6, 7, 8, 9, 10	feet
3	Slab thickness	3, 4, 5	inch
4	Retrofitting method	None, CFRP, GFRP	-
5	Beam span	10, 12, 15	feet
6	WWF locations	Top, Middle, Bottom	-

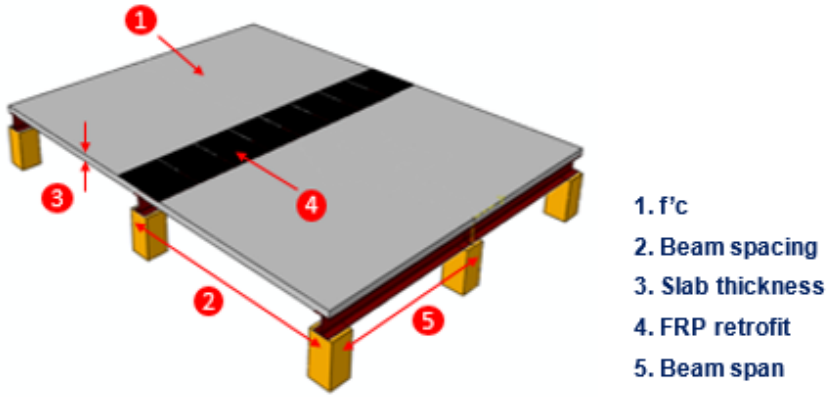

Figure 6-1 Variables in parametric study

houses. The other parameters were support beam spacing, support beam span, and FRP types in strengthening system which are the additional support system and retrofitting techniques of an elevated SOG, and they thereby can be designed before elevating a house. The parameters and the ranges of variation involved in the parametric study were summarized in Table 6-1, and some variables were depicted in Figure 6-1. Each numerical model was simulated with a different combination of parameters and their ranges. A summary of the results from the analyses was presented in Table 6-2.

Table 6-2 Load capacities and failure modes of proposed models

No.	FRP Retrofit	f_c' (ksi)	Slab thickness (in)	Beam spacing (ft)	FRP length (ft)	Load capacity (psf)	Max. corresp. Deflection (in)	Failure mode*
1	None	2.5	3	5	-	185	0.033	FL
2	None	2.5	3	6	-	130	0.040	FL
3	None	2.5	3	7	-	99	0.055	FL
4	None	2.5	4	6	-	208	0.032	FL
5	None	2.5	4	7	-	145	0.034	FL
6	None	2.5	4	8	-	110	0.039	FL
7	None	2.5	4	9	-	93	0.056	FL
8	None	2.5	5	7	-	229	0.031	FL
9	None	2.5	5	8	-	162	0.034	FL
10	None	2.5	5	9	-	126	0.037	FL
11	None	2.5	5	10	-	103	0.050	FL
12	CFRP	2.5	3	6	2	183	0.041	ICD
13	CFRP	2.5	3	7	2	128	0.045	ICD
14	CFRP	2.5	3	8	2.5	96	0.054	ICD
15	CFRP	2.5	4	7	2	215	0.042	ICD
16	CFRP	2.5	4	8	2.5	157	0.046	ICD
17	CFRP	2.5	4	9	2.5	122	0.051	ICD
18	CFRP	2.5	5	8	2.5	235	0.043	ICD
19	CFRP	2.5	5	9	2.5	176	0.044	ICD
20	CFRP	2.5	5	10	2.5	140	0.048	ICD

Failure mode*: FL = Flexural, ICD = Intermediate crack-induced debonding, LTB = Lateral torsional buckling

Table 6-2 Load capacities and failure modes of proposed models (cont.)

No.	FRP Retrofit	f_c' (ksi)	Slab thickness (in)	Beam spacing (ft)	FRP length (ft)	Load capacity (psf)	Max. corresp. Deflection (in)	Failure mode*
21	GFRP	2.5	3	6	2	177	0.039	ICD
22	GFRP	2.5	3	7	2	127	0.045	ICD
23	GFRP	2.5	3	8	2.5	95	0.053	ICD
24	GFRP	2.5	4	7	2	212	0.042	ICD
25	GFRP	2.5	4	8	2.5	156	0.045	ICD
26	GFRP	2.5	4	9	2.5	120	0.050	ICD
27	GFRP	2.5	5	8	2.5	235	0.043	ICD
28	GFRP	2.5	5	9	2.5	176	0.045	ICD
29	GFRP	2.5	5	10	2.5	136	0.047	ICD
30	None	3	3	5	-	222	0.034	FL
31	None	3	3	6	-	153	0.045	FL
32	None	3	3	7	-	111	0.048	FL
33	None	3	3	6	-	243	0.034	FL
34	None	3	3	7	-	169	0.036	FL
35	None	3	4	8	-	129	0.044	FL
36	None	3	4	9	-	107	0.056	FL
37	None	3	4	7	-	260	0.033	FL
38	None	3	5	8	-	189	0.035	FL
39	None	3	5	9	-	147	0.042	FL
40	None	3	5	10	-	121	0.045	FL

Failure mode*: FL = Flexural, ICD = Intermediate crack-induced debonding, LTB = Lateral torsional buckling

Table 6-2 Load capacities and failure modes of proposed models (cont.)

No.	FRP Retrofit	f_c' (ksi)	Slab thickness (in)	Beam spacing (ft)	FRP length (ft)	Load capacity (psf)	Max. corresp. Deflection (in)	Failure mode*
41	CFRP	3	3	6	2	209	0.043	ICD
42	CFRP	3	3	7	2	147	0.049	ICD
43	CFRP	3	3	8	2.5	111	0.058	ICD
44	CFRP	3	4	7	2	248	0.046	ICD
45	CFRP	3	4	8	2.5	184	0.049	ICD
46	CFRP	3	4	9	2.5	141	0.054	ICD
47	CFRP	3	5	8	2.5	255	0.043	LTB
48	CFRP	3	5	9	2.5	205	0.049	ICD
49	CFRP	3	5	10	2.5	160	0.051	ICD
50	GFRP	3	3	6	2	207	0.043	ICD
51	GFRP	3	3	7	2	147	0.048	ICD
52	GFRP	3	3	8	2.5	109	0.057	ICD
53	GFRP	3	4	7	2	244	0.045	ICD
54	GFRP	3	4	8	2.5	184	0.049	ICD
55	GFRP	3	4	9	2.5	141	0.053	ICD
56	GFRP	3	5	8	2.5	250	0.042	LTB
57	GFRP	3	5	9	2.5	205	0.048	ICD
58	GFRP	3	5	10	2.5	160	0.050	ICD

Failure mode*: FL = Flexural, ICD = Intermediate crack-induced debonding, LTB = Lateral torsional buckling

6.3 Interpretation of Results

The numerical results in Table 6-2 were plotted in term of load carrying capacity. The effect of each parameter was also discussed herein.

6.2.1 Effect of WWF Location

As mentioned above, the ACI 360R (2010) requires WWF to be placed in the upper one-third of the slab. In construction practices, however, it is often difficult to follow the requirement. Therefore, the effects of WWF locations were investigated numerically by varying WWF placements in three different locations along the depth of the slab: at 0.5 in from the top surface, at mid-depth, and at 0.5 in from the bottom surface of the slab. Figure 6-2 presents the load-displacement response of a 4-in-thick slab with support beam spacing of 8 ft and beam span of 10 ft. It is observed that the portion of the curve in the linear elastic range is not affected by the locations of WWF reinforcement, and the initial crack in the negative moment region takes place at approximately the same load level in all cases. However, the ultimate load capacity is highest when the reinforcement locates near the top surface of the slab and smallest when the reinforcement was near the bottom surface. The ultimate load capacities are 151, 148, and 144 psf for an elevated slab with WWF reinforcement located near the top surface, at the middle, and near the bottom surface of the slab, respectively. In contrast to the load capacity, .the ductility is slightly higher when the reinforcement is placed near the bottom surface. However, the change in locations of WWF slightly affects to the overall behaviors of the specimen as expected. Therefore, the effect of the

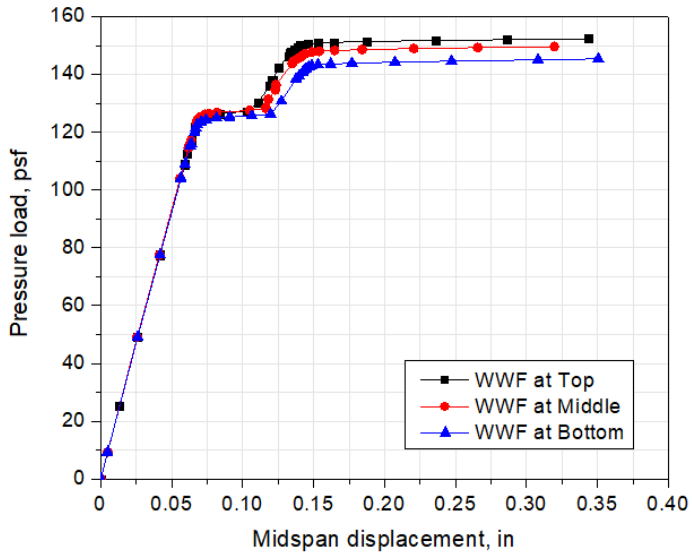

Figure 6-2 Load-displacement relationships based on different WWF locations

WWF location was neglected, and the WWF was simulated at 0.5 in from the bottom surface for all models in the current study.

6.2.2 Effect of Beam Spacing and Slab Thickness

For the examination on the effect of beam spacing and slab thickness on a one-way concrete slab, the compressive strength of concrete was selected to be 2500 psi. Load capacities of un-strengthened concrete slab with three different thicknesses varying from 3 to 5 in supported on different beam spacing ranging from 5 to 10 ft can be found in Figure 6-3. It is observed that the load capacity considerably increases with the decrease of beam spacing for any slab thickness. This is because the flexural bending moment M, linearly related to the flexural stress, are proportional to the square of the one-way slab span l. By keeping beam spacing constant at 7 ft., it can be concluded that the increase of the thickness of

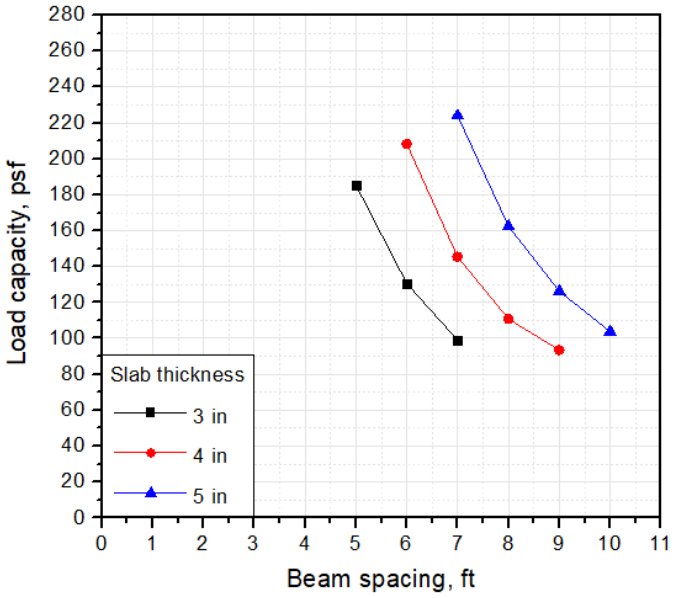

Figure 6-3 Load capacity of un-strengthened specimens for different slab thicknesses and beam spacings

a thinner slab results in significantly more enhancement of load carrying capacity, compared with a thicker slab. This is mainly due to the moment of inertia of a slab which is proportional to the cube of its thickness.

Similar to the un-strengthened slab, the load capacities of the CFRP-strengthened slab with three different thicknesses varying from 3 to 5 in supported on different beam spacing ranging from 6 to 10 ft were plotted in Figure 6-4. The figure shows that the load capacity considerably enhances with the decrease of beam spacing for any slab thickness due to the same reason discussed previously for the un-strengthened slab. At beam spacing of 8 ft., it is indicated that the increase of the thickness of a thinner slab also enhances more load carrying capacity than that of the thickness of a thicker slab does. However, the difference between the load enhancement of thinner slab and thicker slab for strengthened

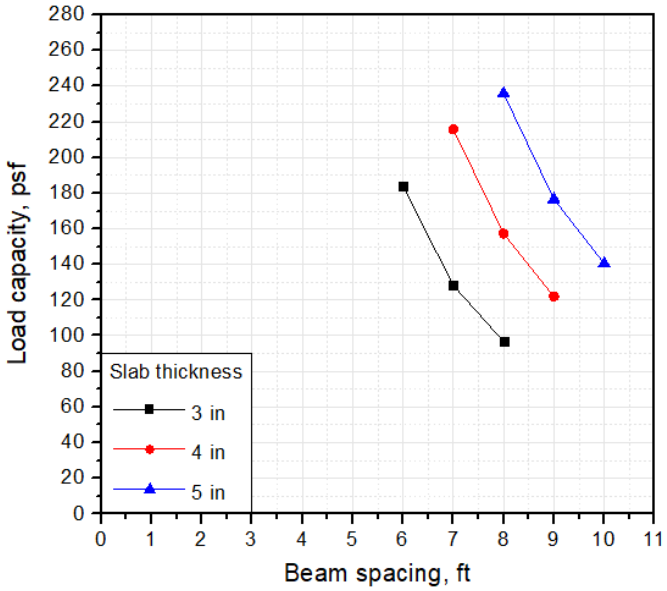

Figure 6-4 Load capacity of strengthened specimens for different slab thicknesses and beam spacings

specimens are less in comparison with un-strengthened specimens. It is because the flexural stiffness of the slabs with different thickness in the negative moment region was upgraded using the same amount of CFRP laminates. Therefore, the percent increase in the stiffness of the strengthened section for a thinner slab is greater. Consequently, this can compensate a thinner slab for its small moment of inertia. It should be noted that the CFRP system has an insignificant influence on the moment of inertia of a composite slab due to its minimal thickness.

6.2.3 Effect of CFRP Strengthening

For the investigation on the effect of CFRP strengthening system on a one-way continuous slab, the compressive strength of concrete was decided to be 2500 psi. Load capacities of un-strengthened and strengthened concrete slab with three

different thicknesses varying from 3 to 5 in supported on different beam spacing ranging from 5 to 10 ft were illustrated in Figure 6-5.

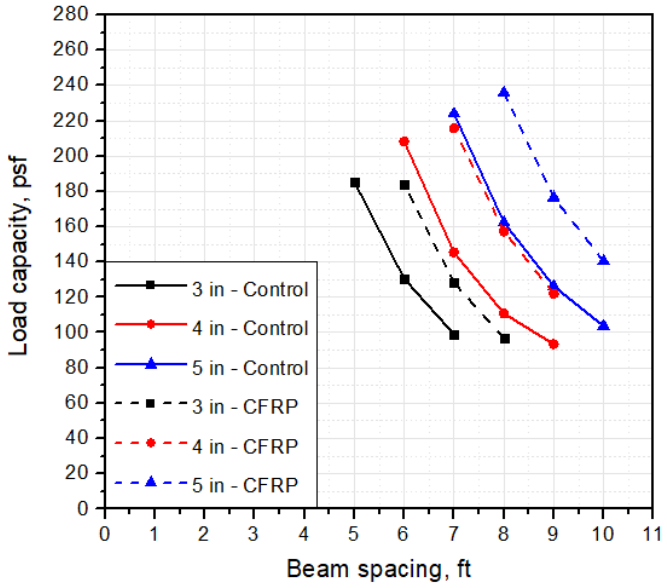

Figure 6-5 Effect of CFRP strengthening on load capacity

From the figure, it is evident that the load capacity enhancement due to the CFRP system increases with the decrease of beam spacing for any slab thickness. It is also observed that the slopes of the curves for the un-strengthened slab and strengthened slab are similar, in particular for the strengthened 4-in-thick slab and the un-strengthened, 5-in-thick slab. This characteristic is related to the flexural crack-induced debonding mode, in which all strengthened slabs in this figure failed. Since the concrete slab and CFRP system were initially assumed to have a perfect bond, tensile strains in CFRP laminates were slightly higher than those in a slab to maintain strain compatibility. Nevertheless, the tensile strength of concrete is substantially less than that of CFRP laminates. Therefore, concrete cracked before

the rupture of CFRP and caused partial debonding at the cracking area. For the foregoing reasons, the strengthened slab behaves similarly to the un-strengthened slab.

6.2.4 Effect of CFRP Types

For the study on the effect of CFRP types on a one-way continuous slab, the compressive strength of concrete was decided to be 2500 psi. Load capacities of CFRP- and GFRP-strengthened concrete slab with three different thicknesses varying from 3 to 5 in supported on different beam spacing ranging from 6 to 10 ft were shown in Figure 6-6. It can be noted that there is no significant difference in load capacities of slabs strengthened by two types of FRP sheets However, the CFRP sheets had a half-thickness of GFRP sheets. This conclusion is confirmed by Hollaway and Leeming (1999).

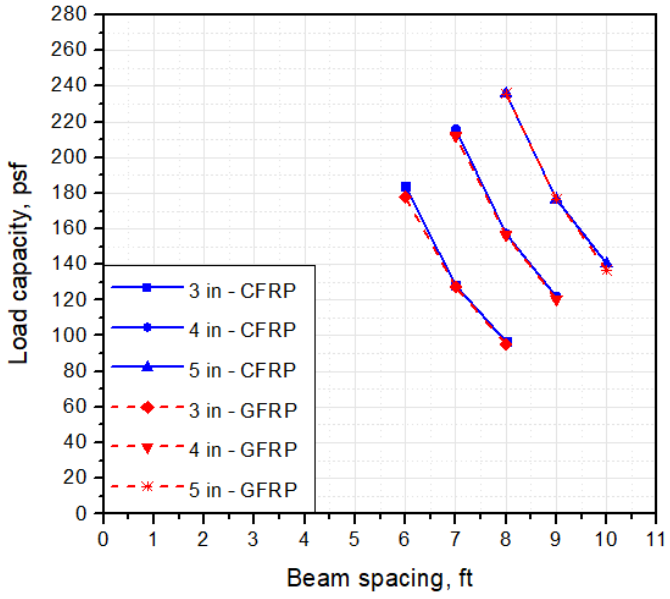

Figure 6-6 Effect of FRP type on load capacity

6.2.5 Effect of Concrete Strength

Although the minimal reinforced concrete slab in the current study failed in tension, a compressive strength was selected for the parameter study instead because it is widely used to identify the concrete strength. Elevated slabs were modeled with two different concrete compressive strengths of 2500 psi and 3000 psi to examine the effect of concrete strength. Load capacities of concrete slabs with three different thicknesses varying from 3 to 5 in supported on different beam spacing ranging from 5 to 10 ft were presented in Figure 6-7.

The enhancements of load carrying capacities due to an increase in compressive strength of concrete are mostly constant for any slab thickness and beam spacing. This is because the constitutive model used in the FEA simulation defines the ascending portion of the stress-strain behavior of concrete under

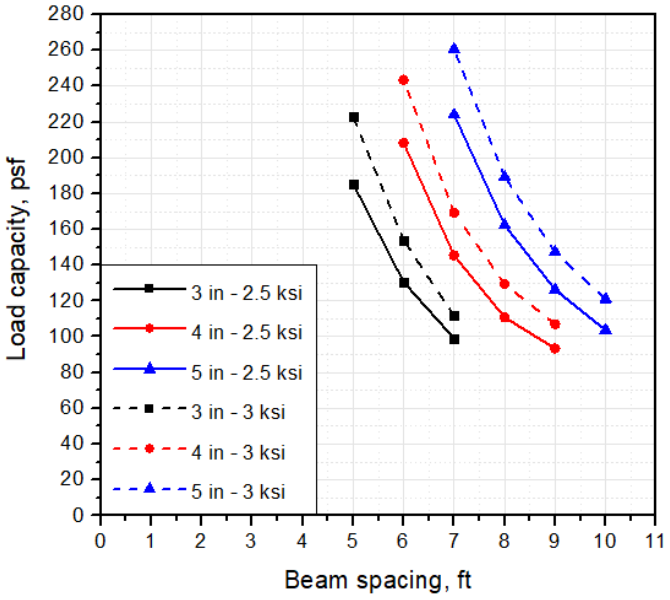

Figure 6-7 Effect of concrete strength on load capacity of un-strengthened specimens

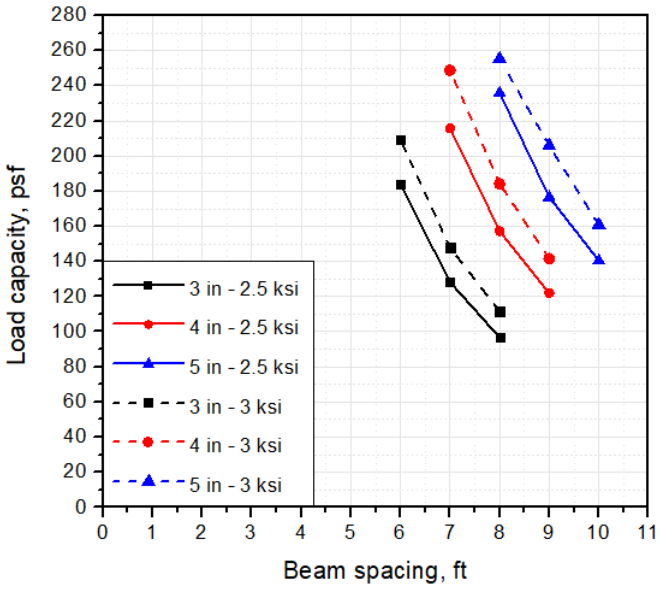

Figure 6-8 Effect of concrete strength on load capacity of CFRP strengthened specimens

tension to be a linear relationship until failure as depicted in Figure 3-6. The tensile strength was assumed to be 10% of the compressive strength of concrete in the analyses. Considering slabs with the same thickness and support beam spacing but different compressive strengths, the tensile stress on top surface increased proportionally to an increase of the applied load. Consequently, load capacity enhancement of a slab is directly proportional to an increase of the tensile strength.

Similar to the un-strengthened slab, the load capacities of the CFRP-strengthened slab were plotted in Figure 6-8. It is observed that the enhancements of load carrying capacities due to an increase in compressive strength of concrete are nearly constant for any slab thickness and beam spacing except for the 5-in-thick slab with beam spacing of 8 ft. This was due to the failure of the support beam in lateral-torsional buckling mode, which was discussed in the next subsection.

6.2.6 Lateral Torsional Buckling

The CFRP-strengthened slab with the thickness of 5 in and beam spacing of 8 ft was examined in detail. The crack pattern depicted in Figure 6-9 indicates that the failure of the elevated slab was caused by the failure of a support beam before the crack propagated through the top surface of the slab.

The deformed shapes and stress contour of the internal support beam at a total load of 225 psf and 264 psf are illustrated in Figure 6-10 (a) and (b), respectively. It was observed that the large deformation initially occurred in the web at the mid-depth of the beam. Moreover, the stress contour at a total load of

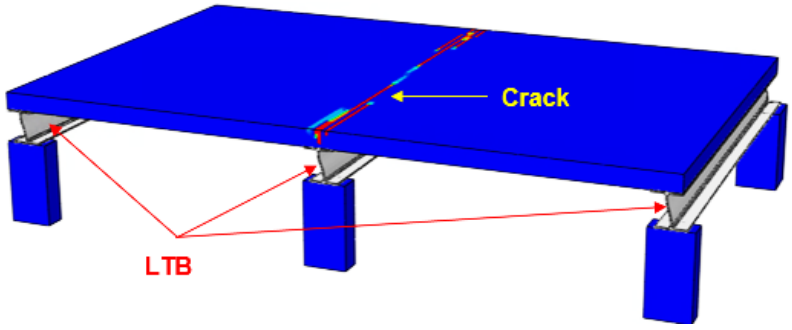

Figure 6-9 Lateral torsional buckling of steel beams and crack patterns

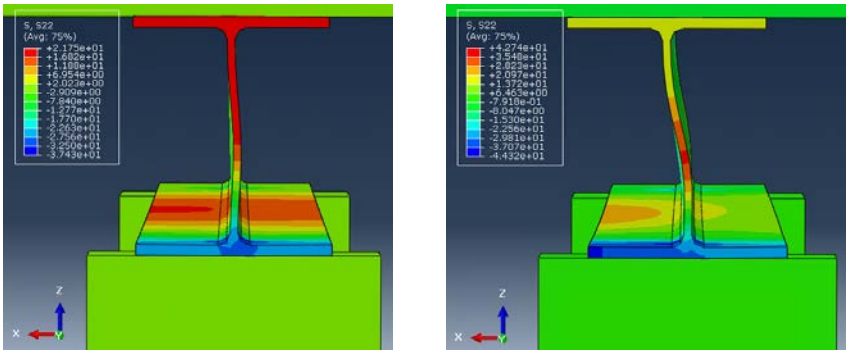

(a) At total load of 255 psf (b) At total load of 264 psf

Figure 6-10 Deformed shape and stress contour of the internal beam

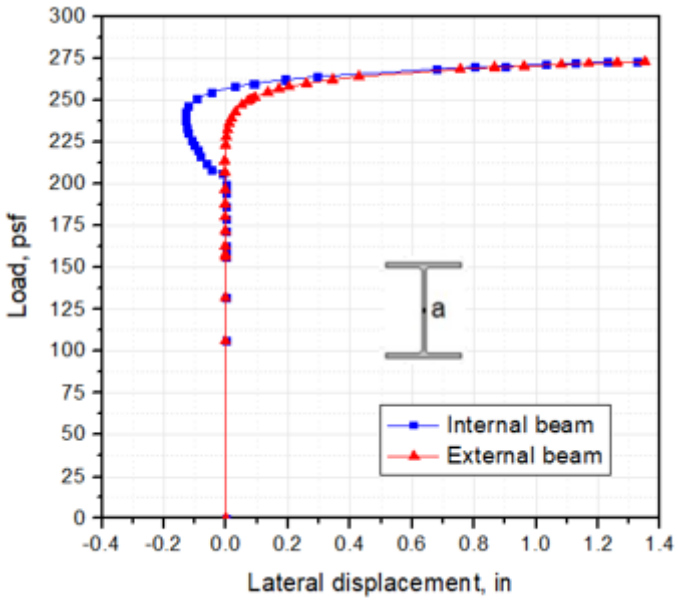

Figure 6-11 Load-displacement relationship at mid-depth of support beam

225 psf indicates the high compressive stress located on the top half of the beam causing the lateral torsional buckling.

Since the support beam began buckling at the mid-depth, the load-displacement relationship at point “a” of internal and external beam were plotted as shown in Figure 6-11. It can be concluded from the figure that the external beam started to deformed at load level of approximately 207 psf, while the internal beam buckling at a total load of approximately 243 psf. As the load increases, the lateral displacement significantly enhances until the specimen collapses at the load of approximately 264 psf

6.4 Soil-Structure Interaction

Soils beneath a foundation often cause problems with respect to the serviceability performance of SOG houses. The settlements in soils under the combination of factored dead and live load create stresses which can result in cracking of the slab. This issue is particularly common in light-reinforced or plain concrete slabs because such slabs are relatively thin and brittle. Elevating damaged or cracked SOG is considered an extremely high threat to the safety of the occupants. Therefore, FEA models of a typical SOG on different types of soils were performed to examine the structural behaviors of the slab influenced by the response of soils.

6.3.1 Texas Soil

Since Texas has a wide diversity of climates, landscapes, and geologies, there are more than 1300 different types of soils according to the Natural Resources Conservative Service (2018). However, in the current study, the FEA models were simulated with three basic soil types: loose sand, medium sand, and soft clay. Expansive clay soil is a severe hazard for the overlying structures because of the high shrink-swell potential that is related to a change in moisture content. Soils with some clay minerals such as montmorillonite have the most shrink-swell capacity. Figure 6-12 depicts the abundance of montmorillonite in the United States. Therefore, high swelling soils can scarcely be found in the coastal areas adjacent to the Gulf of Mexico where residential houses are prone to severe flooding.

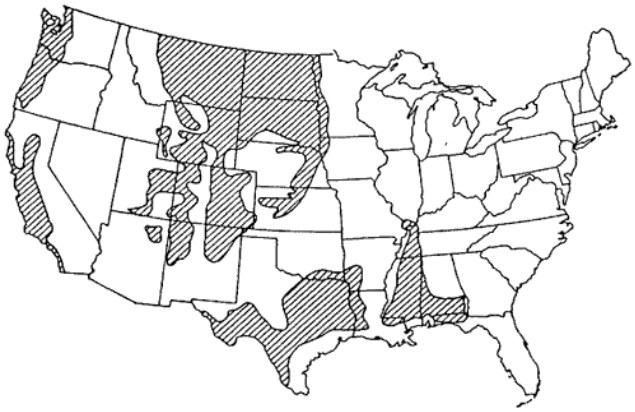

Figure 6-12 General abundance of montmorillonite in near outcrop bedrock formations (Chen, 2012)

6.3.2 Numerical Model

A 3D finite element model was developed for simulation of SOG and soil using the Mohr-Coulomb failure criterion for soil continuum which was defined as an elastic-perfectly plastic model. Young's modulus E and Poisson's ratio ν were utilized to define the stress-strain behavior of the model in the elastic range. The failure criterion was defined by two parameters: the internal friction angle φ and cohesion c. Dilation angle ψ was used to describe an amount of the change in volumetric strain regarding the change in shear strain. Table 6-3 summarizes the material properties of three different soil types used in the analyses. Normal and Tangential contact behaviors were assigned to model the slab-to-soil interaction for which the master surface was the bottom surface of the slab and the slave surface was the top surface of the soil. Surface-to-surface contact was implemented because it yielded a high accuracy of the results in comparison with node-to-node contact (Hibbit et al., 2007; Sinha and Hanna, 2016).

A relatively fine mesh was adopted in the vicinity of the slab and a mesh became coarser at a distance from the slab with a smooth transition as shown in Figure 6-13. The typical slab was 32 ft wide x 50 ft long x 4 in thick as presented in Figure 3-2. The soil was initially modeled with the dimensions of 3B wide x 3B long x 1.5B deep where B is slab width according to the soil model done by Abdelmalak (2007). The soil dimensions were adjusted based on the results of the analyses until the restrained nodes at the boundaries were slightly or not at all affected by external loads in terms of displacement and stress (Figure 6-13 and 6-14). The proper dimensions of 80 ft wide x 80 ft long x 100 ft deep were eventually achieved. Since geometries, material properties, load were symmetric in two directions, only one quarter of the SOG and soils were simulated using symmetry boundary conditions to reduce computational resources and time. A summary of the boundary conditions was illustrated in Figure 6-13. The factored dead and live load were combined and applied on the slab. The live load was taken to be 40 psf following the minimum requirement for residential homes in ASCE 7-10 standard.

Table 6-3 Material properties of soils

Parameters	Loose sand	Medium sand	Soft clay
Young's modulus, psi	2900	4350	2176
Poisson's ratio	0.35	0.35	0.2
Internal friction angle, º	35	40	20
Dilation angle, º	5	10	0
Cohesion, psi	0.725	0.725	1.45

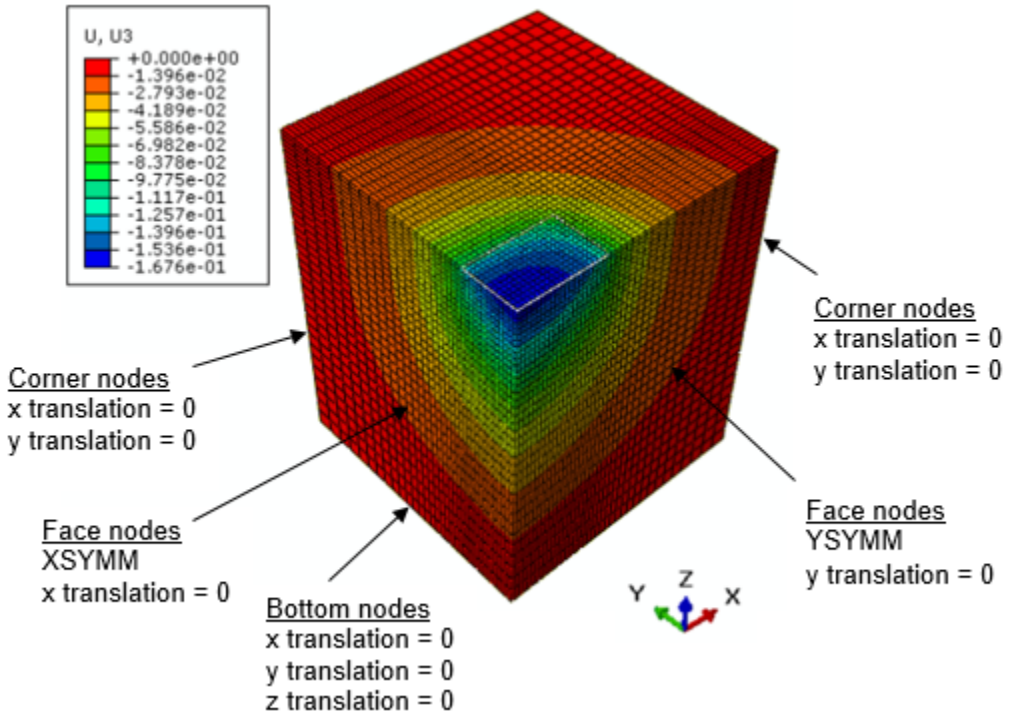

Figure 6-13 Meshing, boundary condition, and vertical displacement contour of SOG and soft clay

To produce a credible model and obtain accurate results, the model validation was conducted during the development of the models. The numerical results were compared with the pressure isobars proposed by Bowles (2001). Figure 6-15 shows the pressure isobars, also called pressure bulbs, which is a line of constant vertical stress beneath a continuous and square footing. The magnitude of the stresses are expressed in term of an applied pressure load, and the stress contour are related to the width of the footing. It can be noted that there was a good correlation between the numerical results and the theoretical results of pressure isobars.

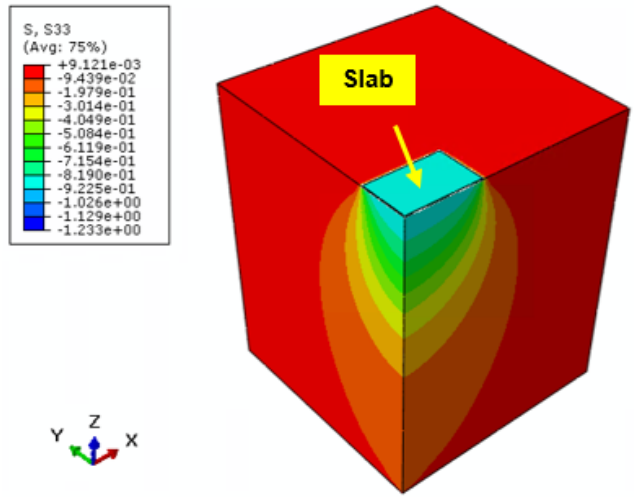

Figure 6-14 Vertical stress contour of SOG and soft clay

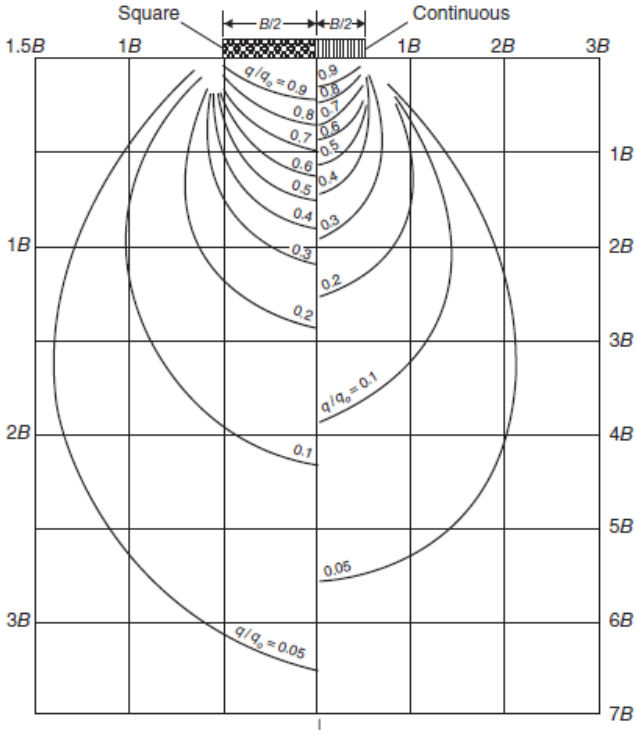

Figure 6-15 Pressure isobars (also called pressure bulbs) for square and continuous footings (Bowles, 2001)

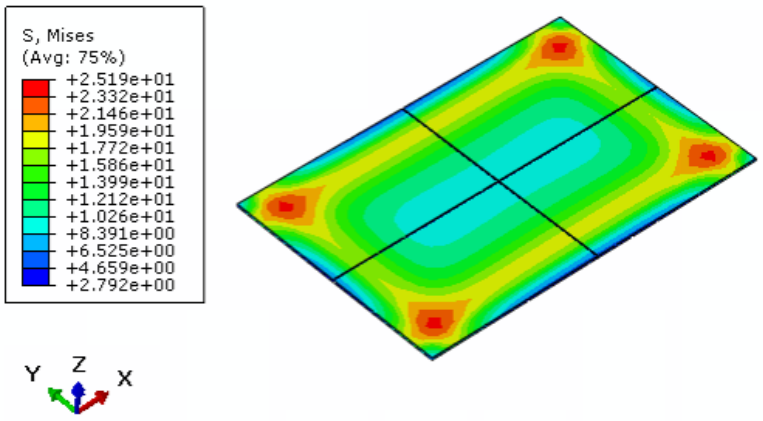

Figure 6-16 Stress contour of SOG

The results of the analyses indicated that the maximum deflection occurred at the center of the slab. The maximum stresses took place at the corners of the slab while relatively high stresses were located at approximately 4 feet from the edge along the parameter of the slab as shown in Figure 6-16. Since a concrete slab curled to a concave configuration under the pressure load, the bottom surface of the slab was under tension. Maximum deflections, stresses, and strains of a slab on different soil types were summarized in Table 6-4. Out of three cases, a slab on soft clay was experienced the largest tensile stress of 25 psi which is substantially less than the tensile strength of concrete. It can be concluded that

Table 6-4 Summary of numerical results of SOG

Soil type	Max. deflection (in)	Max. tensile stress (psi)	Max tensile strain (με)
Loose sand	0.12	21	5.9
Medium sand	0.08	16	4.7
Soft clay º	0.17	25	7.2

SOG on Texas soils is most likely undamaged under the minimum required live load for residential houses. However, the tensile stress of the SOG is significantly increased after elevation. Therefore, an elevated SOG must be supported by the appropriate beam and column spacing and also strengthened to provide adequate safety for homeowners.

Chapter 7
Conclusions and Recommendations

7.1 Summary of Findings and Conclusions

The current research aim to evaluate and develop a better understanding on elevated slabs on grade strengthened with FRP laminates. The structural behaviors of a SOG before and after elevation were investigated through experimental and theoretical study. This study was successful in determining the response of an elevated SOG and providing appropriate strengthening techniques to improve structural capacities of such slabs. The following conclusions can be drawn from this study:

- A single-layer externally-bonded CFRP is effective in delaying the crack initiation and propagation, as well as enhancing the flexural load capacity of 30.3% over the control slab.
- Strengthening an elevated SOG with CFRP application results in a decrease of overall deflection and ductility of the structure.
- The modes of failure changed from brittle flexure failure to intermediate flexural crack-induced debonding.
- Crack initiation and crack development of the slab are related to the stiffness of the support beams.
- The effects of internal WWF locations to the overall responses of the specimen are insignificant.

- The load capacity substantially increases with the decrease of beam spacing for an un-strengthened and strengthened slab.
- The increase of the thickness of a thinner slab results in significantly more enhancement of load carrying capacity, compared with a thicker slab for an un-strengthened and strengthened slab.
- The CFRP system exhibited more effectiveness on the load capacity enhancement with less support beam spacing.
- For the FRP sheets used in the current study, GFRP laminates needed to be two times thicker than CFRP laminates in order to provide the same tensile stiffness.
- Load capacity enhancement of a slab is directly proportional to an increase of the concrete tensile strength.
- In construction practices, the locations of additional columns and supported steel beams should be determined based on the interior layout of an elevated house to provide sufficient spaces over the floor for CFRP application.

7.2 Future Research

Since the available methodology and know-how for an elevated SOG house is almost nonexistent, several more investigations are need to be done. The following are the recommendations for future research work:

- More experimental tests on elevated slabs are recommended to be carried out for the numerical model validation in order to provide more accurate results.
- The effect of additional parameters are needed to be examined including:
  - Type of slab-to-beam and beam-to-column connection
  - FRP-strengthened area such as the positive moment region
  - Type of support beam
  - Size of support beam
- The performance of CFRP strengthening system on repairing the cracked SOG after elevation is suggested to be investigated.
- Since a grid pile system also appears to be widely used to support elevated houses, it will be useful to study the structural behaviors of an elevated SOG on a grid pile system
- The current numerical study did not investigate the effects of expansive soils on a SOG foundation. It is suggested to develop the numerical models of a SOG under a more severe scheme by incorporating soils with high shrink-swell potential.

Appendix A
Preliminary Design

Slab Design

General information

A 50 ft x 32 ft slab with a thickness of 4 in. was taken as a typical SOG. The tensile strength of slab was taken to be 250 psi. This analysis example uses the Flexure Formula, in which the slab is divided into longitudinal 1-ft strips, assumed to be supported on rigid beams.

Factored dead and live loads

$$DL_{slab} = \frac{4}{12}\, x\, 150 = 50\, psf$$

$$LL_{slab} = 40\, psf$$

$$TL_{slab} = 1.2(50) + 1.6(40) = 124\ psf$$

Flexural capacity of the slab

A 1-ft strip of the slab is equally divided to seven spans using eight support beams. Each span is approximately 7.15 ft.

$$M^{-}_{Max} = -0.106\, wl^2 = -0.106\,(124)(7.15)^2 = -670\, lb \cdot ft$$

$$I_{slab} = \frac{bh^3}{12} = \frac{(12)(4)^3}{12} = 64\ in^4$$

$$\sigma_x = \frac{Mc}{I} = \frac{(670\, x\, 12)x\, 2}{64} = 251.25\ psi \geq 250\, psi$$

Thus, the minimum beam spacing that causes crack on the slab under the combined load is 7.15 ft.

Appendix B
Material Properties

Concrete properties

MIX DESIGN PARAMETERS

[1] **Minimum Compressive Strength: 2500 psi @ 28 Days** — **Sack Content: 4.50**

Air Content: 1.5% +/- 1% — **Fly Ash Content: 20%**

[2] **Slump Range (inches): 4 +/- 1" (After the addition of WR Admixtures)**

W/Cm Ratio (lb/lb): 0.58 (6.56 gal/sk) — **Theoretical Plastic Unit Weight: 149.9 pcf**

One Cubic Yard Mix Proportions

Materials	ASTM Standards			Weights per Cubic Yard, SSD	Absolute Volume
Cement	ASTM C 150	Type I/II Cemex		338 lbs.	1.72 cu.ft.
Fly Ash	ASTM C 618	Class C Charah		85 lbs.	0.53 cu.ft.
Coarse Aggregate	ASTM C33	Size #57	1" Limestone	1850 lbs.	11.15 cu.ft.
Fine Aggregate	ASTM C 33	Bristol Sand		384 lbs.	2.31 cu.ft.
Fine Aggregate	ASTM C 33	Bridgeport Sand		1145 lbs.	6.95 cu.ft.
Admixture 1	ASTM C 494	Type A (Sika 686)	5.0 oz./cwt.	21.2 oz.	
City Water	ASTM C1602		29.5 gal.	246 lbs.	3.94 cu.ft.
				Air Void	0.41 cu.ft.
					27.00 cu.ft.

[1]This design will meet or exceed design strengths when tested and evaluated in accordance with applicable ASTM test methods and standards, and when concrete is placed and cured using recommended construction practices. Only strength specimens molded and initially cured per Sec. 10 ASTM C 31-03a will be considered for acceptance, in accordance with ACI 318 Sec. 5.6.

[2]Slump achieved after the addition of water-reducing admixtures.

[3]Admixture dosages and Type will vary, depending on average concrete temperatures and specific job conditions.

Strength Comparisons

Laboratory Trial Batches - 20% Flyash, MRWR

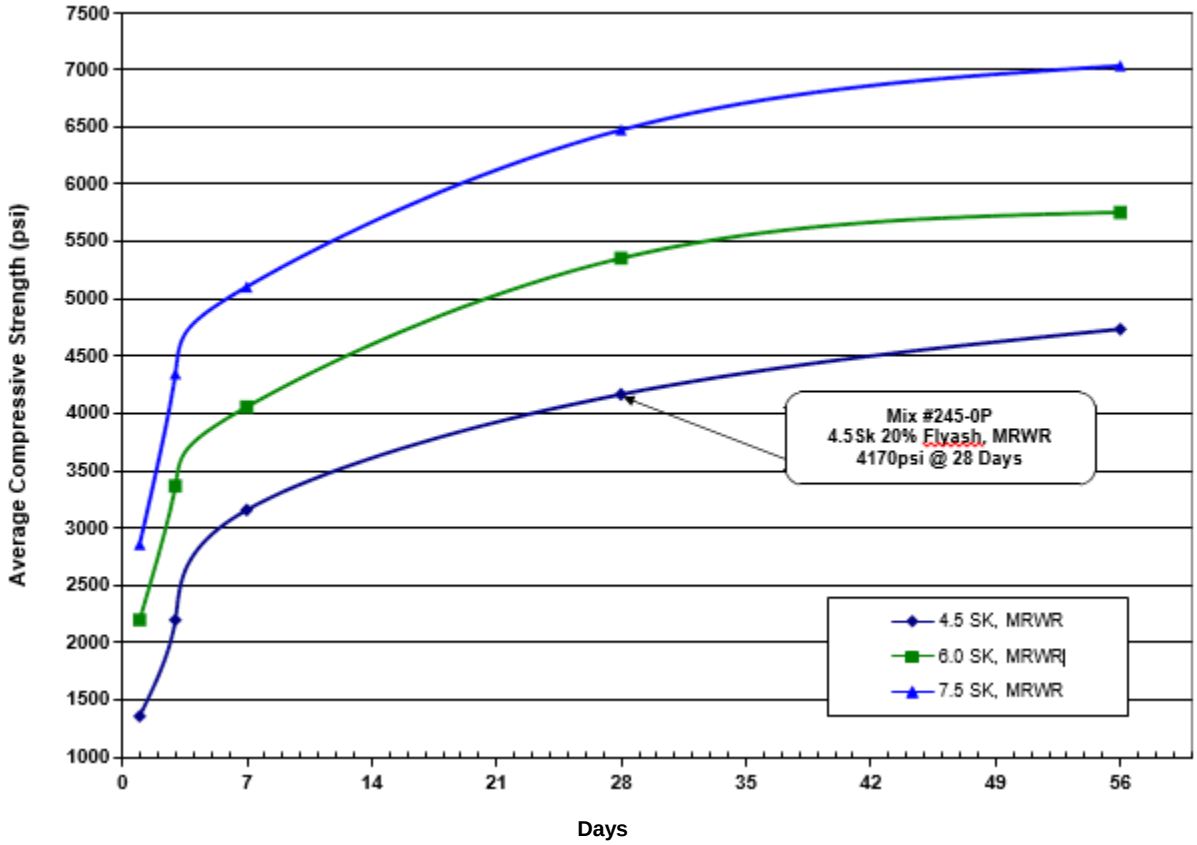

		1		2		3	
		4.5 SK, MRWR		6.0 SK, MRWR		7.5 SK, MRWR	
Mix		245-0		260-0		275-0	
Ash Grove Cement - Type I/II			**423**		**564**		**705**
Cemex Balcones - Type I/II		**338**		**451**		**564**	
Boral Class F		**85**	**20%**	**113**	**20%**	**141**	**20%**
Perch Hill Size #57		**1850**	**2.68**	**1850**	**2.68**	**1850**	**2.68**
Hanson Bristol		**388**	**2.658**	**350**	**2.658**	**313**	**2.658**
Bridgport C33		**1164**	75%	**1051**	75%	**940**	75%
Design Water		**246**	After Dosing Admixture-->	**256**	After Dosing Admixture-->	**265**	After Dosing Admixture-->
Actual Water Used-->		**259**		**267**		**276**	
Water/Cementitious Ratio		0.58		0.45		0.38	
Percent Water Reduction							
W/C+P Ratio (Actual)		0.61		0.47		0.39	
Sika 686	Dose, oz / cwt	**6.0**		**6.0**		**6.0**	
	Dose, oz / yd	25.4		33.8		42.3	
Sika AEA	Dose, oz / cwt						
	Dose, oz / yd						
	Dose, oz / cwt						
	Dose, oz / yd						
	Dose, oz / cwt						
	Dose, oz / yd						
	Dose, oz / cwt						
	Dose, oz / yd						
	Dose, oz / cwt						
	Dose, oz / yd						
Designed Air%		**1.5%**		**1.5%**		**1.5%**	
Time Batched		9:51	10:10	10:12	10:47	11:14	11:29
Slump as Batched/spread		4.00		5.50		5.50	
Unit Weight (PCF)		36.90	148.19	36.85	147.99	36.90	148.19
C231 Air**%**(pressure method)		2.7%		2.3%		2.0%	
Air / Concrete Temp. (°F)		70		70		70	
Yield (cf/cy)			27.56		27.59		27.56
Time of Set (hrs)	**150 psi**						
	Initial (500 psi)						
Compressive Strengths (psi)	**11/4/2015**	**4**	**" Molds**	**12.57**	**Square inch of surface area**		
		Load	PSI	Load	PSI	Load	PSI
	11/05/2015	17100	1360	27657	2200	35931	2860
	Ave. 1 Day:		**1360**		**2200**		**2860**
	11/07/2015	26908	2140	41894	3330	54230	4320
	11/07/2015	28320	2250	42818	3410	55100	4380
	Ave. 3 Day:		**2200**		**3370**		**4350**
	11/11/2015	40500	3220	51351	4090	62125	4940
	11/11/2015	39493	3140	50461	4020	64544	5140
	11/11/2015	39209	3120	51378	4090	65954	5250
	Ave. 7 Day:		**3160**		**4060**		**5110**
	12/02/2015	51336	4090	68638	5460	81520	6490
	12/02/2015	53155	4230	67083	5340	80450	6400
	12/02/2015	52581	4180	66325	5280	82150	6540
	Ave. 28 Day:		**4170**		**5360**		**6480**
	12/30/2015	59613	4740	72407	5760	88521	7040
	Ave. 56 Day:		**4740**		**5760**		**7040**

	AASHTO-M295 Class "C" Requirements	ASTM C-618 Class "C" Requirements	Actual
Fineness (+325 Mesh)	34% Max	34% Max	14.70%
Moisture Content	5.0% Max	5.0% Max	0.08%
Density g/cm^3 C188	3.0% Max	3% Max	2.59
Density Variation	5.0% Max	5.0% Max	3.14%
Loss on Ignition	5.0% Max	6% Max	0.33%
Soundness	0.8% Max	0.8% Max	0.01%
S.A.I., 7 Days	75% Min	75% Min	104.70%
S.A.I., 28 Days	75% Min	75% Min	107.20%
Water Req. % Control	105% Max	105% Max	95.00%
Silica SiO_2	****	****	38.01%
Aluminum Oxide Al_2O_3	****	****	21.08%
Ferric Oxide Fe_2O_3	****	****	6.01%
Total	50% Min	50% Min	65.10%
Sulfur Trioxide SO_3	5% Max	5.0% Max	1.44%
Calcium Oxide CaO	****	****	24.42%
Magnesium Oxide MgO	****	****	5.18%
Available Alkalies as Na_2O	1.50% Max	****	1.29%

Steel properties

	CUSTOMER SHIP TO	CUSTOMER BILL TO	GRADE	SHAPE/SIZE	DOCUMENT ID
			A992/A572-50	Wide Flange Beam/ 10x33 / 250x49.1	0000127104
	SALES ORDER	CUSTOMER MATERIAL NO.	LENGTH	WEIGHT	HEAT/BATCH
			40’00”	15,840 LB	59075202/02

CUSTOMER PURCHASE ORDER NUMBER	DATE	SPECIFICATION/DATE or REVISION
	06/25/2017	ASTM A6-14 ASTM A709-15 ASTM A992-11 (2015), A572-15 CSA G40.21-13 345WM

CHEMICAL COMPOSITION

C	Mn	P	S	Si	Cu	Ni	Cr	Mo	Sn	V	Nb	Al
%	%	%	%	%	%	%	%	%	%	%	%	%
0.08	0.95	0.010	0.036	0.29	0.30	0.10	0.13	0.010	0.006	0.002	0.016	0.004

CHEMICAL COMPOSITION

CE A6
%
0.30

MECHANICAL PROPERTIES

YS 0.2%	UTS	YS	UTS	Y/T ratio	G/L	G/L	Elong.
PSI	PSI	MPa	MPa	%	Inch	mm	%
53974	69440	372	479	0.780	8.000	200.0	23.50
54118	70588	373	487	0.770	8.000	200.0	23.40

COMMENTS/NOTES

Appendix C
ABAQUS Input

Compressive behavior of concrete with compressive strength of 2500 psi for CDP material model

Stress (σ_c)	Strain (ε_c)	Inelastic strain ($\tilde{\varepsilon_c^{in}}$)	d_c
0	0	-	-
898	0.00025	-	-
1250	0.00041	0	0
1836	0.00075	0.0002390	0
2108	0.00100	0.0004133	0
2282	0.00125	0.0006148	0
2390	0.00150	0.0008348	0
2454	0.00175	0.0010672	0
2487	0.00200	0.0013080	0
2499	0.00225	0.0015547	0
2500	0.00230	0.0016044	0
2486	0.00275	0.0020581	0.0054
2469	0.00300	0.0023130	0.0124
2446	0.00325	0.0025692	0.0213
2422	0.00350	0.0028261	0.0312
2395	0.00375	0.0030836	0.0420
2367	0.00400	0.0033412	0.0530
2339	0.00425	0.0035990	0.0642
2311	0.00450	0.0038570	0.0756
2283	0.00475	0.0041148	0.0868
2255	0.00500	0.0043725	0.0980

Tensile behavior of concrete with compressive strength of 2500 psi for CDP material model

Stress (σ_t)	Strain (ε_t)	Cracking strain ($\tilde{\varepsilon_t^{ck}}$)	d_t
0	0	-	-
250	0.00008772	0	0
192.5	0.00010965	0.00004211	0.23
112.5	0.00035087	0.00031140	0.55
25	0.00076315	0.00075439	0.90

Tensile behavior of WWF for bilinear elastic-strain hardening material model

Stress (σ_t)	Plastic strain ($\tilde{\varepsilon_t^{pl}}$)
65000	0
75000	0.012

Tensile behavior of steel for bilinear elastic-strain hardening material model

Stress (σ_t)	Plastic strain ($\tilde{\varepsilon_t^{pl}}$)
50000	0
65000	0.18

CFRP-concrete interfacial properties for surface-based cohesive behavior material model and damage model

K_{nn}	K_{ss}	K_{tt}	Normal	Shear-1	Shear-2
1469	582	582	1.72	3.21	3.21

Appendix D

Design Chart

Load capacities of elevated SOG without FRP strengthening system

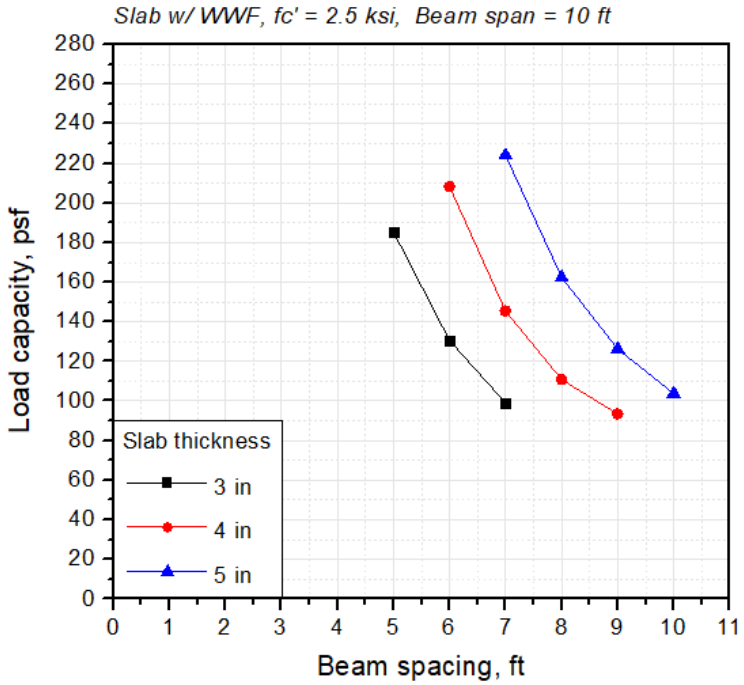

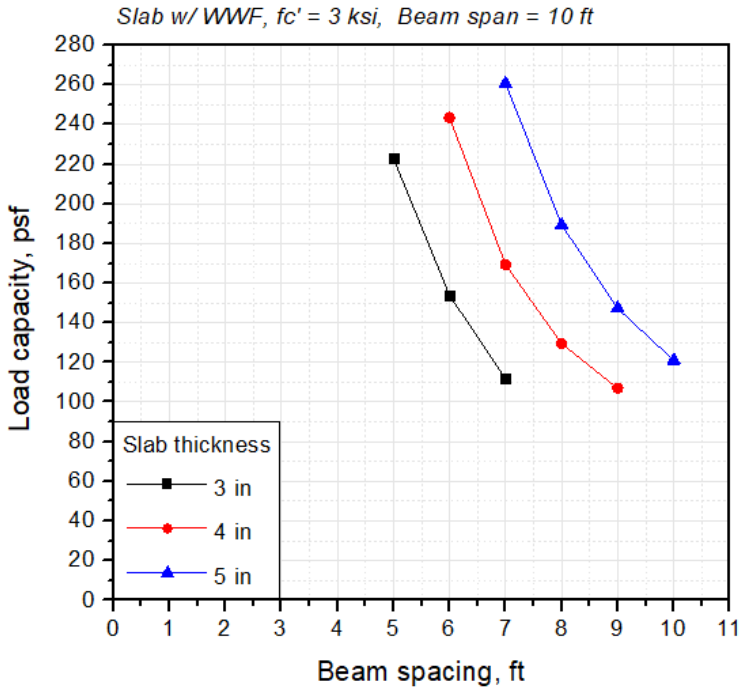

Load capacities of elevated SOG with CFRP strengthening system

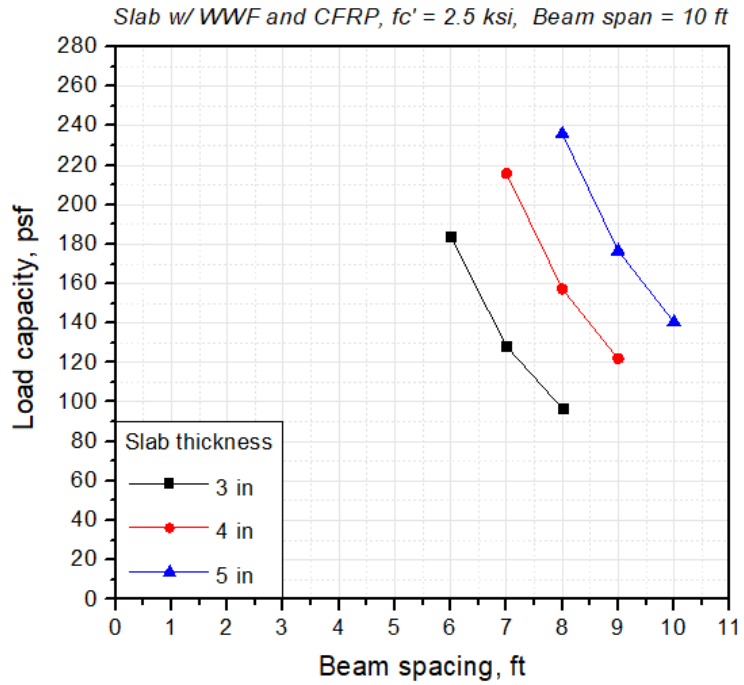

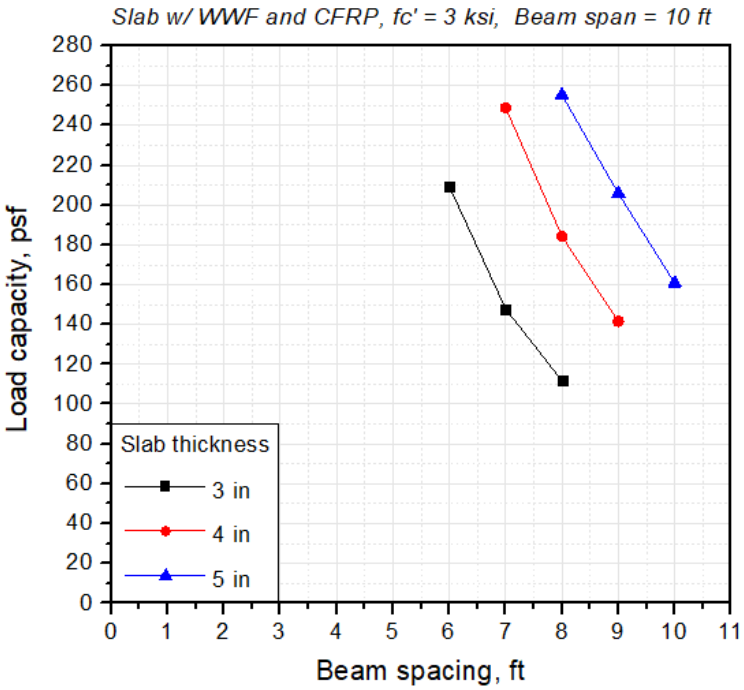

Load capacities of elevated SOG with GFRP strengthening system

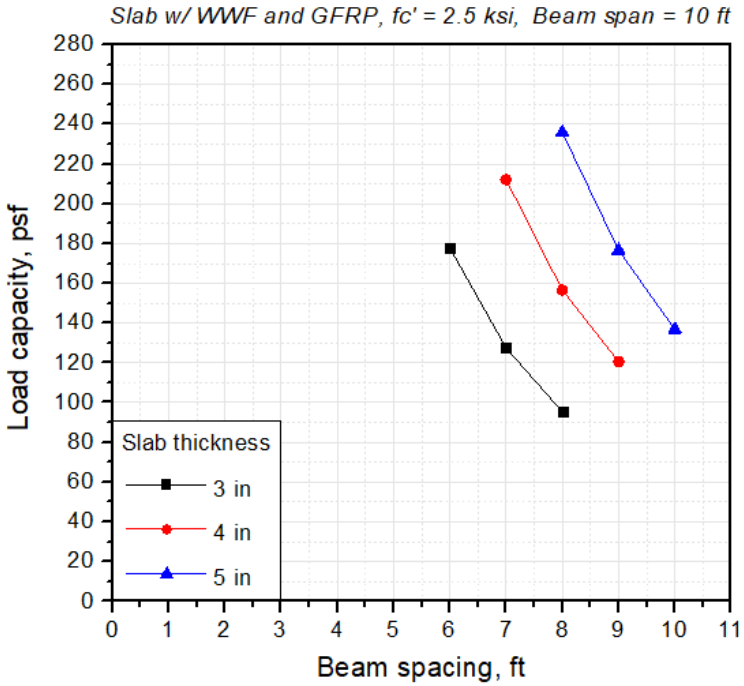

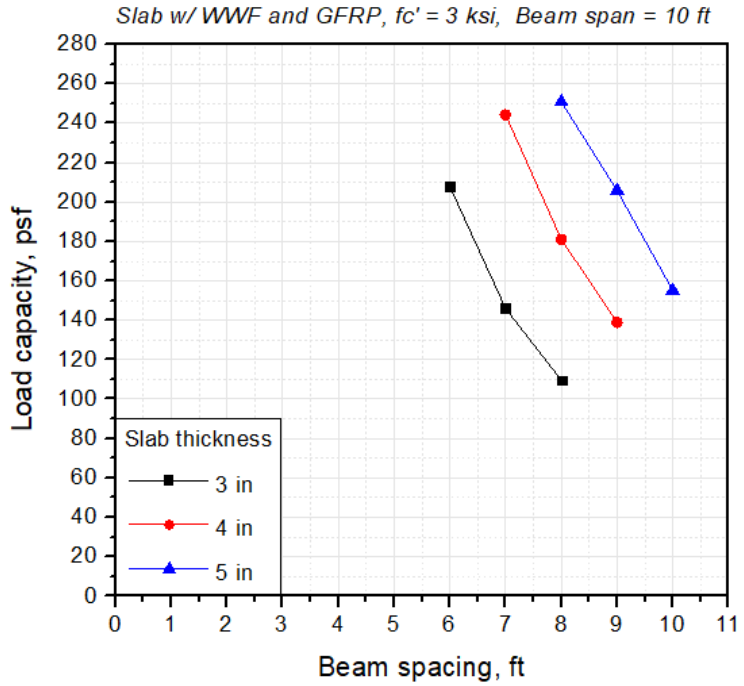

References

ABAQUS, V. (2014). “ABAQUS standard user’s manual.” *Version 6.14, vol. I–III*, Pawtucket (America): Hibbitt, Karlsson & Sorensen, Inc.

Abdelmalak, R. I. (2007). *Soil structure interaction for shrink-swell soils “A new design procedure for foundation slabs on shrink-swell soils.”* Texas A&M University.

Abdulrahman, B. Q., Wu, Z., & Cunningham, L. S. (2017). “Experimental and numerical investigation into strengthening flat slabs at corner columns with externally bonded CFRP.” *Construction and Building Materials*, *139*, 132-147.

ACI (American Concrete Institute). (2010). “Guide to design of slabs-on-ground.” *ACI 360R-10*, Farmington Hills, MI.

ACI (American Concrete Institute). (2010). “Specification for Tolerances for Concrete Construction and Materials and Commentary.” *ACI 117-10*, Farmington Hills, MI.

ACI (American Concrete Institute). (2013). “Building Code Requirements and Specification for Masonry Structures and Companion Commentaries.” *ACI 530/530.1-13*, Farmington Hills, MI.

ACI (American Concrete Institute). (2014). “Building code requirements for structural concrete.” *ACI 318-14*, Farmington Hills, MI.

ACI (American Concrete Institute). (2014). “Residential code requirements for structural concrete and commentary.” *ACI 332-14*, Farmington Hills, MI.

ACI (American Concrete Institute). (2017). “Guide for the design and construction of externally bonded FRP systems for strengthening concrete structures.” *ACI 440.2R-17*, Farmington Hills, MI.

AISC (American Institute of Steel Construction). (2011). “Steel construction manual.” *AISC 325, 14th Edition,* Chicago, IL.

Al-Rousan, R., Issa, M., & Shabila, H. (2012). Performance of reinforced concrete slabs strengthened with different types and configurations of CFRP. *Composites Part B: Engineering*, *43*(2), 510-521.

Arduini, M., Nanni, A., & Romagnolo, M. (2004). "Performance of one-way reinforced concrete slabs with externally bonded fiber-reinforced polymer strengthening." *ACI Structural Journal*, *101*(2), 193-201.

Arkitektura development Inc. (2018, May 5). "Portfolio of recent elevation projects." Retrieved from http://arkdevinc.com/home-elevation/

Arockiasamy, M., Amer, A., & Shahawy, M. (1996). "Concrete beams and slabs retrofitted with CFRP laminates." In *Engineering Mechanics* (pp. 776-779). ASCE.

ASCE (American Society of Civil Engineers). (2010). "Minimum design loads for buildings and other structures." *ASCE 7-10,* Reston, VA.

ASTM. (2006). "Standard specification for structural steel shapes." *ASTM A992/A992M-06a, ASTM International,* West Conshohocken, PA.

ASTM. (2010). "Standard test method for determining tensile properties of fiber reinforced polymer matrix composites used for strengthening of civil structures." *ASTM D7565/D7565M-10, ASTM International,* West Conshohocken, PA.

ASTM. (2017). "Standard test method for compressive strength of cylindrical concrete specimens." *ASTM C39/C39M-17b, ASTM International,* West Conshohocken, PA.

ASTM. (2017). "Standard test method for splitting tensile strength of cylindrical concrete." *ASTM C496/C496M-17, ASTM International,* West Conshohocken, PA.

Attari, N., Amziane, S., & Chemrouk, M. (2012). "Flexural strengthening of concrete beams using CFRP, GFRP and hybrid FRP sheets." *Construction and Building Materials*, *37*, 746-757.

Balendran, R. V., Rana, T. M., & Nadeem, A. (2001). “Strengthening of concrete structures with FRP sheets and plates.” *Structural Survey*, *19*(4), 185-192.

Banu, D., & Taranu, N. (2010). “Traditional solutions for strengthening reinforced concrete slabs.” *Buletinul Institutului Politehnic din lasi. Sectia Constructii, Arhitectura*, *56*(3), 53.

Belarbi, A., & Acun, B. (2013). “FRP systems in shear strengthening of reinforced concrete structures.” *Procedia Engineering*, *57*, 2-8.

Beneberu, E. S. (2016). *Hydrocarbon Pool Fire Performance of Fiber Reinforced Polymer (FRP) Strengthened and Thermally Insulated Bridge Girders* (Doctoral dissertation).

Bisby, L. A., & Williams, B. K. (2004). “An introduction to FRP strengthening of concrete structures.” *ISIS Educational Module, 4*, 1-39.

Bowles, J. E. (2001). “Foundation analysis and design.” *5th edition*, McGraw-Hill, New York.

Bukhari, I. A., Vollum, R. L., Ahmad, S., & Sagaseta, J. (2010). “Shear strengthening of reinforced concrete beams with CFRP.” *Magazine of Concrete Research*, *62*(1), 65-77.

Carolin, A. (2003). “Carbon Fiber Reinforced Polymers for Strengthening of structural elements.” *Doctoral Thesis*, Luleå University of Technology.

Carreira, D. J., & Chu, K. H. (1985). “Stress-strain relationship for plain concrete in compression.” In *Journal Proceedings* (Vol. 82, No. 6, pp. 797-804).

Carreira, D. J., & Chu, K. H. (1986). “Stress-strain relationship for reinforced concrete in tension.” In *Journal Proceedings* (Vol. 83, No. 1, pp. 21-28).

Census Bureau (2008). (2017, March 8) “Building permits survey.” Retrieved from http://www.census.gov/construction/chars/completed.html

Chajes, M. J., Januszka, T. F., Mertz, D. R., Thomson, T. A., & Finch, W. W. (1995). “Shear strengthening of reinforced concrete beams using externally applied composite fabrics.” *Structural Journal*, *92*(3), 295-303.

Chen, C. C., & Li, C. Y. (2000). “An experimental study on the punching shear behaviour of RC slabs strengthened by GFRP.” *Trita-BKN. Bulletin*, *57*, 415-422.

Chen, F. H. (2012). *Foundations on expansive soils* (Vol. 12). Elsevier.

Chen, S., & Gu, P. (2005). “Load carrying capacity of composite beams prestressed with external tendons under positive moment.” *Journal of Constructional Steel Research*, *61*(4), 515-530.

Daly, A. F., & Witarnawan, W. (1997, October). “Strengthening of bridges using external post-tensioning.” In *Conference of eastern Asia society for transportation studies, Seoul, Korea*.

Deuring, M. (1994). “Brandversuche an nachträglich verstärken Trägern aus Beton,” *EMPA Report No. 148795*. EMPA, Dübendorf, Switzerland.

Ebead, U., & Marzouk, H. (2002). “Strengthening of two-way slabs using steel plates.” *Structural Journal*, *99*(1), 23-31.

Erki, M. A., & Heffernan, P. J. (1995). “Reinforced concrete slabs externally strengthened with fibre-reinforced plastic materials.” In *RILEM PROCEEDINGS* (pp. 509-509). CHAPMAN & HALL.

Federal Emergency Management Agency (FEMA). (2013). “Foundation requirements and recommendations for elevated homes.” *Hurricane Sandy Recovery Fact Sheet No.2*, Washington, D.C.

Federal Emergency Management Agency (FEMA). (2014). “Homeowner’s guide to retrofitting.” *FEMA P-312*, Washington, D.C.

Federal Emergency Management Agency (FEMA). (2017, September 22). “Historic disaster response to hurricane Harvey in Texas.” HQ-17-133, Retrieved from https://www.fema.gov/news-release/2017/09/22/historic-disaster-response-hurricane-harvey-texas

Federal Emergency Management Agency (FEMA). (2018, February 28). “Policies in force by occupancy type.” Retrieved from http://bsa.nfipstat.fema.gov/reports/1011.htm

GangaRao, H. V., & Vijay, P. V. (1998). “Bending behavior of concrete beams wrapped with carbon fabric.” *Journal of structural engineering*, *124*(1).

Gere, J. M., & Timoshenko, S. P. (1997). Mechanics of materials, 1997. *PWS-KENT Publishing Company, ISBN 0, 534*(92174), 4.

Gilbert, R. I., & Warner, R. F. (1978). “Tension stiffening in reinforced concrete slabs.” *Journal of the structural division, 104*(12), 1885-1900.

Hibbit, H. D., Karlsson, B. L., and Sorrensen, P. (2007). *Abaqus theory manual*, SIMULIA, Providence, RI.

Hollaway, L. C., & Leeming, M. (Eds.). (1999). *Strengthening of reinforced concrete structures: Using externally-bonded FRP composites in structural and civil engineering*. Elsevier.

Hollaway, L. C. (2010). “A review of the present and future utilisation of FRP composites in the civil infrastructure with reference to their important in-service properties.” *Construction and Building Materials, 24*(12), 2419-2445.

Horse Structural Strengthening Materials (2018, March 2). “Epoxy bonded steel plate reinforcement on the bridge” Retrieved from http://www.horseen.com/project/Epoxy-bonded-steel-plate-reinforcement-on-the-bridge

Horse Structural Strengthening Materials (2018, March 2). “Epoxy bonded steel plate reinforcement on the bridge” Retrieved from http://www.horseen.com/steel-plate-bonding-system/steel-plate-bonding

Hsu, L. S., & Hsu, C. T. (1994). “Complete stress-strain behaviour of high-strength concrete under compression.” *Magazine of Concrete Research*, *46*(169), 301-312.

INOUE, S., Nishibayashi, S., Kuroda, T., & OMATA, F. (1996). “Fatigue strength and deformation characteristics of reinforced concrete beams strengthened with carbon fiber-reinforced plastic plate.” *Transactions of the Japan Concrete Institute*, *17*, 149-156.

IRC (International Residential Code). (2015). *A Member of the International Code Family*. Country Club Hills, IL.

Janner, J. (2015, May 24). “Hundreds of homes washed away by deadly Texas flooding.” Retrieved from https://www.cbsnews.com/news/homes-washed-away-deadly-texas-flooding-blanco-river/

Kaiser, H. P. (1989). “Strengthening of reinforced concrete with epoxy-bonded carbon-fiber plastics.” *Doctoral Thesis, Diss. ETH*.

Khalifa, A., Belarbi, A., & Nanni, A. (2000). “Shear performance of RC members strengthened with externally bonded FRP wraps.” In *Proceedings (CD-ROM) of Twelfth World Conference on Earthquake, Auckland, New Zealand, January*.

Klaiber, F. W., Dunker, K. F., Wipf, T. J., & Sanders Jr, W. W. (1987). *Methods of strengthening existing highway bridges* (No. 293).

Lam, L., & Teng, J. G. (2001). “Strength of RC cantilever slabs bonded with GFRP strips.” *Journal of Composites for Construction*, *5*(4), 221-227.

Lorenc, W., & Kubica, E. (2006). “Behavior of composite beams prestressed with external tendons: Experimental study.” *Journal of constructional steel research*, *62*(12), 1353-1366.

Lu, X. Z., Teng, J. G., Ye, L. P., & Jiang, J. J. (2005). “Bond–slip models for FRP sheets/plates bonded to concrete.” *Engineering structures*, *27*(6), 920-937.

Lubliner, J., Oliver, J., Oller, S., & Onate, E. (1989). “A plastic-damage model for concrete.” *International Journal of solids and structures*, *25*(3), 299-326.

Macdonald, M. D., & Calder, A. J. J. (1982). “Bonded steel plating for strengthening concrete structures." *International Journal of Adhesion and Adhesives*, *2*(2), 119-127.

Meier, U. (1992). “Carbon fiber-reinforced polymers: modern materials in bridge engineering.” *Structural Engineering International, 2(1), 7-12.*

Meier, U. (1995). “Strengthening of structures using carbon fibre/epoxy composites.” *Construction and Building Materials*, *9*(6), 341-351.

Mosallam, A. S., & Mosalam, K. M. (2003). “Strengthening of two-way concrete slabs with FRP composite laminates.” *Construction and building materials, 17*(1), 43-54.

Nanni, A. (1999). “Composites: Coming on Strong.” *Concrete Construction*, *V.44*, p.120.

Natural Resources Conservation Service (NRCS). (2018, May 25). “The soil orders of Texas.” Retrieved from https://www.nrcs.usda.gov/wps/portal/nrcs/detail/tx/home/?cid=nrcs144p2_003094

Nayal, R., & Rasheed, H. A. (2006). “Tension stiffening model for concrete beams reinforced with steel and FRP bars.” *Journal of Materials in Civil Engineering*, *18*(6), 831-841.

Norris, T., Saadatmanesh, H., & Ehsani, M. R. (1997). “Shear and flexural strengthening of R/C beams with carbon fiber sheets.” *Journal of structural engineering*, *123*(7), 903-911.

Peshkam, V., & Leeming, M. (1994). “Application of composites to strengthening of bridges: Project ROBUST.” In *Proceedings 19th International BPF Composites Congress*.

Phillip, D. (2017, August 29). “Texas, Louisiana begin long recovery from catastrophic flooding as the remnants of hurricane Harvey move northeast.” Retrieved from http://www.businessinsider.com/tropical-storm-harvey-hurricane-updates-map-texas-where-landfall-damage-2017-8

Raithby, K. (1980). “External strengthening of concrete bridges with bonded steel plates.” *APWA reporter*, 18-p.

Ritchie, P. A., Thomas, D. A., Lu, L. W., & Connelly, G. M. (1990). “External reinforcement of concrete beams using fiber-reinforced plastics.” *ACI Structural Journal*, *88*(4), 490-500.

Saafi, M., Toutanji, H. A., & Li, Z. (1999). “Behavior of concrete columns confined with fiber reinforced polymer tubes.” *ACI materials journal*, *96*(4), 500-509.

Saenz, L.P. (1964). “Discussion of equation for stress-strain curve of concrete by Desayi, P. and Krishnan, S.” *ACI Structural Journal, 61, 1229-1235.*

Saibabu, S., Lakshmanan, N., Murthy, A. R., Ganapathi, S. C., Jayaraman, R., & Senthil, R. (2009). “External prestressing technique for strengthening of prestressed concrete structural components.” *Practice Periodical on Structural Design and Construction*, *14*(2), 90-98.

Santoh, N., Kimura, H., Enomoto, T., Kiuchi, T., & Kuzuba, Y. (1993). “Report on the use of CFCC in prestressed concrete bridges in Japan.” *Special Publication*, *138*, 895-912.

Seim, W., Hörman, M., Karbhari, V., & Seible, F. (2001). “External FRP poststrengthening of scaled concrete slabs.” *Journal of Composites for Construction*, *5*(2), 67-75.

Seniwongse, M. S. (2008). “Rehabilitation and Strengthening of Concrete Structures Using Carbon Fiber Reinforced Polymer.” In *AEI 2008: Building Integration Solutions* (pp. 1-10).

Shahawy, M., & Beitelman, T. E. (1999). “Static and fatigue performance of RC beams strengthened with CFRP laminates.” *Journal of Structural Engineering*, *125*(6), 613-621.

Sharaf, M. H., Soudki, K. A., & Van Dusen, M. (2006). “CFRP strengthening for punching shear of interior slab–column connections.” *Journal of Composites for Construction*, *10*(5), 410-418.

Sinha, A., & Hanna, A. M. (2016). “3D numerical model for piled raft foundation.” *International Journal of Geomechanics*, *17*(2), 04016055.

Suntharavadivel, T. G., & Aravinthan, T. (2005). “Overview of external post-tensioning in bridges.” In *Proceedings of the 2005 Southern Region Engineering Conference (SREC 2005)* (pp. 29-38). Engineers Australia, Toowoomba Local Group.

Taerwe, L., Khalil, H., & Matthys, S. (1997). “Behaviour of RC beams strengthened in shear by external CFRP sheets.” In *Proceedings of the Third International Symposium on Non-Metallic (FRP) Reinforcement for Concrete Structures (FRPRCS-3), Sapporo (Japan), 14-16 oktober Volume 1*.

Tao, Y., & Chen, J. F. (2014). “Concrete damage plasticity model for modeling FRP-to-concrete bond behavior.” *Journal of Composites for Construction*, *19*(1), 04014026.

Teng, J. G., Smith, S. T., Yao, J., & Chen, J. F. (2003). “Intermediate crack-induced debonding in RC beams and slabs.” *Construction and building materials*, *17*(6-7), 447-462.

Thomsen, H., Spacone, E., Limkatanyu, S., & Camata, G. (2004). “Failure mode analyses of reinforced concrete beams strengthened in flexure with externally bonded fiber-reinforced polymers.” *Journal of composites for construction*, *8*(2), 123-131.

Van Gemert, D. (1980). “Force transfer in epoxy bonded steel/concrete joints.” *International Journal of Adhesion and Adhesives*, *1*(2), 67-72.

Wahalathantri, B. L., Thambiratnam, D. P., Chan, T. H. T., & Fawzia, S. (2011). “A material model for flexural crack simulation in reinforced concrete elements using ABAQUS.” In *Proceedings of the first international conference on engineering, designing and developing the built environment for sustainable wellbeing* (pp. 260-264). Queensland University of Technology.

Wang, J. (2002). *Punching Shear Behaviour of RC Flat Plates Externally Strengthened with FRP Systems* (Doctoral dissertation, National University of Singapore).

WRI (Wire Reinforcement Institute). (2003). “Formulas for success innovation ways to reinforce slabs-on-ground.” *TECH FACTS 705-R-03*, Hartford, CT.

WRI (Wire Reinforcement Institute). (2003). “Welded wire reinforcement (WWR) in concrete pan joist slab construction.” *TECH FACTS 205-R-03*, Hartford, CT.

WRI (Wire Reinforcement Institute). (2007). “A design of slab-on-ground foundations.” *TECH FACTS 700-R-07*, Hartford, CT.

Yan, H., Lavandera, E. (2016, April 20). “Houston flooding: 7 dead, 1,200 rescued -- and more rain to come.” Retrieved from https://www.cnn.com/2016/04/19/us/houston-texas-flooding/index.html

Zhang, J. W., Teng, J. G., Wong, Y. L., & Lu, Z. T. (2001). Behavior of two-way RC slabs externally bonded with steel plate. *Journal of Structural Engineering*, *127*(4), 390-397.

Biographical Information

Natawut Chaiwino completed his Bachelor's degree in Civil Engineering from Kasetsart University, Thailand in 2005 and Master's degree in Structural Engineering from University of Houston, United States in 2009. He worked as a structural engineer for design and consulting firms from 2010 to 2011, and as a Lecturer at Rajamangala University of Technology Thanyaburi in Thailand from 2011 to 2014. His research interest includes Fiber Reinforced Polymer (FRP) for structural strengthening, design of reinforced concrete structures, and finite element analysis.